The thesis committee for Connor Dixon Mulkay certifies that this is the approved version of the following thesis:

Investigating the Utilization of Surfactant in Liquid Unloading Experiments of a Propped Fracture

APPROVED BY

SUPERVISING COMMITTEE

Mukul Sharma, Supervisor

Hugh Daigle

Investigating the Utilization of Surfactant in Liquid Unloading Experiments of a Propped Fracture

by

Connor Dixon Mulkay

Thesis

Presented to the Faculty of the Graduate School

of the University of Texas at Austin

in Partial Fulfillment

of the Requirements

for the Degree of

Master of Science in Engineering

The University of Texas at Austin

May 2019

Acknowledgements

Firstly, I would like to express gratitude to my supervising professor, Dr. Mukul Sharma, for his guidance and supervision throughout this project and during my time at the University of Texas at Austin. I am also appreciative of Dr. Hugh Daigle for being the second reader of my thesis and for allowing me to operate his NMR equipment. I would also like to thank Rod Russell for his limitless advice, expertise, and help in the laboratory. I am also very grateful for Jin Lee for all the work she does in the office and for always finding time to help me with anything, no matter how large or small the issue may it be.

I also like to thank Kay Cawiezel and her team at BP for making this project possible and for their suggestions throughout this endeavor. I would also like to thank my coworker Williams Ozowe for all his assistance in the lab and for being a soundboard for me as I interpreted experimental results.

Finally, I would like to thank the rest of my family and friends for their advice, love, and support.

Abstract

Investigating the Utilization of Surfactant in Liquid Unloading Experiments of a Propped Fracture

Connor Mulkay, M.S.E.

The University of Texas at Austin, 2019

Supervisor: Mukul Sharma

The United States currently leads global production of oil and gas fundamentally in part due to its successful large shale plays. Advancements in technology and research have allowed the US to apply production techniques that increase recovery from these unconventional reservoirs; one of these principally being fracing. Through fracing, large fractures are created in the highly impermeable rock, thus increasing the amount of surface area for hydrocarbon flow and unlocking profitable production. After these fractures are created, the high amount of production only continues for a relatively short amount of time, after which production steeply slows down. Most companies react to this by drilling and fracing a new well in a different location. If these fractures could be improved so that the reduction in productivity is slowed down, companies would not have to drill as many well thereby saving money and causing less environmental disturbances.

An idea to mitigate the productivity decline is by quickly unloading the built-up liquid in a newly created fracture. If suspended in a fluid for a period of time, gravitational forces cause

proppant to settle in the lower part of the fracture. As the liquid slowly seeps into the formation, closure stresses from the surrounding rock begin to exceed pressure in the fracture and the upper part of the fracture closes off due to a lack of proppant. The surface area of the fracture promoting hydrocarbon flow is then drastically reduced. The closed off fracture could also potentially close off routes of flow if it is a critical pathway. A hypothesis is that if the built-up fluid in the fracture is unloaded quickly, the fracture will have a more homogenous distribution and will promote better fluid flow, thus slowing down the productivity decrease that is normally observed.

Surfactants are already used for a variety of applications in the oil and gas industry. This thesis involves conducting experiments using surfactants to remove the built-up fluid in a fracture. Investigations are performed with different combinations of fluids typically used in industry. A fracture model made out of plastic plates is filled with proppant and a test fluid, and air is injected at the bottom of the fracture. The volume of liquid that exits the fracture is recorded as time passes. Results show that surfactant significantly improves the volume of unloaded liquid, even when in contact with oil at S_o = 30% in the fracture. Results from these experiments are not meant to be directly applied to the field, as experiments are not conducted at reservoir conditions. They are intended as a preliminary investigation into the potential of surfactant additives in hydraulic fracturing fluid.

Table of Contents

List of Figures

List of Tables

Chapter 1: Introduction

1.1 Motivation

In an effort to meet the world's growing global energy demands, hydraulic fracturing is one of many solutions developed and applied most significantly in the United States to bolster the economic recovery of hydrocarbons. This technology has been used for decades; however, since the early 2000s, when the shale revolution kicked off, fracturing has become an increasingly important method for accessing new reserves and accelerating production. Currently more than half of all US oil production is from hydraulically fractured wells. According to the International Energy Agency, US oil production will cover 80% of new global demand for oil in the next three years, as production is believed to increase nearly 30% in this time. This growth comes primarily from hydraulic fracturing, mainly in the West Texas region (Worland, 2018).

The process of hydraulic fracturing involves injecting hydraulic fracturing fluid down the well and into a formation at very high pressures. The fluid fractures the rock and propagates outwards in complex geometries. Proppant suspended in the fluid acts as a wedge to hold the fracture open. As a result, there is a large increase in surface area of pathways for hydrocarbons to flow to the wellbore. Industry typically refers to this as stimulation, as production rates can increase from between 1.5 to 30 times the pre-fracture rate of flow. Companies often use a well's productivity index to describe its flow potential. This value is the ratio of the surface flow rate at standard conditions and the drawdown (the difference between the reservoir pressure and the bottom hole pressure). Immediately after stimulation, the increase in flow rate drives the

productivity index up to very high values. Unfortunately, this stimulation doesn't seem to last. After only a couple of months, the productivity declines quite rapidly. Usually the easiest response to this loss of production is to drill a new well. Although significant advancements and industry experience has reduced costs in drilling and fracturing, research into increasing production from already fractured wells would reduce the cost of development and the environmental impact. Even better would be methods of slowing down the rapid productivity decline.

Productivity index decline is well-understood in conventional reservoirs, however in unconventional plays that rely on hydraulic fracturing for production, the phenomenon is more complex. Unconventional wells involve various evolving flow regimes during their early history, in addition to the decaying ability for a fracture to flow fluid, which could be affected by various mechanisms that are difficult to investigate (Sarna, Xing, Mork, & Ershaghi, 2014). These qualities make simulation difficult and decline behavior confusing. Clay swelling, fines migration, proppant embedment, and closing of fractures are some mechanisms believed to be large influences.

There are numerous research efforts investigating these qualities, however the topic of interest for this thesis involves the closing of fractures due to low fracture fluid recovery. Very little frac fluid is actually recovered to the surface after a fracturing job is performed, resulting in a loss of thousands of gallons of liquid (Abbasi, Dehghanpour, & Hawkes, 2012). Various studies reveal the fluid retention downhole is likely caused by low water relative permeability and high capillary pressure (Gdanski & Walters, 2010; Ghanbari & Dehghanpour 2016). To further inhibit recovery, the tortuous nature of pathway geometry of the hydraulic fracture limits movement in the vertical direction, affecting liquid transport (Fisher & Warpinski 2012). Built-up liquid in the fracture is unfavorable for production for a couple of reasons. Results from 3-D simulation of liquid loading reveal hydrocarbon flow from the formation into a hydraulic fracture is impeded by

a lower pressure differential between the fracture and surrounding matrix (Agrawal & Sharma, 2015). Having a low pressure drawdown has huge impacts on well production rates. Furthermore, leakage into formation can result in unfavorable fracture closure. Numerous numerical studies reveal fracture closure to reduce the aperture, or fracture volume, leading to a loss of fracture conductivity which hurts production. These studies involve investigating a variety of mechanisms for fracture closure (Fredd, McConnell, Boney, & England, 2001; Alramahi & Sundberg, 2012; Cho, Ozkan, & Apaydin, 2013). However, a challenge in these models arises when estimating the proppant concentration distribution. There is difficulty in creating a fracture with a uniform distribution of proppant. Over time, gravity causes the particles to settle towards the bottom, leaving the upper part of the fracture without proppant (Acharya, 1984; Warpinski, 2010). Figure 1 displays what the resulting aperture looks like after liquid is produced or leaked into the formation and far field stresses exceed the pore pressure.

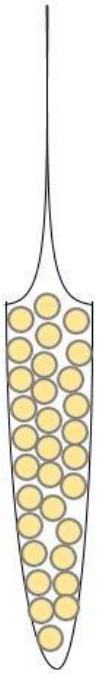

Figure 1 - The cross section of a hydraulic fracture after proppant has settled and closure stress has closed the upper aperture.

Because networks of fractures act as vehicles that allow hydrocarbon to flow more easily to the wellbore, fracture conductivity can be harmed if critical pathways are disrupted. A decrease in effectiveness of critical fracture pathways reduce flow capabilities of any fractures beyond that point and hurt production. 3D hydraulic fracturing simulation shows how non-uniform proppant distribution affects discrete fracture networks (McClure, Babazadeh, Shiozawa, & Huang, 2016). The results involve complex geometries of both propped and unpropped fractures. Unpropped fractures limit conductivity, where the aperture is controlled by its asperities. If completely closed, pathways of fractures beyond the closed fracture could be rendered ineffective.

Sharma and Agrawal (2013) have given recommendations for operators to combat liquid loading under different scenarios. The easiest way to minimize loading within fractures would be to maximize the drawdown pressure. Some concerns with this involve pre-maturely closing the fracture network, and causing retrograde condensate dropout, gas relative permeability reduction, and eventual condensate loading. To avoid further damage, they recommend the use of surfactants or energized fracturing fluid alternatives.

1.2 Objective

If one could unload liquid from the fracture without having to increase drawdown pressure, then there would be less damage to the formation, thus lessening the decline in productivity index. The productive life of the well would also be increased, and there would be less of a need to drill new wells to maintain steady field production levels. The purpose of this thesis is to experimentally investigate the potential of unloading liquid built-up in a fracture through foam transport when surfactant is added to hydraulic fracturing fluids. It is believed that successful unloading would mitigate detrimental effects due to non-uniform proppant distribution, proppant embedment and fracture closure, as well as improve the relative permeability for gas. It is important that the fluid

be unloaded before leakage into the formation, which usually occurs in the first couple days after fracture creation. Therefore, unloading with surfactant will be considered successful if a substantial amount of liquid can be removed from a fracture in the first 48 hours.

It must be stated that the intention of this thesis is not to identify a surfactant that generates stable foam at reservoir conditions in contact with oil, but to demonstrate that the application of foam in a hydraulic fracture is worth further research.

Chapter 2: Background

2.1 Surfactants

Surfactants are a group of chemicals that reduce interfacial tension and, therefore, act as surface active agents. They are often described as molecules with a hydrophilic "head" and a hydrophobic "tail." Because of this structure, the molecule tends to migrate to an oil-water interface. Above the critical micellar concentration, surfactants often form micelles.

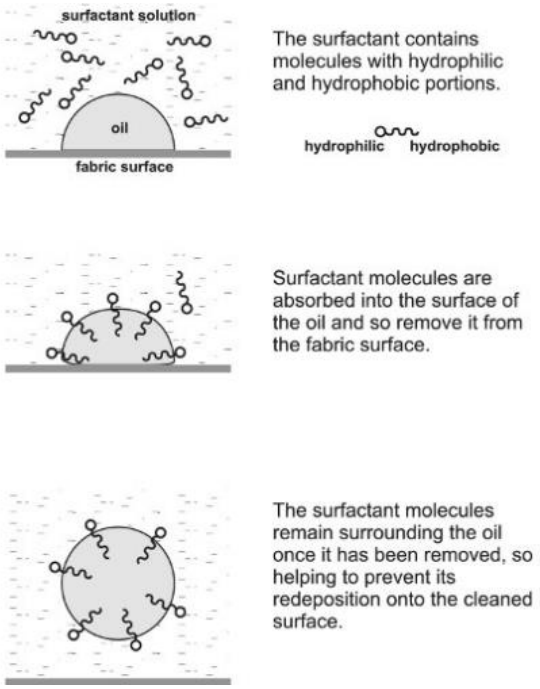

Figure 2 - Surface active agents at interfaces. (From Lichtarowicz, 2013)

The shape and size of a micelle is a function of the surfactant's molecular geometry, thermodynamic conditions, and the solution's concentration, pH, and ionic strength. Surfactants have many practical uses – from household applications, cleaning dishes to industrial applications

such as making paper softer and more absorbent (Kumar & Mittal, 1999; American Chemistry Council, 2019). Oil industry applications are numerous, even across various disciplines including drilling, secondary recovery, enhanced oil recovery, and pipeline transportation. Table 1 lists a partial list of these practices.

Table 1 - Some oil and gas industrial applications of surfactants. (From Schramm, Laurier, Stasiuk, & Marangoni, 2003)

Gas/liquid systems	
	Producing oil well and well-head foams
	Oil flotation process froth
	Distillation and fractionation tower foams
	Fuel oil and jet fuel tank (truck) foams
	Foam drilling fluid
	Foam fracturing fluid
	Foam acidizing fluid
	Blocking and diverting foams
	Gas-mobility control foams
Liquid/liquid systems	
	Emulsion drilling fluids
	Enhanced oil recovery in situ emulsions
	Oil sand flotation process slurry
	Oil sand flotation process froths
	Well-head emulsions
	Heavy oil pipeline emulsion
	Fuel oil emulsions
	Asphalt emulsion
	Oil spill emulsions
	Tanker bilge emulsions
Liquid/solid systems	
	Reservoir wettability modifiers
	Reservoir fines stabilizers
	Tank/vessel sludge dispersants
	Drilling mud dispersants

The ionic charge of the hydrophilic group designates if a surfactant is anionic, cationic, or nonionic. Anionic surfactants are most commonly used in the petroleum industry due to their limited adsorption and effectiveness in sandstone reservoirs, however all three have been used (Negin, Ali, & Xie, 2017). There is currently much ongoing research for new applications of all

three types of surfactants, as well as research for creating new, stable surfactants that can be used in specific environments or systems, as the performance of surfactants are influenced by temperature, salinity, and rock composition in addition to its concentration and molecular structure.

2.2 Improving Displacement

Waterflooding is a production method utilized to produce hydrocarbons after primary and secondary recovery. This unrecoverable oil is referred to as residual oil. One topic of interest for EOR researchers is using surfactants in waterfloods to recover the capillary trapped residual oil. The ideal surfactant increases the capillary number and reduces the mobility ratio to recover as much of the remaining oil as possible.

$$Mobility\ Ratio = \frac{\frac{k_{rdisplacing}}{\mu_{displacing}}}{\frac{k_{rdisplaced}}{\mu_{displaced}}}$$

$$Capillary\ Number = \frac{v\mu_{displaced}}{\sigma}$$

Where: k_r = relative permeability
μ = viscosity
v = velocity
σ = surface tension

This same principle can be applied to a proppant pack. Surfactants should be able to increase the capillary number (recover more liquids) and reduce the mobility ratio (improve the sweep efficiency). The capillary number is typical controlled during EOR by reducing the interfacial tension to near zero. The mobility ratio can be controlled by increasing the viscosity of the displacing fluid by using foams or polymers (Mejia, 2018). Polymer additives are not favorable

for fracturing applications as they increase the viscous pressure drop in the tubing and casing. However, to some extent surfactants can realize the same effects. The ideal surfactant for unloading should maximize the capillary number while minimizing the mobility ratio with the addition of other frac fluid components. While fracturing fluid contains friction reducers that lower viscosity, the addition of surfactant generates foam when in contact with gas. The foam has a much higher viscosity, called apparent viscosity as it contains multiple phases, which favorably drives the mobility ratio down.

The apparent viscosity of foam is dependent on many factors including the quality of the foam, bubble sizes, and proppant packing (Falls, Musters, & Ratulowski, 1989). For the purposes of this experiment, the apparent viscosity will not be measured, however it will be controlled mainly by the concentration of surfactant added. It is desired to reach a mobility ratio lower than 1.0. Saffman-Taylor fingering initiates when the ratio is greater than one due to viscous instabilities during displacement, as seen in Figure 3. A less-than-one mobility ratio results in more uniform, piston-like displacement resulting in better sweep efficiency. It is expected that increasing the concentration of surfactant will increase the foam viscosity, improve sweep efficiency and result in better liquid unloading.

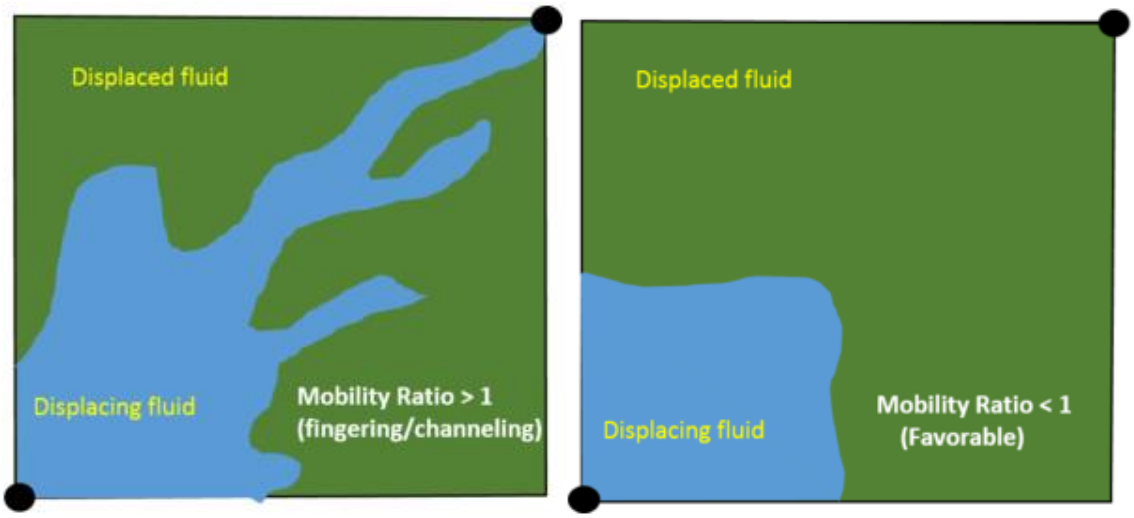

Figure 3 - Viscous fingering occurs when the mobility ratio is greater than one and results in inefficient displacement. (From Green & Willhite, 1998)

2.3 Foam Stability

Continuous, effective displacement assumes that foam is able to remain stable. Unfortunately, maintaining stable foam is not as trivial as generating foam. Stability depends on the foam's elasticity, disjoining pressure, resistance to ripening, resistance to drainage, and resistance to defects (Abbott, 2017).

2.3.1 Film Stability

A stable foam requires bubbles that remain unharmed after being moved, compressed, and deformed. Foam stability depends on the visco-elastic properties of the surfactant films that separate the gas bubbles (Wang & Yoon, 2008; Abbott, 2017). Higher surfactant concentration, smaller bubble sizes and more elasticity in the foam lamella (surfactant films) generally promote foam stability.

2.3.2 Disjoining Pressure

By its very nature, the curvature of films in a foam creates capillary forces that inherently force the liquid to flow, which would result in thinning of the film until it disappears completely. Thus according to DLVO theory, there exists some force, or disjoining pressure, that counter-balances capillary pressure and prevents thinning. Disjoining pressure has been found to be the summation of the effects of van der Waals forces, electrostatic forces, and steric interactions (Sedev & Exerowa, 1999). This is represented in the following equation.

$$\Pi = \Pi_{vw} + \Pi_{el} + \Pi_{st}$$

The electrostatic forces are determined by ionic strength and surface potential, and are the most important determiners of disjoining pressure. Essentially, the salinity, type of salt, and hydrophilic and hydrophobic components in the surfactant govern disjoining pressure. Salt concentration and pH have a strong influence on foam stability (Aronson, Bergeron, Fagan, & Radke, 1994; Behera, Varade, Ghosh, Paul, & Negi, 2014). For foam to remain stable, the disjoining pressure sets a limit on film thickness and controls the equilibrium bubble size.

2.3.3 Ostwald Ripening

Heterogeneous bubble sizes tend to encourage coarsening, or Ostwald ripening, as larger bubbles grow in size and smaller bubbles shrink due to inter-bubble gas diffusion caused by differences in capillary pressure. This process is represented in Figure 4.

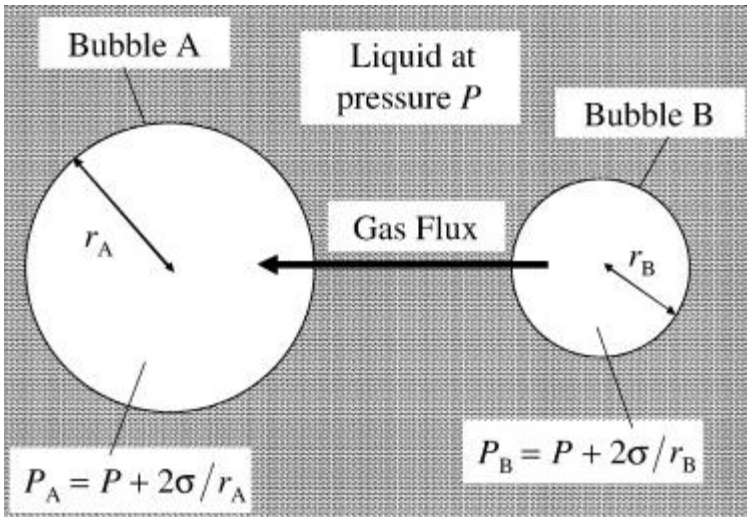

Figure 4 - Illustration of Ostwald ripening caused by capillary pressure differences. (From Stevenson, 2010)

Ostwald ripening can be problematic, as the small bubbles shrink until they no longer exist, and the large bubbles become weaker and less stable as they grow. To mitigate effects of ripening, the gas diffusion rates must be minimized. This can be done either by lowering the solubility of gas, or decreasing the permeability of diffusion across the film wall. Additives of different gases or chemicals can be used to combat both these phenomena. The addition of nitrogen is often practiced in foam applications because of its low solubility in water. Among other additives that lower gas solubility are certain water-soluble polymers such as sodium carboxymethyl cellulose (CMC) and guar gum, (Princen & Mason, 1965; Sarma, Pandit, & Khilar, 1988; Stevenson, 2010). Many studies are currently being performed to further understand gas diffusion and the contribution of film permeability (Tcholakova et al., 2011).

2.3.4 Drainage Effects

Free drainage occurs in foam due to the natural difference in densities between the gas and liquid. Over time gravity causes liquids to pass through channels between bubbles, often referred to as Plateau borders, to settle below some equilibrium level. Determining the rates of drainage is

a complex concept, however it is known to be highly dependent on the viscosity of the liquid, size of the bubbles, as well as how the surfactant responds to flow (slip conditions vs no slip conditions) (Koehler, Hilgenfeldt, & Stone, 2000). Gas flow through a proppant pack in a hydraulic fracture does not allow free drainage to occur, as the system contains forced flow. However, the foam in the proppant pack endures similar consequences as a foam encountering free drainage would. In both situations, liquid is being removed, either by gravitational effects or intentional forced transport.

When the liquid volume fraction, ε, is less than 0.05, bubbles have well defined edges and are labelled as "dry foam", while when greater than 0.36 there is random close packing of solid spheres with no deformity and are labelled as "wet foam" (Saint-Jalmes, 2006). Free drainage can be slowed down by increasing the viscosity of the liquid. However, in a hydraulic fraction, lowering the liquid volume fraction is actually the goal, meaning that the effectiveness of the foam to unload fluid from the fracture will decrease with time as the foam transforms from wet to dry.

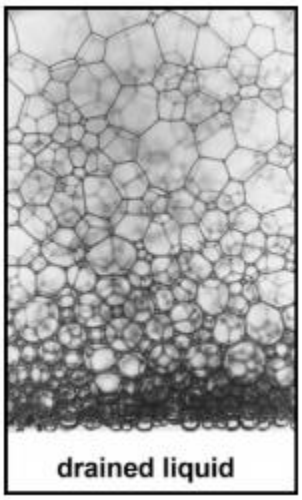

Figure 5 - A foam at equilibrium after being allowed to drain freely. At the top is dry foam with polyhedral bubbles and Plateau borders, while the bottom is wet. The first layer contains spherical gas bubbles, indicating ε > 0.36. (From Saint-Jalmes, 2006)

Figure 5 shows a photograph of a foam that has reached equilibrium, resulting in bubbles with different liquid volume fractions and, therefore, forming different shapes.

2.3.5 Effect of Impurities and Additives

Finally, the stability of foam can be affected by additives, or other fluids or particles that can interact with the system. In a hydraulic fracture, this could be the interaction of foam with a hydrophobic material such as oil or oil-coated particles. If oil becomes concentrated enough when in contact with foam, it can spread over the lamellar surfaces, causing bubble swelling, film thinning and eventual rupture. Rupture can also occur due to oil's hydrophobic nature affecting the stability of the thin surfactant films (Aveyard, Cooper, Fletcher, & Rutherford, 1993).

For the purposes of our experiment, foam is generated when air mixes with the surfactant SDS (sodium dodecyl sulfate) solution in either water or broken hydraulic fracturing fluid. Because many influencers on the stability of foam are dependent on temperature, pressure, and chemistry of fluids involved, the chemicals utilized in this experiment do not completely represent a real fracture. However, if a proper mixture of surfactant and hydraulic fracturing fluid can be identified to be stable at reservoir conditions, the results of these experiments should identify the capabilities of an ideal mixture.

2.4 Broken Hydraulic Fracturing Fluid

There are many types of fluids utilized in hydraulic fracturing, and they are often grouped into categories of being water-based, oil-based, or energized (containing gas). Their critical functions are to be able to suspend and deliver proppant as a fracture is generated, control leak-off into the surrounding formation, and to transmit pressure from the surface to the fracture tip. Depending on a formation's requirements, there are a variety of different additives that can be

included in the fluid including proppant, cross-linkers, gels, breakers, friction reducers, fluid loss controllers, clay stabilizers, bactericides, polymer stabilizers, pH buffers, and surfactants (U.S. Department of Energy, 2009). Because frac fluid can differ greatly from well to well, and identifying a stable foam at reservoir conditions is beyond the scope of this thesis, the recipe for the fracturing fluid utilized in these experiments is not complex. Only a proprietary mixture of friction reducers is mixed with an oxidative breaker and surfactant.

Chapter 3: Experimental Assembly, Materials, Preparation, and Procedure

Foaming agents were tested in the laboratory for their ability to unload fluid from a simulated fracture. A hydraulic fracture cell was filled with proppant and completely saturated with the fluid to be tested. Part of the experimental setup can be seen in Figure 6.

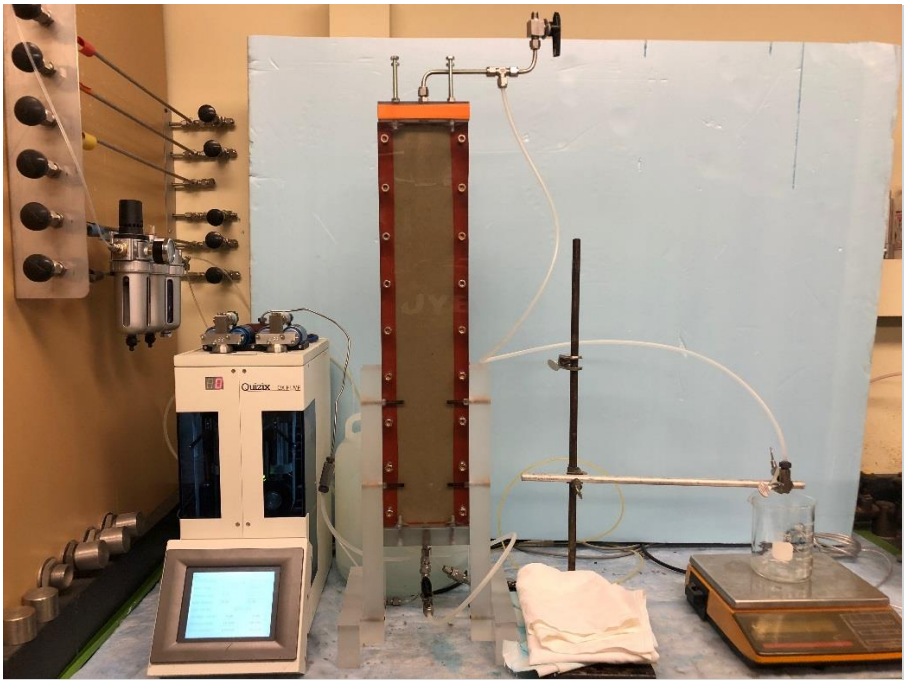

Figure 6 – Integral equipment for the fracture testing assembly are pictured including the mass balance, collection beaker, fracture cell, dual syringe pump, dehydrator and deoiler.

Gas flow through the fracture is simulated by injecting air into the bottom of the proppant pack. The air then travels through the proppant and pushes the test fluid out the top of the cell, where its mass can be recorded. Tests were performed using different concentrations of surfactant and with different air injection flow rates. Both tap water and broken hydraulic fracturing fluid were used as solvents for the surfactant.

3.1 Description of Equipment

Figure 7 displays the schematics for the experimental setup. Following the image is a list of the equipment used with a description of its purpose or its specifications.

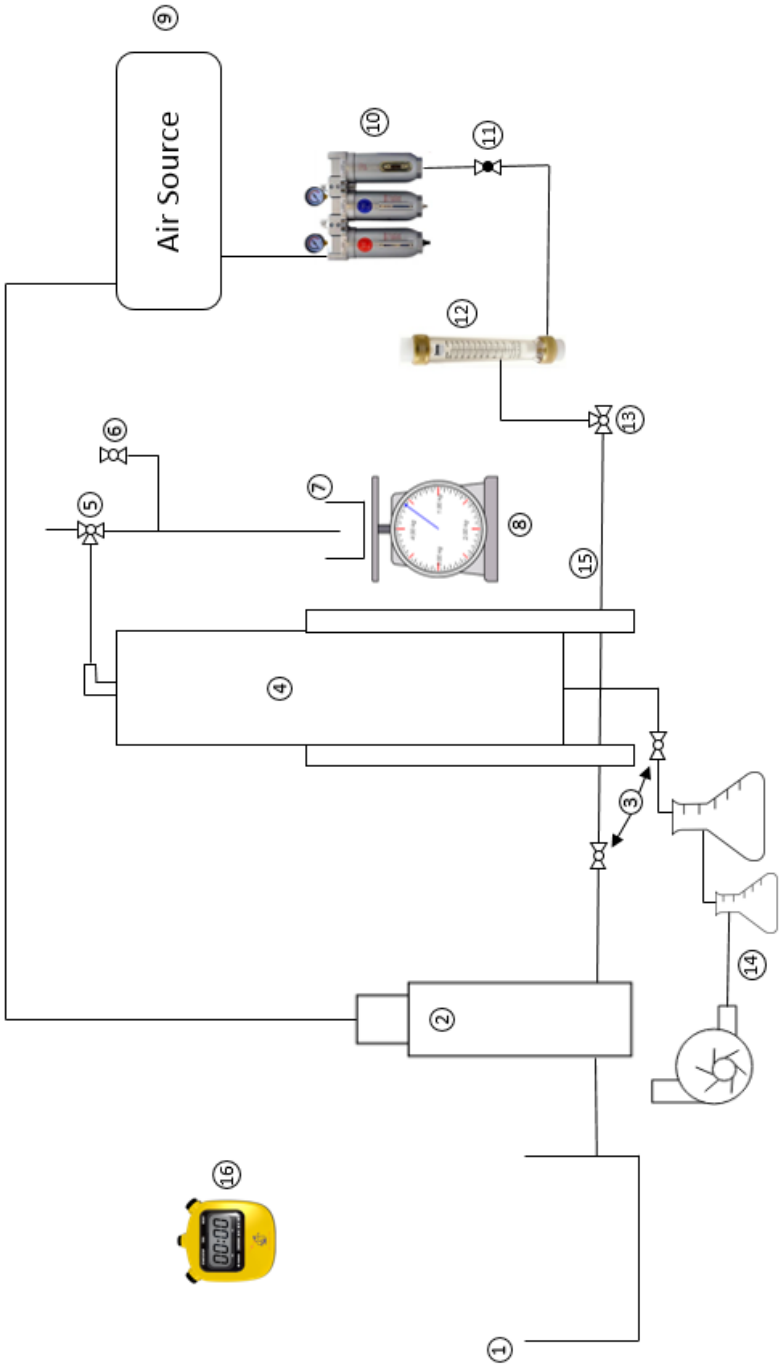

Figure 7 - Schematic of experimental setup for testing the unloading of fluids from fracture cell.

1) Fluid Reservoir— A beaker or tank contains liquids to be delivered to testing cell. It should hold at least 200 mL of liquid at minimum in order to fill the entire volume of the cell, pump syringes, and tubing and can be filled with either tap water or broken hydraulic fracturing fluid.
2) Dual Syringe Pump— A reciprocating positive displacement pump is used to load liquid into the cell during experiment preparation. It can maintain either constant pressure or constant flow rate injection depending on what the operator requires. During preparation, liquid flow rates were delivered at rates less than 50 mL/min.
3) Ball Valves— These valves control the connection between the pumps and the closed system of the test cell assembly. When open they allow flow, and when closed they prevent flow. During experimentation, they need to be closed to ensure all airflow is directed into the test assembly.
4) Test Cell Assembly— The fracture is mimicked out of 1" thick transparent polyethylene plates. The plates have a height of 23" and width of 5.125". A rubber seal coated with silicon gen sits between the plates, causing the actual fracture width to be closer to 3.375". See Figure 8 for 3D-CAD views of the rubber seals as well as the assembly as a whole. The fracture thickness is dependent on how tightly the plates are fastened onto the rubber seal. For these experiments, the thickness is approximately 0.125". Seals and silicon are also applied to the top and bottom of the fracture to ensure there is no leakage. A hole is drilled into the top plate that acts as the fracture outlet. Half-inch Swagelock tubing is fastened into the outlet as a connection to tubing. The assembly also has legs that allow it to stand vertically. After filled with US Mesh 12-30 glass reflective beads, the pore volume is approximately 69.5 mL.

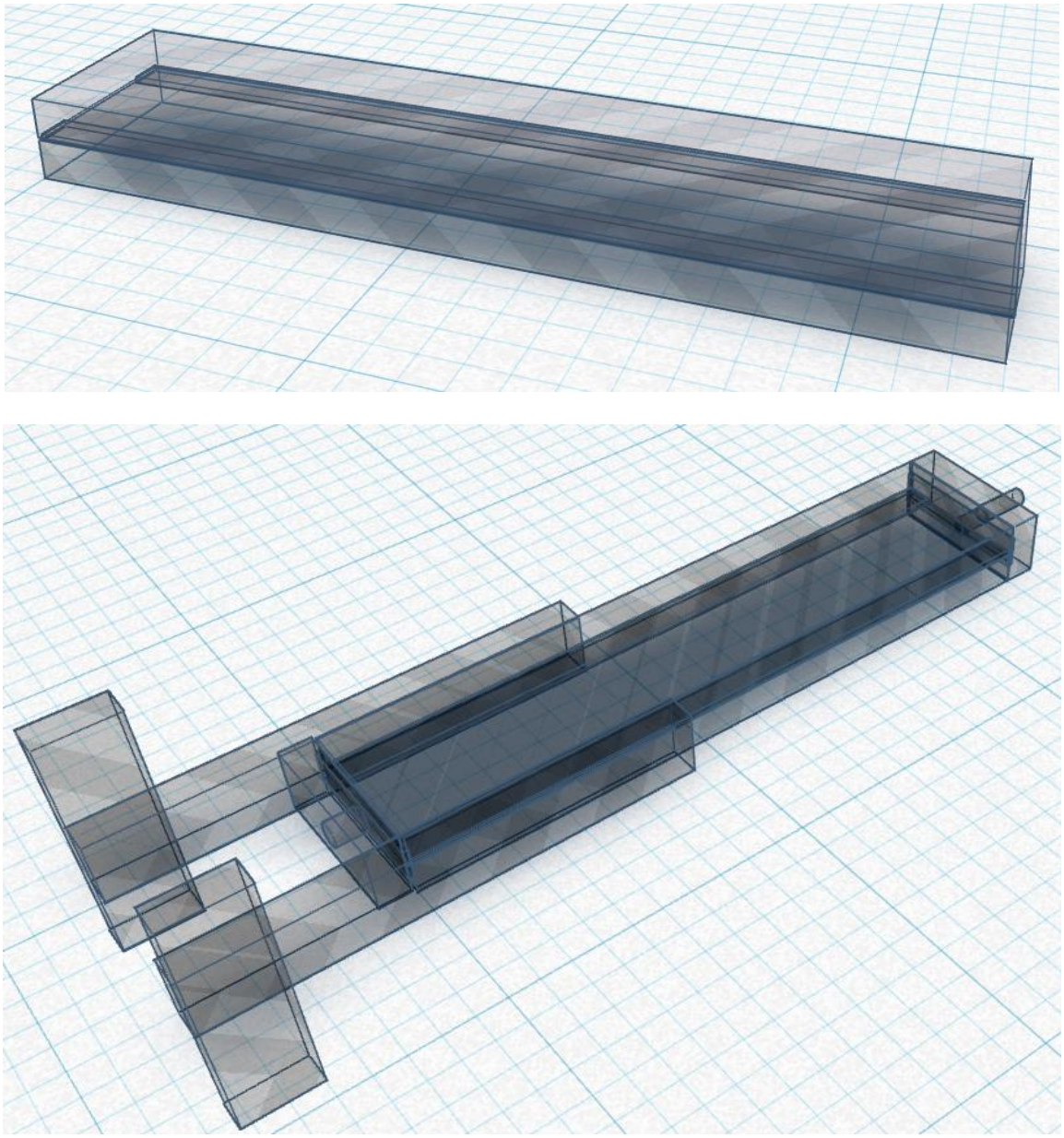

Figure 8 - Views of the fracture cell with CAD software. The top image depicts the two plastic plates separated by rubber sealing that form the walls of the fracture. The bottom image shows the entire fracture assembly including its legs.

5) Three-way Ball Valve— This valve can close off or open the system to the atmosphere, or it can pass fluid through to the collection beaker

6) Ball Valve— Located at the end of a section of branched off tubing that can be opened or closed to the atmosphere, this valve can create or break a siphon effect on the tubing

transporting unloaded fluid. For more accurate measurements, unloaded fluid in the liquid phase should not be slowed down by the siphon. Liquid cannot not use the valve as a pathway for flow due to gravitational effects. However, when the unloaded fluid is a foam, the flow can overcome gravity to escape through the valve, and so the valve must be closed off after foam inception.

7) Collection Beaker— A graduated cylinder is used to catch unloaded fluid. The capacity of the beaker exceeds the volume of fluid in the fracture.
8) Mass Balance— The mass of fluid that exits the fracture is recorded by a balance. The collection beaker sits on top, and the balance is tared before beginning the experiment. The maximum allowed weight is 3500 g with a precision of 0.01 g
9) Air Source— Shop air is readily available at a delivered pressure of approximately 70 psi. The dual syringe pump requires a connection to the air source to manipulate its actuators.
10) Dehydrator and Deoiler— A series of filters cleans the shop air as it removes any trace amounts of water and oil.
11) Globe Valve— Manipulating this valve regulates the flow rate of air delivered to the fracture cell.
12) Floating Ball Flowmeter— This analog flowmeter indicates the air flow rate to be injected into bottom of fracture cell with a maximum possible reading of 250 mL/min. The precision of the readings are varied, however in the region of interest (0 - 20 mL/min) it is 1 mL/min.
13) Three-Way Ball Valve— This valve can deliver air to either the environment or into bottom of cell. Diverting air into the environment allows the operator to reach a desired air injection rate before actually delivering air into the cell.

14) Vacuum Pump with Dehydrators— The vacuum can be utilized to removed residual fluids and air from test cell during test preparation. This allows for more homogeneous fluid saturation and more accurate measurements of fluid contained in the fracture. A pair of dehydrators are used to protect the vacuum pump from damage.
15) Swagelok Tubing— Both quarter-inch and eighth-inch Swagelok tubing and connections are used. The majority of tubing is plastic for easier viewing and is feasible because of the lack of pressure requirements.
16) Stopwatch— A stopwatch is used as a timer for indicating when to record mass measurements.

3.2 Other Materials

- Tap Water— A test fluid to be loaded inside the fracture cell.
- Broken Hydraulic Fracturing Fluid— A test fluid to be loaded inside the fracture cell. It is created by adding a proprietary high viscosity friction reducer to water, and then mixed with an oxidative agent and introduced to heat to break polymerized chains.
- Sodium Dodecyl Sulfate— Also referred to as SDS or sodium lauryl sulfate, it is the surfactant to be mixed in concentrations of 0.05% and 0.1% with the test fluids. It is an anionic surfactant.
- US Mesh 12-30 Glass Reflective Beads— Advertised by Cole Safety Products as Type 4, “Airport Quality” Reflective Beads. It is used to as proppant in the fracture.
- Dye— Water soluble dye is added to both types of test fluids to color the fluid red. Ensures ease of visibility in the fracture cell to distinguish fluid saturation and distribution.

- EXXSOL™ D110— A petroleum-based solvent used in industrial applications such as manufacturing process solvent, metal working, and coatings. It is a mineral oil used to investigate foam interactions with oil.

3.3 Obtaining Repeatability

For test repeatability, there are some features of both the assembly design as well as test preparation that were applied for consistent results. Most of these features are attempts to combat the difficulty in fully saturating the fracture cell in a consistent manner. Figure 9 depicts the bottom section of the hydraulic fracture cell with no fluid added, showing non-uniform proppant packing.

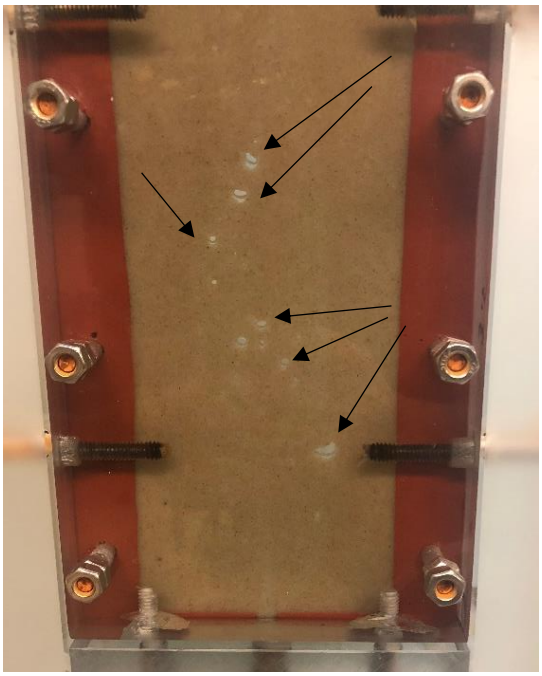

Figure 9 - After each time a test run is performed, the proppant must be reorganized into a uniform distribution free from void spaces. Some void spaces are depicted here by the arrows.

Even though the proppant was originally well-packed when added to the cell, a test run mars the uniform distribution as the injected air pushes the particulates around, thus creating these void spaces. The void spaces are detrimental to the experiment for a couple of reasons: preferential pathway for flow, fluid settling, all of which hinders test repeatability. If the void spaces are

allowed to remain in the proppant pack when the cell is saturated with the testing fluid, the fluid flows preferentially through the spaces to the top of the fracture and leaves the proppant away from the spaces unwetted and unconnected. Even after pumping the test fluid into the cell for extended periods of time (a couple days), regions of the fracture remain unsaturated. Ceasing the injection sometimes even reveals more unsaturated regions at the top of the cell, as some of the saturation seemed to be "held in place" by the fluid velocity. Once no longer flowing, fluid settling could take place as gravity took control and moved the fluid to other regions. Obviously real propped fractures in the ground do not have perfect proppant distributions; however, imperfections in the experiment's distribution were believed to drastically affect test repeatability.

Attempts to correct the imperfect saturation involved adding the testing fluid to the fracture at differing flow rates, both fast and slow. Fast flow rates would preferentially follow the void pathways all the way to the top of the cell, leaving most of the sand unsaturated, as seen in Figure 10.

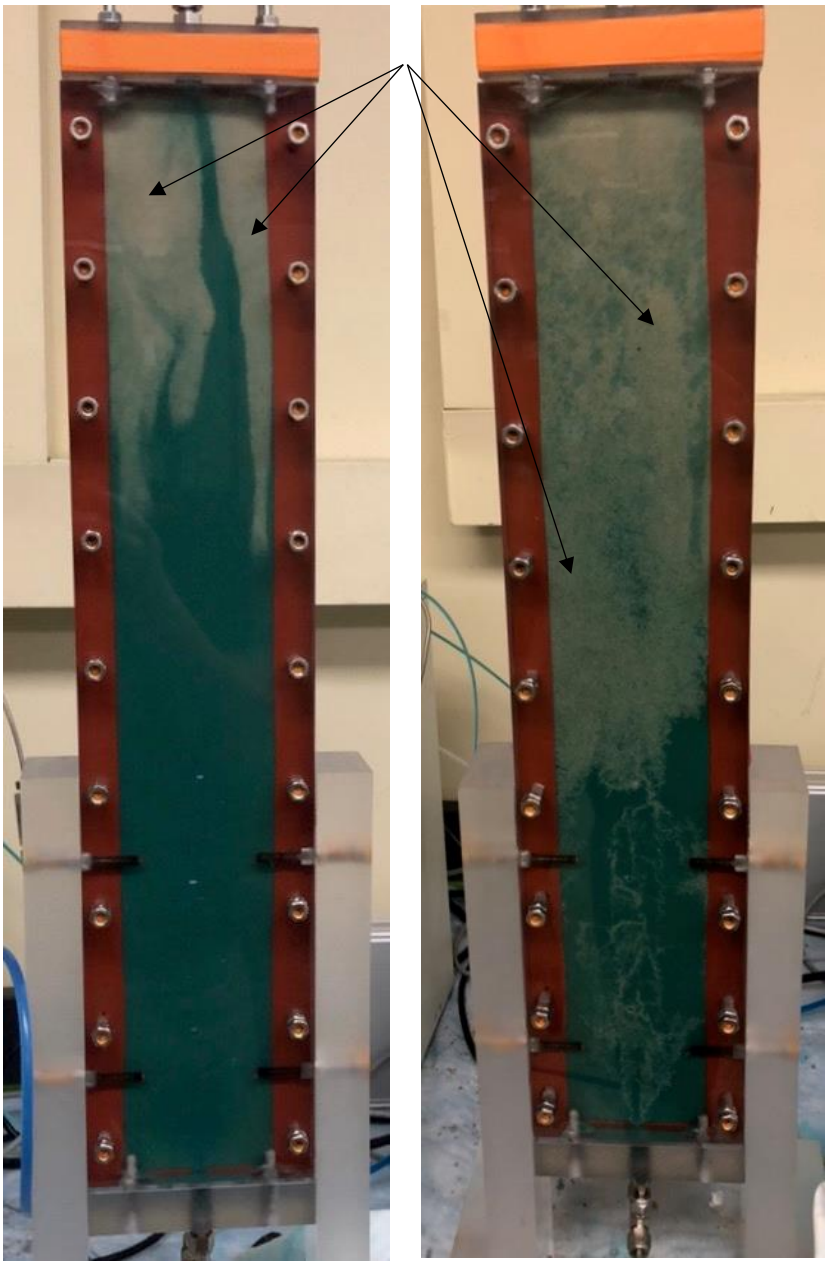

Figure 10 - Regions of the fracture remain unsaturated when fluid is injected at high flow rates, indicated by the lack of blue coloring.

Slower flow rates would seem to overcome the preferential void pathways and gave the appearance of saturating most of the packed proppant. However, settling effects were quite apparent after injection was stopped. Figure 11 shows the change in saturation after the pump is turned off.

Figure 11 - Low flow rates did not fully saturate the fracture either, revealed when the pump is turned off.

A combination of different stages of fast and slow injection over the course of a couple of hours appeared to fully saturate the cell even when turning off the pump; however, the void spaces remained to be a problem for test repeatability. Figure 12 reveals that either the void spaces, assembly design, or test procedure produced inconsistent test results. The unloading tests were performed with air injection rates of 5 ml/min to unload water. They were conducted solely for the purpose of observing the repeatability of the experiment. The different trials were performed with the same procedure, however the resulting data revealed to be inconsistent.

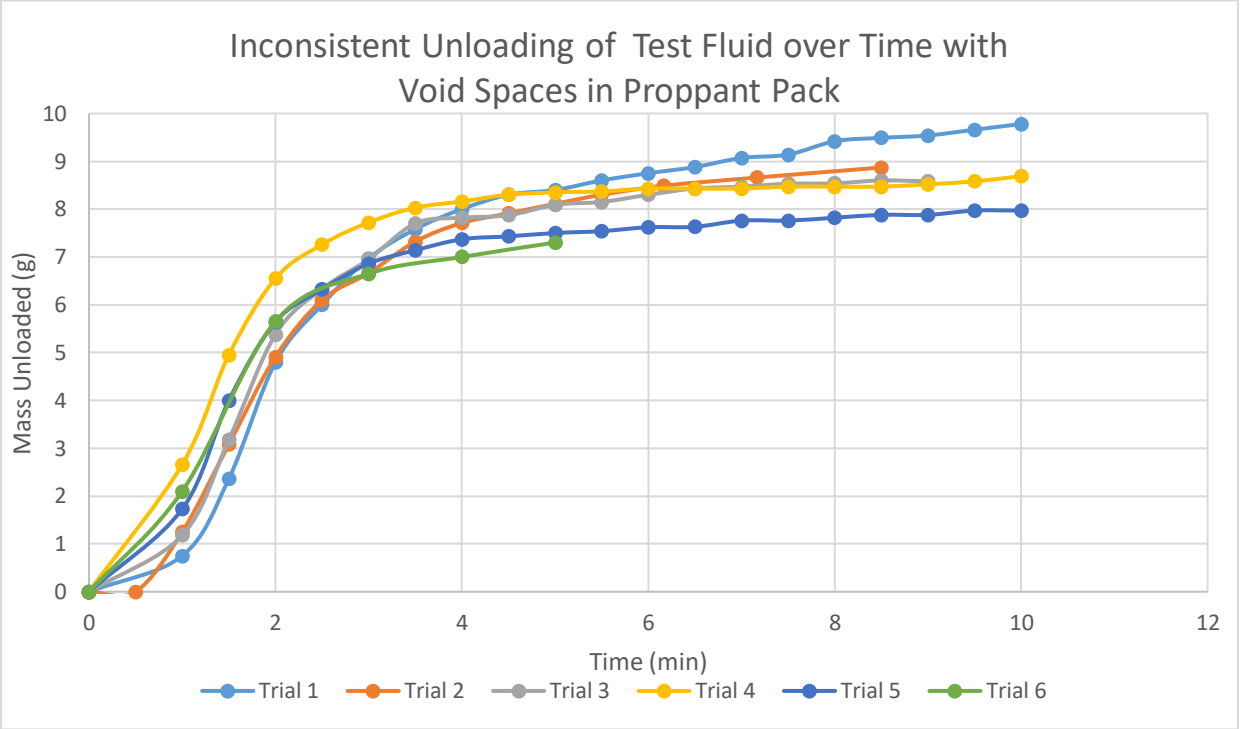

Figure 12 - Inconsistent results from initial testing.

After more trial and error, a process was found to successfully remove all void spaces. This process must be done right after a test run has been performed, or air has agitated the proppant pack. Testing fluid must be injected slowly, at rates around 2 mL/min. As the water level rises just above the void space, tapping on the plastic side of the fracture with a heavy instrument (handle of a screwdriver) will cause the air trapped in the void to migrate up to the water level, resulting

in a new void higher up the fracture. Constant attention from the operator is required to fully drift the void up to the top end of the proppant pack. The flow rate may be increased up to 10-15 mL/min as the void reaches higher. This process results in packing the proppant very well, and it reveals an open gap at the top between the proppant pack and the outlet of the fracture. Instead of adding more proppant, the gap was left to act as an obstacle to exaggerate possible benefits of foam transport. Real fractures in the field are imperfect, so this was an attempt to have some level of imperfection while maintaining the ability to obtain consistent results.

To further obtain homogeneous saturation throughout the cell, the sand proppant was replaced with reflective glass beads of larger diameters. US Mesh 12-30 glass beads were eventually used during the experiment. Because the beads contained a blue tint, test fluids were dyed red as contrast for visual purposes.

Plumbing changes to the inlet of the fracture allowed for a vacuum to be applied when preparing the cell. A valve at the top of the fracture can be utilized to either allow air to flow from the atmosphere, through the pack, and into the vacuum, or to completely close the system off. The vacuum removes all remaining fluid in the cell, allowing the experimenter to know exactly how much fluid is in the fracture after subsequently re-loading the cell. A vacuum pump was modified with a globe valve to restrict the delivered pressure, thereby not damaging the fracture cell itself. Testing of the seals were periodically performed to ensure the assembly's integrity.

During a test run, it was noticed that different phases of test fluid exit the fracture at different times. The initial-time unloading phase is strictly liquid. Even when unloaded in small amounts, a siphon effect occurs in the tubing. Because the mass unloaded was recorded over time, the siphon effect was detrimental to the experiment. Even though test fluid had left the fracture, it couldn't yet be recorded because instead of reaching the balance it was held up in the tubing. A

valve was added after the outlet of the fracture and connected to the tubing to control this flow. Opening the valve to the atmosphere breaks the siphon and allows liquid to flow freely and smoothly. However, this open valve affects the flow of foam during late-time of the experiment. Having it open, the foam preferentially flows out this valve and spills into the lab where it makes a mess and the mass is not measured. As a result, the testing procedure was modified to start the experiment with this anti-siphon valve open at the beginning of the experiment, but it is closed the moment that foam appears in the beginning of the tubing.

Some additional alterations to the assembly design were made. Because of the broken siphon, liquid unloading needed the tubing to be angled downward at all points along the tubing. Any coiling or curving upwards would cause pooling in the tube. Over the course of the experiments, the length of the tubing changed as various plumbing alterations were made. The length has a minimal effect on the time it takes for the fluid to exit the fracture and reach the balance. Because the differing tubing length would require the positions of nearby equipment to change, the shape of the tubing path would change as well. Although this doesn't necessarily affect the fluid flow, it was critical to check the tubing for any detrimental upward curving before starting a test run. Another assembly alteration made to encourage consistent fluid unloading across test runs was to lower the vertical distance the fluid needed to travel after exiting the fracture and before reaching the horizontal tubing. It was believed the gap created from the de-voiding process was enough of a vertical obstacle that the extra height from tubing was unnecessary. Also, the observer can visually see the gap as an obstacle, however they can't physically view fluid flow through the metal vertical tubing. The metal vertical distance was reduced to 1.75", from the outlet of the fracture to the "floor" of the horizontal tubing.

Also to encourage repeatability, a testing procedure was created and strictly followed. Comparing Figure 13 to Figure 12 shows experimental repeatability was definitely improved. By conducting proper preparation and implementation of the devised test procedure on the modified assembly, experimental results can be trusted and compared across different fluid types and injection rates. The different trials were performed under the same conditions and procedure (injection rate of 5 mL/min).

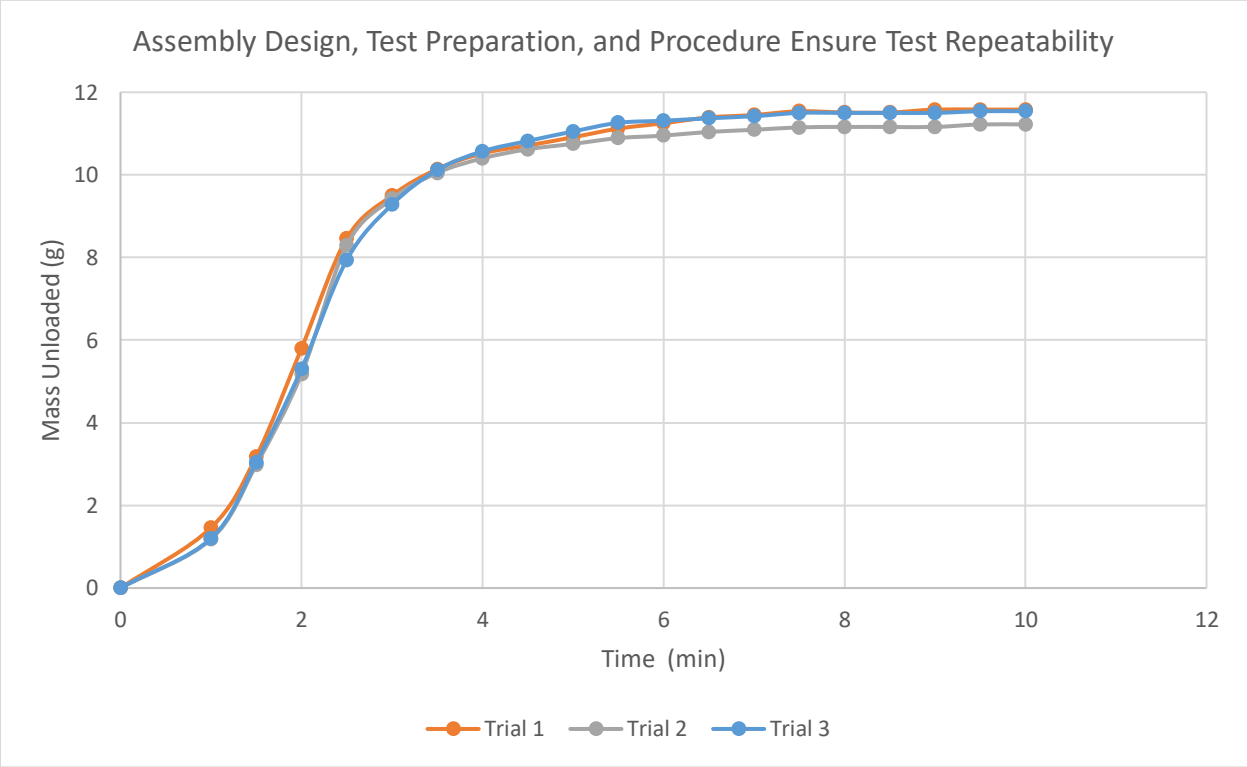

Figure 13 – Experimental repeatability drastically improved after modifications were made.

3.4 Experimental Procedure

The initial cases were performed to determine the capability of foam to transport fluid in general, so water was used as the initial liquid to investigate. Different amounts of sodium dodecyl sulfate were added to create solutions of 0% SDS, 0.05% SDS, 0.1% SDS. After being loaded in

the test cell, tests were run at different flow rates of injected air from the bottom: 5, 10, 15, and 20 mL/min.

The next objective was to determine the foam's capability to transport fluid if the solvent were to be hydraulic fracturing fluid. The experiment was then run with the exact same test parameters held constant, with frac fluid used instead of water. The results of these tests can be found in the Results section. The testing procedure for all cases are as follows:

Fluid Unloading Test Procedure

- A previously manufactured simulated fracture assembly is filled with US Mesh 12-30 reflective glass beads. The fracture width is approximately two proppant diameters. As the beads are added to the fracture, the assembly is agitated in order to somewhat pack the proppant together. Upon filling the cavity, the top plate is screwed into place to complete the propped fracture assembly.

- The fluid to be tested is then prepared with a mass balance and stirring rods (adding surfactant or creating frac fluid). The fluid is then injected into the bottom of the empty propped fracture cell at a low flow rate (0.5-2 mL/min) while tapping on the walls with the handle of a screwdriver to ensure quality packing. Flow rate may be increased up to 15 mL/min as the fluid level rises higher. Pumping occurs until the moment fluid appears at the cell outlet.

- In an effort to maintain consistent initial starting cell volumes, the cumulative volume entering the cell is recorded by the pump. If the cell is filled and the volume is less than 60 mL, then then the pumping process needs to be repeated. The fluid is allowed to drain out the bottom of the fracture, and a vacuum is utilized to evacuate anything remaining. The

cumulative volume counter is reset, and the fluid is injected again to fill the fracture with at least 60 mL of volume. After this requirement is satisfied, the cell is completely prepared.

- Data is recorded as a stopwatch is started, and air is injected at a specified flow rate into the bottom of the cell. The injected air migrates through the fracture and pushes fluid out the top of the cell. The unloaded fluid is recorded with a balance at specific time intervals.
- A valve connected to the tubing is used to combat a siphon effect. The experiment must start with the valve open so that liquid falls freely. The moment that foam appears in the tubing, the valve must be shut to ensure the foam travels through the entirety of the tube.
- The experiment is stopped when the test fluid ceases to unload from the fracture.
- The masses recorded during the experiment are converted to volume from their respective fluid density and can then be interpreted.

3.5 Definitions

$$Volumetric\ Sweep\ Efficiency = \frac{Volume\ of\ Fluid\ displaced}{Volume\ of\ Reservoir}$$

$$Volume\ Fraction\ Unloaded = \frac{Volume\ of\ fluid\ unloaded\ from\ the\ cell}{Initial\ volume\ of\ fluid\ in\ cell}$$

$$Unloading\ Limit = Maximum\ possible\ total\ volume\ fraction\ to\ be\ unloaded\ at\ t = \infty$$

$$Critical\ Volume\ Fraction = The\ value\ of\ volume\ fraction\ at\ which\ unloading\ rate\ ceases\ to\ be\ linear\ and\ the\ mechanism\ of\ transport\ changes$$

$$Displacement\ Unloading\ Rate = \left.\frac{dV_{unloaded}}{dt}\right|_{volume\ fraction < critical\ volume\ fraction}$$

$$V_{unloaded} = Volume\ of\ fluid\ unloaded$$

Chapter 4: Fluid Unloading Test Results

4.1 Overview of Cases

Initial testing began with water and different concentrations of SDS. Hydraulic fracturing fluid and different concentrations of SDS followed afterwards. See Table 2 for the description of each case to be tested and the density used to convert mass unloaded to fluid unloaded. Densities were experimentally found. Each case was performed with four different air injection rates: 5, 10, 15, and 20 mL/min. One easily recognizes the role that surfactant plays in altering the transport of fluid through porous media, both from visually seeing the effects through the plastic plates of the assembly and from analyzing the data of volume unloaded over time.

Table 2 - Case Numbers and Densities of Test Fluids

Case Number	Fluid Type Involved	Density of Fluid (g/cm^3)
1	Only Water	0.998
2	0.05% SDS in Water	1.005
3	0.1% SDS in Water	1.007
4	Only Broken Hydraulic Frac Fluid	1.011
5	0.05% SDS in Broken Frac Fluid	1.015
6	0.1% in Broken Frac Fluid	1.018

4.2 Case 1

When the simulated fracture is prepared with absolutely no surfactant, air migrates upwards with viscous fingering throughout the entirety of the fracture from the start of injection. Reaching the gap at the top, bubbles are released and escape through the outlet. Some fluid is moved by the air and manages to unload. At all flow rates tested, this purely water saturated fracture ceased to unload liquid after approximately 15 minutes. Viscous fingering persists throughout the entirety of the injection time, however there does appear to be two different modes of transport during the period of unloading: displacement and splashing. Figure 14 depicts four test runs with different air injection rates. It reveals the different modes of transport, as the displacement occurs in the early time of the experiment and splashing occurs during the late time.

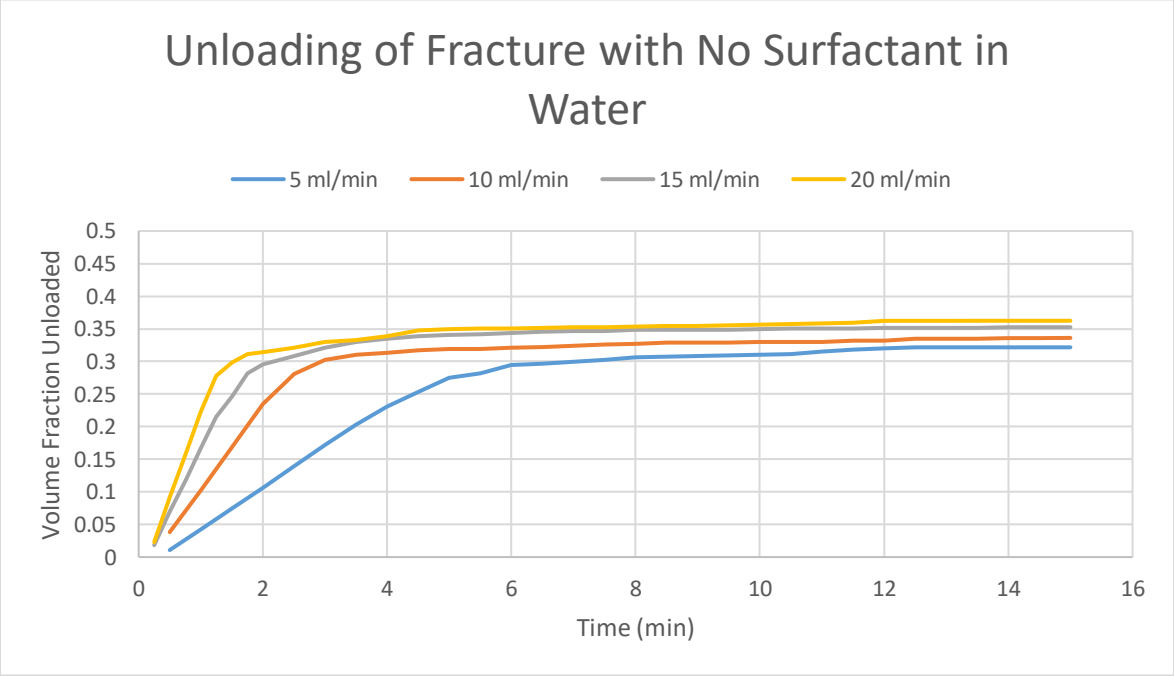

Figure 14 – Results of Case 1 involving water and no surfactant.

4.2.1 Displacement Transport

Transport through displacement occurs because of the incompressibility of water. During the early time, the majority of the fracture is saturated with water; because water is incompressible, it is moved by the addition of gas to exit the system. Although visually looking through the walls the unloading looks sporadic due to Saffman-Taylor fingering, in reality the unloading rate is constant over time as shown by the numerical data. Saffman-Taylor fingering is explain in Section 2.2. While constant, the magnitude of the unloading rate does appear to be dependent on the rate the air is injected. Figure 15 depicts the experimental data during the early time with linear regression applied. It is easy to conclude the two fluid rates have a directly proportional relationship and the experimental data to be accurate due to the strong R^2 values.

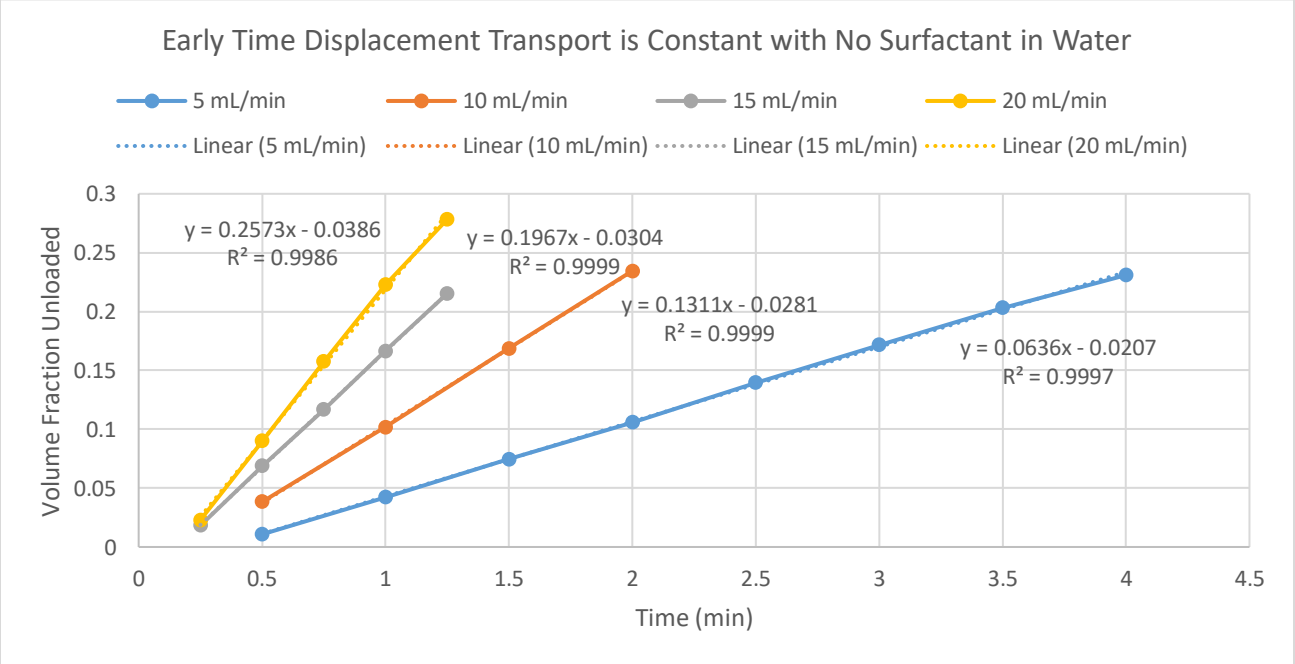

Figure 15 – This graph is the early time data of Figure 14, showing the linearity of displacement transport at all flow rates.

Table 3 - Early Time Volumetric Flow Rates of Air and Liquid

Air Injection Rate (mL/min)	Liquid Unloading Rate (mL/min)
5	4.4004
10	9.0735
15	12.911
20	17.809

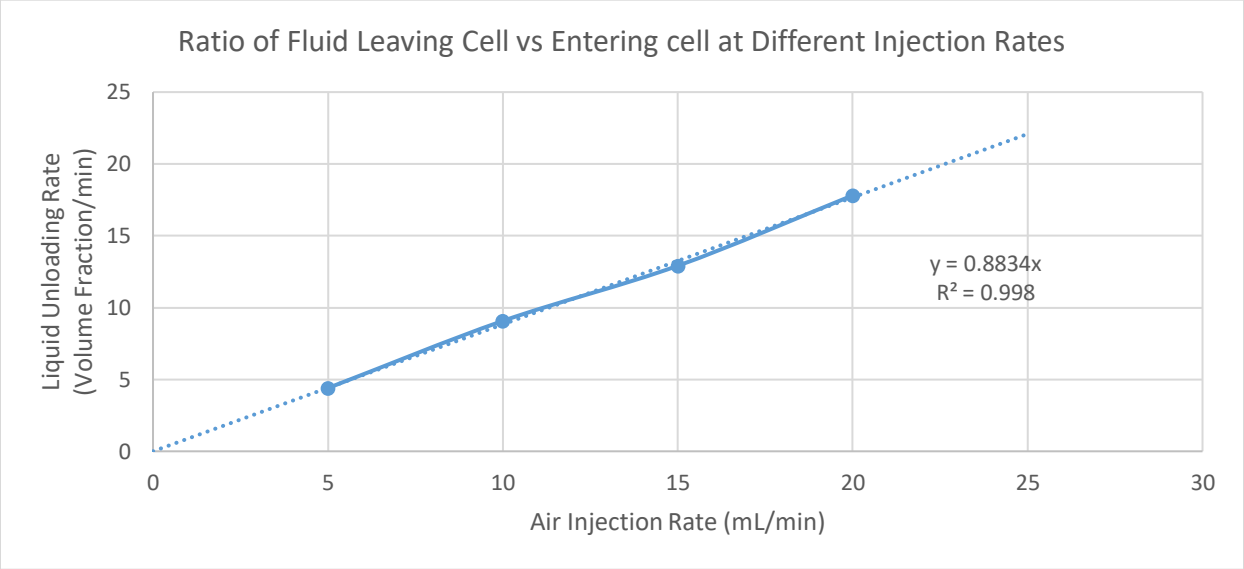

Figure 16 – Plotting two volumetric flow rates against each other reveal the ratio is not unity, indicating some fluid compression taking place.

The slopes of the lines in Figure 15 allow for the creation of Table 3 and Figure 16, however they are in terms of volumetric flow rates rather than volume fraction rates. These units are more relatable, and allow the observer to notice that the volumetric flow rate of air entering the cell is greater than the volumetric flow rate of liquid leaving the cell. The difference must be due to the compression of air once inside the fracture. Figure 16 is actually the plot of the table, revealing the compression to be constant for the different flow rates during times of displacement transport. The liquid to air ratio is 0.8834 after linear regression is constrained to pass through the origin.

4.2.2 Liquid Removal after Breakthrough of Gas

Regardless of the air injection rate, unloading remains constant until a critical volume fraction of liquid has been unloaded. In this case, the critical volume fraction is approximately 0.28. After this point, the ability for air to displace water significantly decreases. At the top of the fracture cell, one can observe that the fracture contains enough air that there is now a disconnection between liquid and the fracture outlet. The displacement that occurs during late time is quite different from the early time behavior. Instead of escaping through the outlet, the liquid's position in the cell is simply moved around within the fracture. The method of transport of unloading during this time takes the form of gas bubbling through the proppant pack. Although no longer being pushed upward, the water is agitated by the introduction of gas. This occurs because the air continuously changes its preferential pathways created by the Saffman-Taylor fingering. Also because air is now able to travel to the outlet, bubbles are crossing across the built-up fluid in the gap with no proppant (see Figure 17).

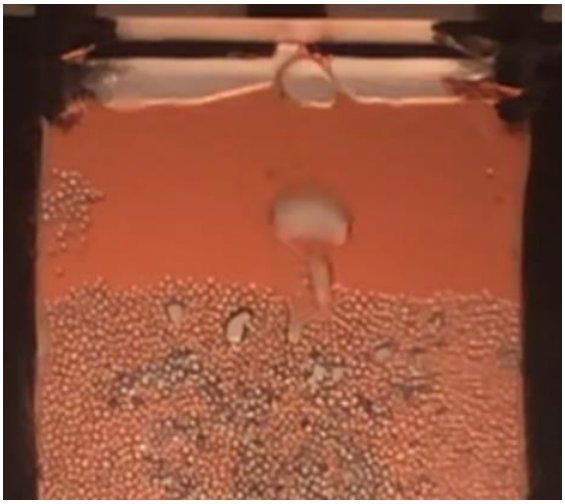

Figure 17 - After the critical volume fraction of liquid is displaced, the upper region of the fracture develops a gap. The transport mechanism transitions from displacement to gas bubbling through the proppant pack when there is no surfactant.

The agitation and the bubbles combine to toss the built-up liquid around the gap, resulting in the stochastic ejection of water. The rate of unloading decays nonlinearly as the mechanism of transport transitions to this sporadic removal of liquid, where it levels off to a very low rate. This continues for a long time until the gap between the liquid and outlet becomes too great. It is at this point that the simulated proppant pack has reached its unloading limit. The addition of air into the system no longer reduces the volume of fluid. Referring again to Figure 14, the total volume fraction unloaded after reaching the unloading limit depends on air injection rate. Increasing the injection rate causes an increase in total volume fraction unloaded. Comparing the slowest and fastest injection rates in this particular case, air injection at 5 mL/min resulted in a total volume fraction unloaded of 0.3216, while an injection at 20 mL/min resulted in a total volume fraction unloaded of 0.3624. Although these final values are quite similar with only a 4.08% difference of fracture volume, it is worth noticing the time to reach these values. The slower injection rate reached its final value after taking 15 minutes to level off. The faster injection rate reached this same value of 0.3216 after 2.5 minutes. In other words, not only does a faster air injection rate result in more fluid unloaded, but it does so in significantly less time. In this situation, by increasing the rate air is injected into the system by a factor of 4, the time it took the majority of total fluid to be unloaded decreased by a factor of 6. Remembering time plays a huge role in the creation of real fractures in the field due to proppant distributions from proppant settling, this is an important observation. This suggests that initial gas production could have a role on shaping the distribution of proppant during fracture creation and propagation as it may affect the volume of recovered hydraulic fracturing fluid and thus time until fracture closure.

4.3 Case 2

Satisfied with the previous results as a Base Case scenario, test runs were then performed with the addition of the sodium dodecyl sulfate surfactant to the water at a concentration of 0.05%. In addition to the caution mentioned in the methods section, preparation in loading these fracture simulators required more care. If foam were to form during the loading process, then the cell would be considered improperly prepared. The experimental results from tests performed on properly prepared fractures with 0.05% SDS in water can be seen in Figure 18. There are two stark differences that are immediately apparent between these results and from Case 1: the unloading limits and the time to reach the unloading limits.

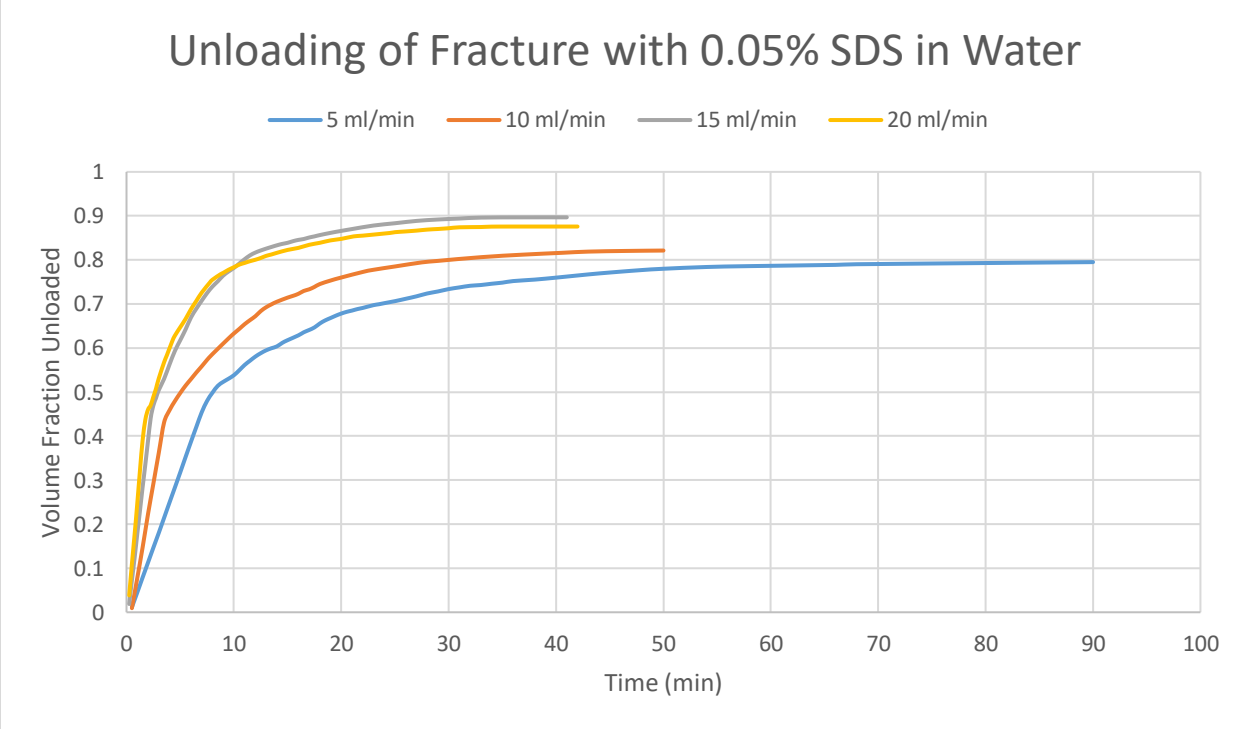

Figure 18 - Results of Case 2 involving water and a surfactant concentration of 0.05%.

In Case 2, appreciably more fluid is removed from the fracture. Interesting to note, the unloading limit increased a proportional amount across all air injection rates with the addition of surfactant. These unloading limits increased by a factor of 2.471 ± 0.064. In other words, the addition of surfactant to a concentration of 0.05% leads to almost 2.5 times the amount of fluid removed in this particular experimental setup for each injection rate, with the best performance resulting in almost 90% fluid unloaded from the fastest injections. The unloading curves at injection rates of 15 and 20 mL/min appear almost identical, suggesting that there is some limiting phenomenon. It is likely that there exists some critical flow rate of gas, beyond which an increase in flow rate does not increase unloading performance.

Unloading also occurs over a much greater period of time with the surfactant added. For the slowest injection rate, complete unloading took six times as long with SDS, while the other injection rates unloaded for approximately four times longer. While maximizing effective proppant distribution before aperture closure would require quick unloading, the times involved in this experiment are still much shorter than the 48 hours of time it takes for fluid to drain into the formation, indicating Case 2's increase in time is not a concern.

The unloading time in this case is much greater than Case 1 because the surfactant alters the modes of transport. The early time transport still occurs through displacement, however the air no longer takes the form of viscous fingers. Rather, the air generates a foam that uniformly moves up the entire fracture as if it were a piston pushing the fluid out, suggesting a mobility ratio less than 1. The unloading rate during this time of displacement is slightly higher than in Case 1, indicating that the gas does not need to compress as much when it enters the fracture. Visually, it is easy to see this as the foam is able to sweep a much greater volume of fluid up the column with the piston-like movement. The greater sweep also allows for displacement transport to reach a

higher critical volume fraction, before changing to the second mode of transport. The critical volume fraction in this case occurred around 0.44, however the slowest injection rate reached a slightly higher value of 0.48. See Table 4 for unloading rates during displacement transport for all cases, as well as Figure 25 and Figure 26 for plots containing unloading data on the same timescales.

4.3.1 Foam Bridging

When the air reaches the proppant gap at the top of the fracture, it is in the form of foam. Some splashing does occur as the bubbles float to the outlet, similar to Case 1, and the unloading rate nonlinearly decreases. However, this only occurs for a short period of time. Once an air gap forms between outlet and built-up liquid, the late time mechanism of transport takes the form of foam bridging. Bubbles rise to the top of the fluid column and remain stable. New bubbles that reach the top of the fluid column push the earlier bubbles and raise them into the gap between liquid and outlet, creating a bridge. The continuous generation of more bubbles allows the liquid to use this bridge to exit the fracture as seen in Figure 19.

Figure 19 - Through foam bridging, fluid is still able to unload from the fracture even though there is a large gap separating the outlet from the fluid level. The pictures from left to right depict the activity of the bridging over time. The bridge will exist if bubble generation exceeds escape.

Foam bridging is a far superior transport mechanism than splashing, and is the major reason unloading limits are incredibly high compared to the results lacking surfactant. The water-SDS foam remains stable for quite a bit of time, allowing unloading rates to plateau off before bubbles collapse.

4.4 Case 3

The third case involves a higher concentration of 0.1% SDS in water. The results of these experiments reveal further improvement in our ability to unload liquids. Depending on the air injection rate, unloading limits range from 0.925 to 0.955 as seen in Figure 20. Displacement transport unloading rates are similar to Case 1, as seen again in Table 4.

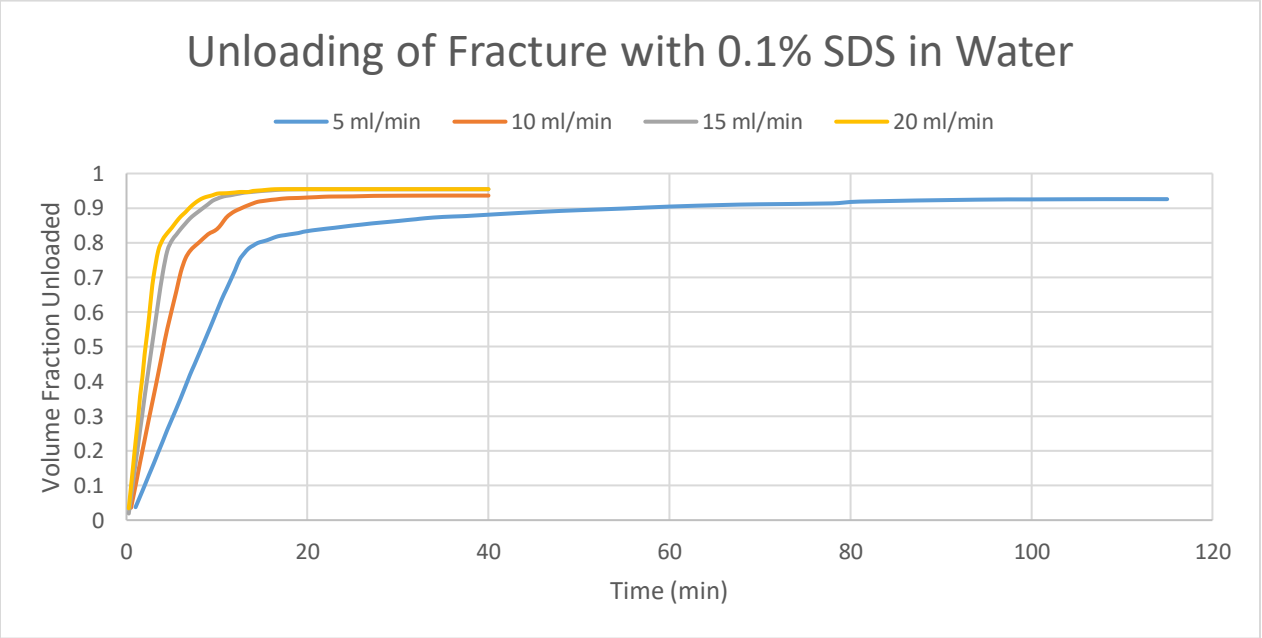

Figure 20 - Results for Case 3 involving water and a surfactant concentration of 0.1%.

The critical volume fraction is also much higher at 0.78, further signifying the critical role SDS plays in improving sweep efficiency from the proppant pack. This means displacement transport is able to unload most of the fluid, placing less demand on foam bridging transport. Because foam bridging is the slower transport mechanism, the time to reach the unloading limit should be much shorter with Case 3 than in Case 2. This is confirmed for all of the injection rates, except for the slowest one. For the injection rate of 5 ml/min, the time to complete unloading is approximately the same at 90 minutes. The other injection rates complete in about 22 minutes.

4.5 Case 4

The following cases investigate if surfactant also increases unloading if the fluid involved is broken hydraulic fracturing fluid. This case is the frac fluid base case, as it has no surfactant added. It was expected to perform similarly to the water base case. For the most part, it does for the two higher injection rates as Figure 21. For the two slower rates, the unloading limits are less than that of water, and the critical volume fractions occur at different values. As there is no surfactant added, the two transport mechanisms appear to be displacement and splashing.

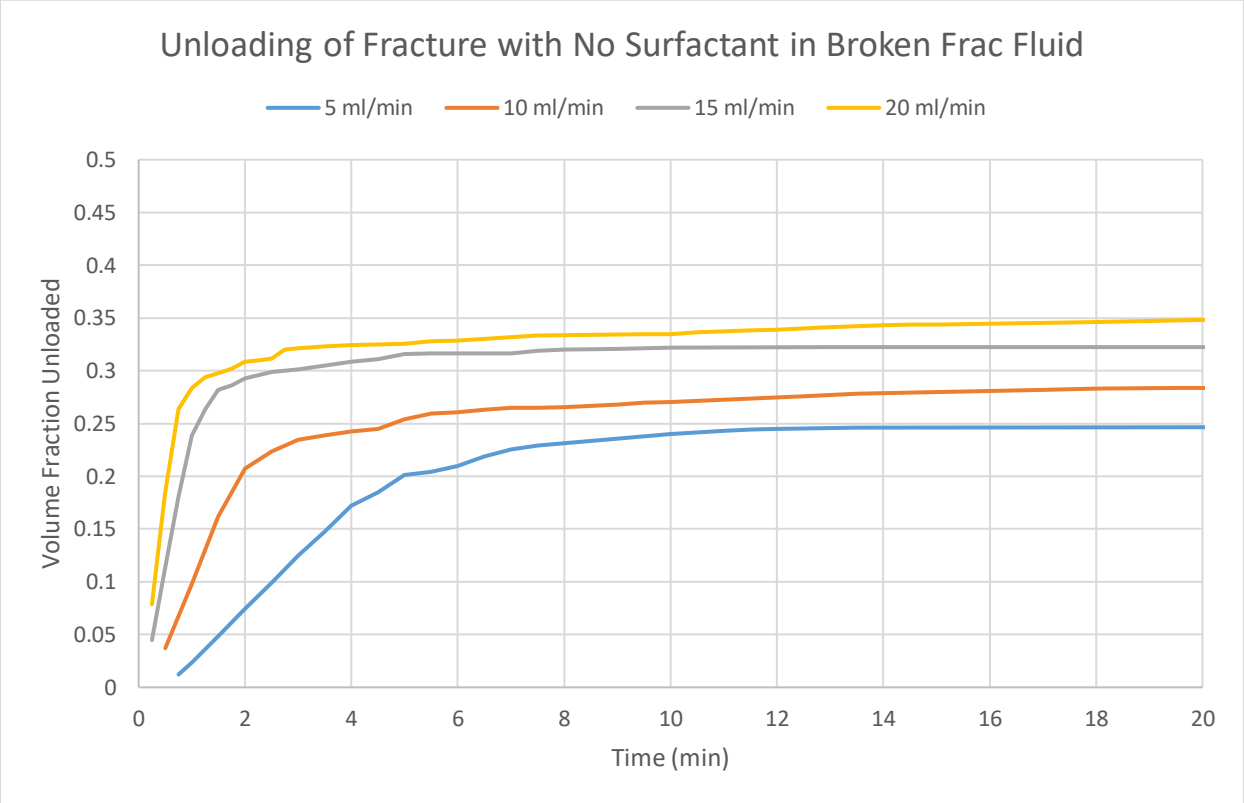

Figure 21 - Results of Case 4 involving broken hydraulic fracture fluid and no surfactant.

4.6 Case 5

With the addition of SDS to the broken frac fluid to a concentration of 0.05%, the unloading ability increases significantly. Similar to Case 4, the higher flow rates approach the same level of success as for the water case, while the lower flow rates fail to maximize displacement transport. The lower critical volume fractions require a higher dependence on foam bridging to unload, resulting in much longer times to complete unloading and also possibly reducing unloading limits as the foam bridge has more time to destabilize. Sweep efficiency within the proppant is also likely to be lower. Air injection at 5 ml/min continued for 180 minutes before unloading finally tapered. It can be noted this 180 minutes is still significantly less than the fluid leakoff time scale of 48 hours to a few days.

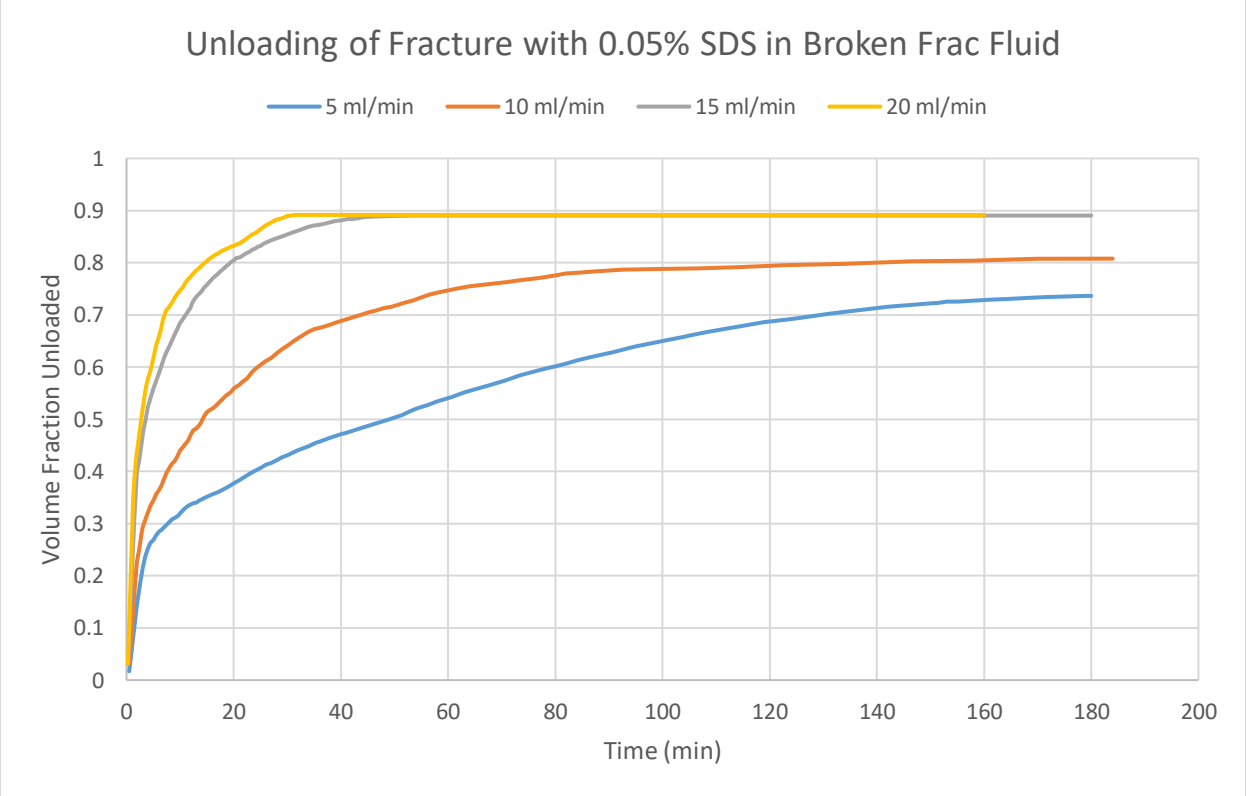

Figure 22 - Results of Case 5 involving broken hydraulic fracture fluid and a surfactant concentration of 0.05%.

4.7 Case 6

Once again, a high concentration of surfactant improves its unloading ability in the frac fluid. Unlike in Case 4 and Case 5, displacement transport is maximized across all injection rates. Like the cases with water, the critical volume fraction at each flow rate is about the same, indicating hydraulic fracturing fluid can realize high sweep efficiency throughout the proppant if there is enough surfactant in solution. The critical volume fraction here was 0.74, which is slightly less than in water, and much greater than other results with frac fluid.

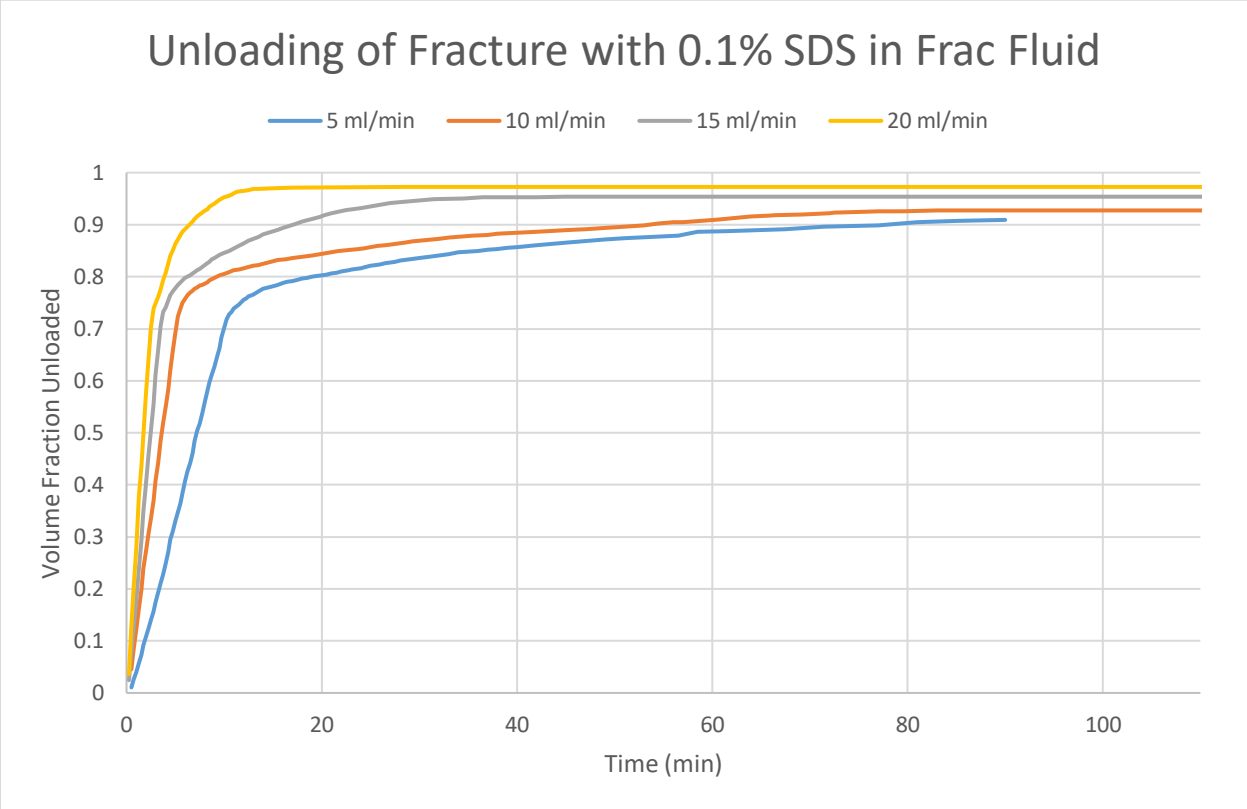

Figure 23 - Results of Case 6 involving broken hydraulic fracture fluid and a surfactant concentration of 0.1%.

By increasing the amount of surfactant, the unloading limits improve dramatically, especially for lower injection rates. The unloading limits even obtain results similar to and sometimes even surpassing water with values between 0.91 and 0.97.

The times to reach unloading limits follow the previous patterns. Because the foam sweeps most of the fluid and minimizes foam bridging, the time to complete unloading is shorter. Depending on the injection rate, time is reduced by a factor of 2 to 2.56 when SDS concentration is doubled.

4.8 Case Comparison

In Cases 1-3 and Case 6, the critical volume fraction occurred at the same value across all flow rates. In Cases 4 and 5, displacement transport terminated at smaller fractions for the slower flow rates. There appears to be a correlation with this phenomenon and the ratio of liquid unloading rate to air injection rate during displacement transport. In Cases 1-3 and Case 6, the rate that fluid unloads increases proportionally as the air injection rate increases. However, in Cases 4 and 5 the proportionality between the two is less strong. This suggests that in these particular cases the sweep efficiency is different thus resulting in different kick-off points to late-time transport. Figure 24 displays the relationships between liquid unloading rate and injection during the early-time transport of displacement. It is important to note that the surfactant does not appear to affect the rate of unloading during this time.

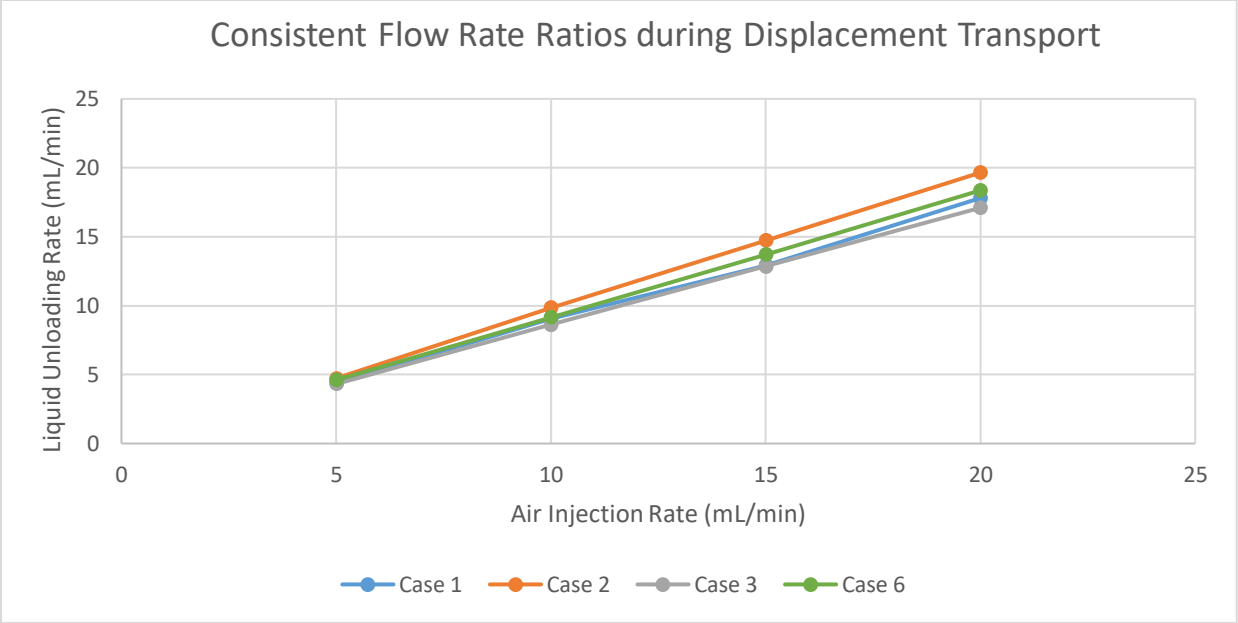

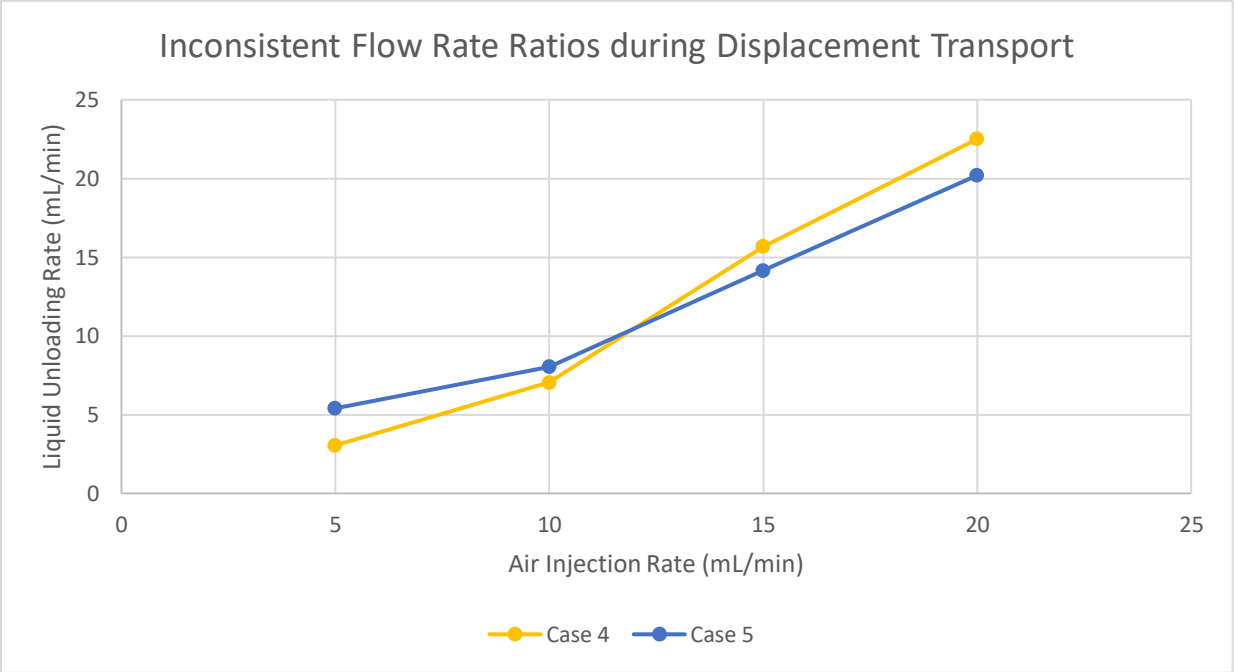

Figure 24 - Volumetric Flow Rate Ratios of Liquid to Air for all Cases

Table 4 - All Early Time Liquid Unloading Rates and Their Ratios to Air Injection

	Liquid Unloading Rates During Displacement Transport (mL/min)					
Air Injection Rate -> (mL/min)	5	10	15	20	Average Flowrate Ratio of Liquid to Air	R^2 Value
Case 1	4.4004	9.0735	12.911	17.809	0.8813	0.998
Case 2	4.731098176	9.852390016	14.72284307	19.65600582	0.9929	0.9999
Case 3	4.3190784	8.6243136	12.8603328	17.1032736	0.8518	1
Case 4	3.05118	7.05446	15.678	22.50255	1.3396	0.9823
Case 5	5.40594	8.038186	14.167768	20.19791	1.0101	0.973
Case 6	4.610315	9.149925	13.717403	18.36297	0.9165	1

Table 4 also shows the numerical values of these rates, as well as the average liquid-to-air flow rate ratio obtained by the slope of linear regression. The R^2 values are another signifier in which cases behaved similar at different conditions. There doesn't appear to be a clear trend with the value of the liquid to air flow rate ratio, although it makes sense for the values to be less than one as air is much more compressible than liquid.

Figure 25 and Figure 26 show all the unloading data plotted on graphs that keep the gas injection rate constant, so one can compare results over the same timescale. This further reinforces our conclusions that the surfactant does not play a role in altering the rate of unloading during displacement transport, but rather it increases the critical volume fraction at which displacement transitions to late time transport. This can be seen as the curves stack on top of each other until reaching their critical volume fraction.

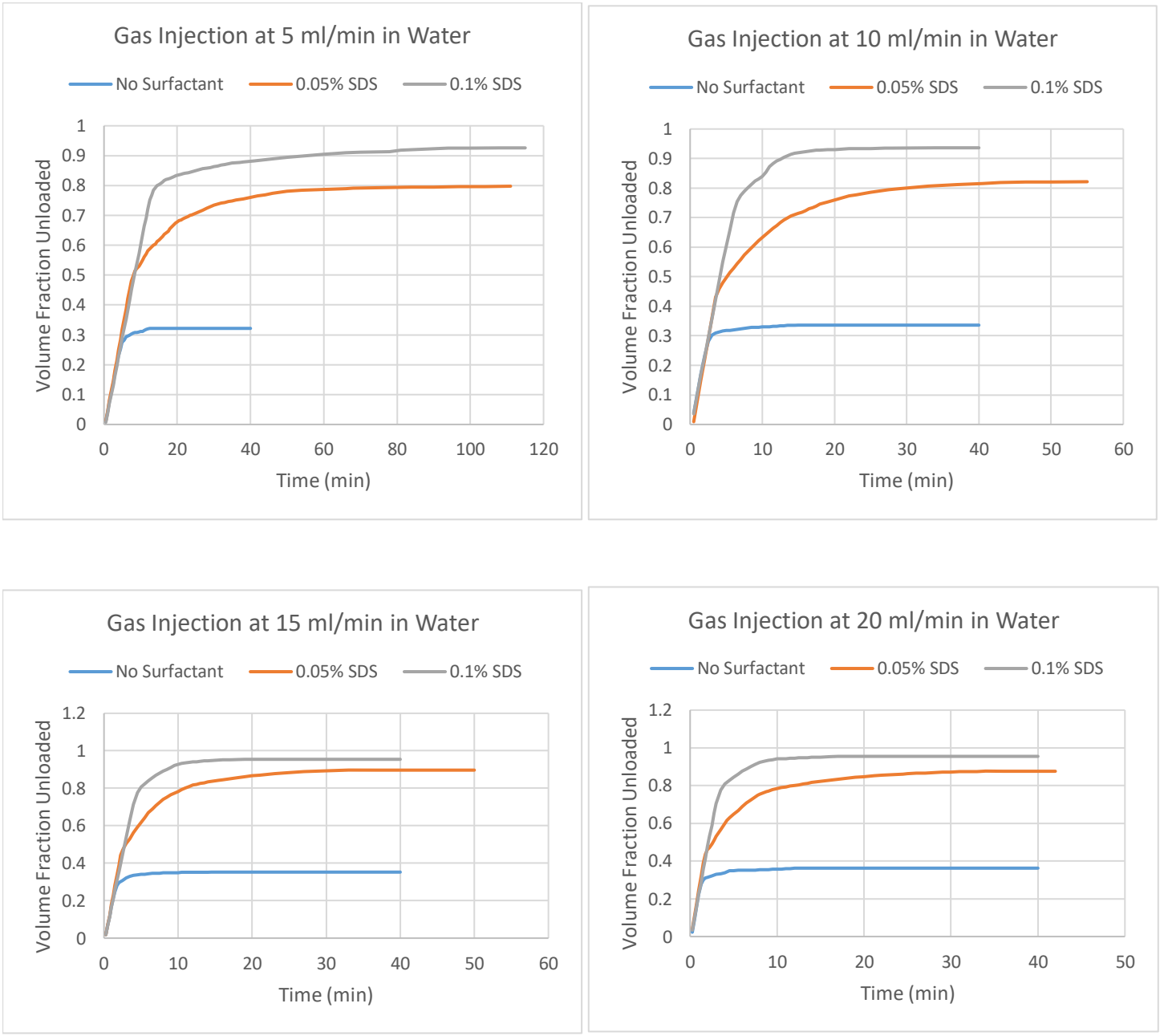

Figure 25 - Unloading results performed with water in the fracture (Cases 1, 2, and 3) are plotted on the same graphs, keeping air injection rates constant. This allows for comparison on the same timescale.

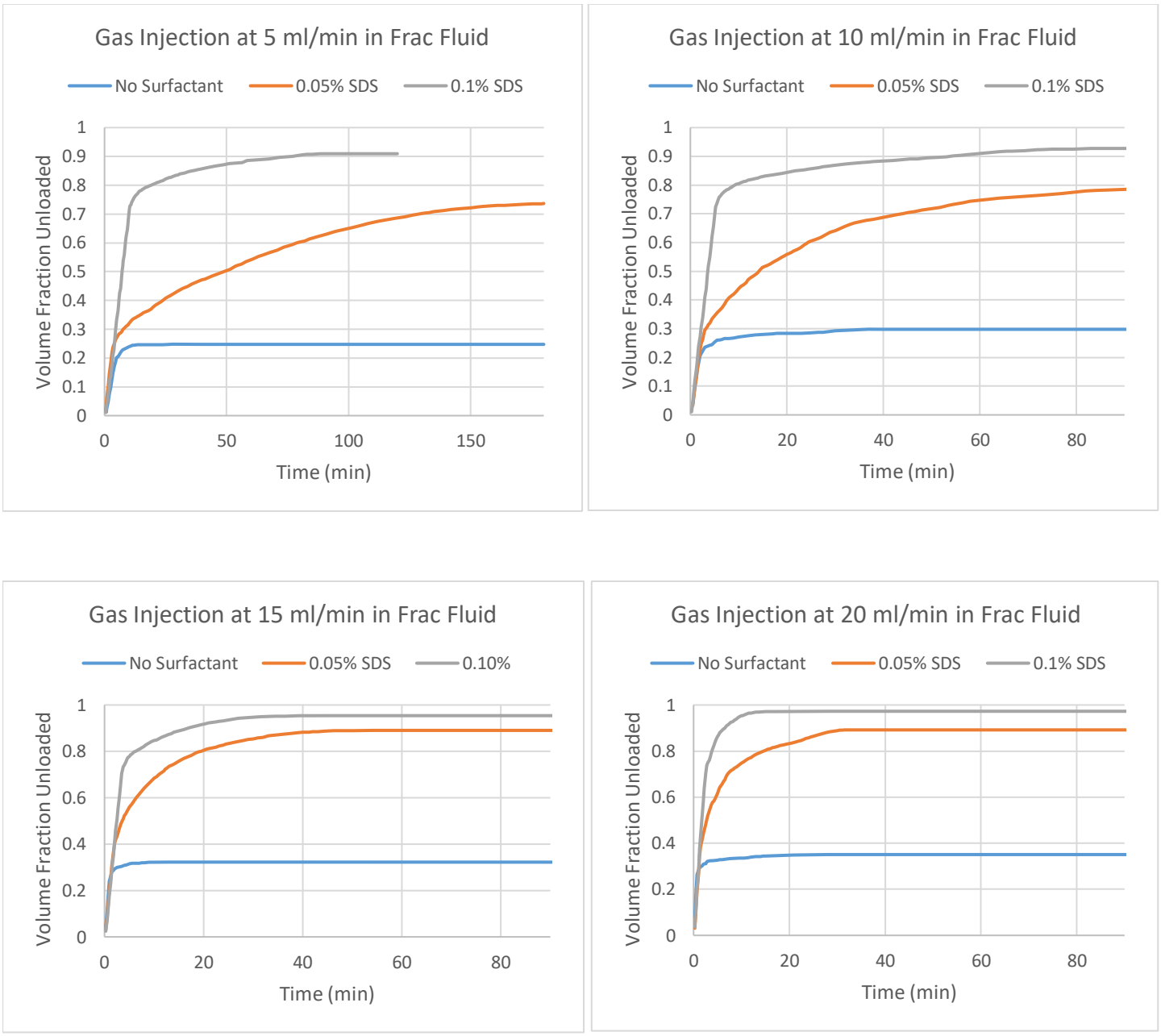

Figure 26 - Unloading results performed with broken hydraulic fracturing fluid in the fracture (Cases 4, 5, and 6) are plotted on the same graphs, keeping air injection rates constant.

At this point it is clear that the addition of surfactant has a very significant effect on liquid removal from the fracture. Figure 27 reveals the role concentration of surfactant plays on both the unloading limit and the time to reach the unloading limit. While both are influenced by the concentration, the time is affected more. Doubling the concentration results in increases of 10-20% of total fraction volume unloaded, however the time can be halved at low injections rates. This suggests that in fractures with high gas production rates, lower concentrations of surfactant would be sufficient for fluid unloading, however wells with lower production rates would benefit by using a higher concentrations of surfactant.

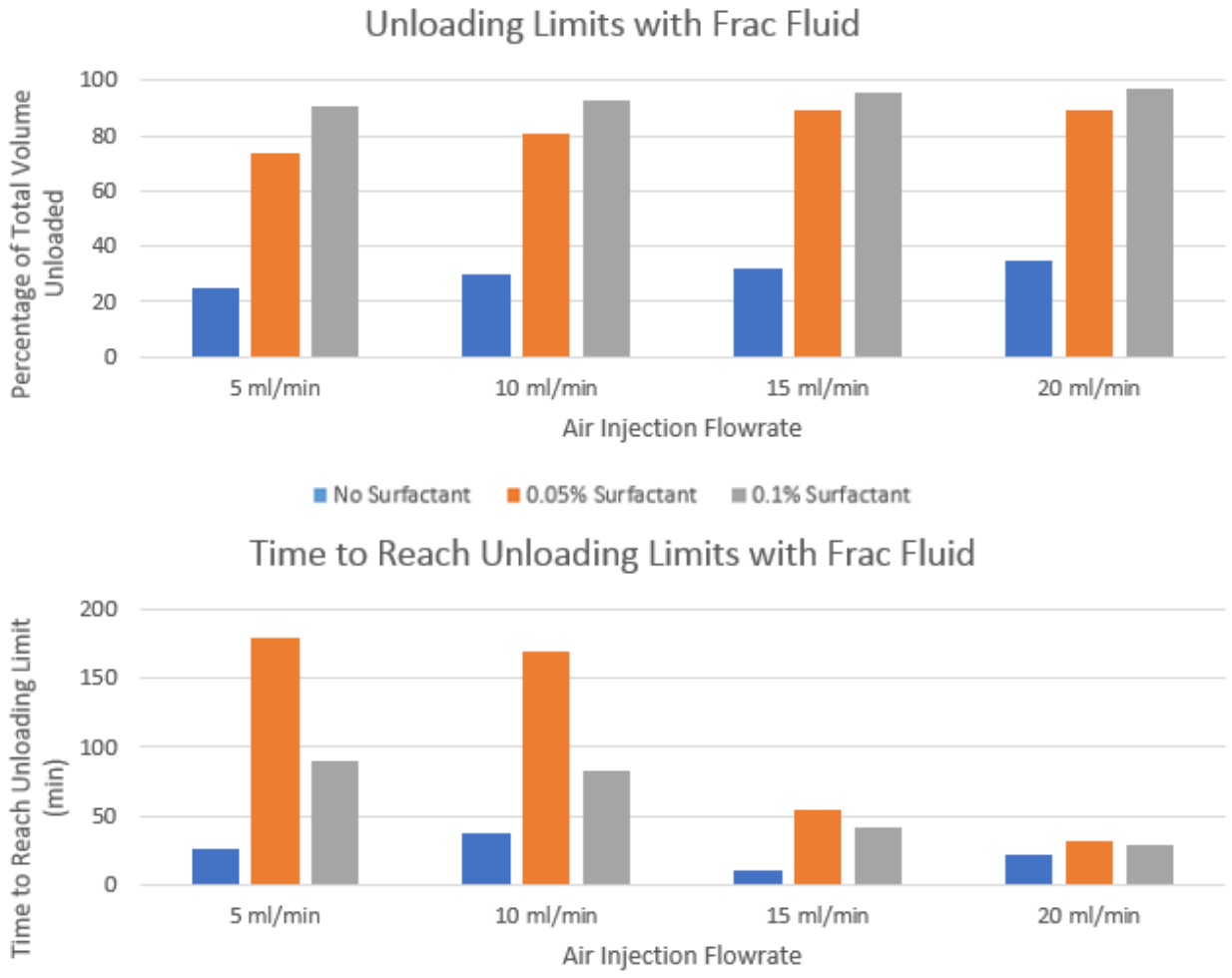

Figure 27 - Endpoint comparison of all test results.

Chapter 5: Oil-Foam Interaction

Although the liquid unloading experiments were not performed under reservoir conditions, it was desired to observe the effects of oil on the results. Oil is known to destabilize foam so it is important to know if the application of surfactants and foam was feasible in oil or gas condensate reservoirs.

5.1 Observing Foam Stability

The simplest method of observing how oil affects foam is by comparing the foam stability of prepared fluids with and without oil added. To do this, a 0.1% SDS solution in hydraulic fracturing fluid was prepared in a container. Another container was prepared with an equal volume of fluid, while 80% of the liquid was the frac fluid solution with surfactant and the other 20% was the mineral oil EXXSOL^{TM} D110. The two containers were sealed and shaken at the same time for approximately 20 seconds. Both fluids produced foam, however of very different qualities. The containers were then allowed to rest without stimulation, and the stability of both foams were observed as time progressed as depicted in Figure 28.

The mixture lacking oil produced a much larger volume of foam with a column of bubbles that filled almost the entire container. The mixture including oil generated a smaller amount of foam of two different types. Bubbles in the oil column formed minutely sized bubbles, while an equal volume of larger bubbles floated on top. The bubbles in the oil column were small because oil negatively affects foam stability and forces bubble size to be smaller. It is probable that the foam column on top is formed from oil-free solvent and surfactant as the bubbles are larger. As

bubble stability is also affected by volume fraction of liquid, the columns of bubbles in both mixtures degenerated as time passed and free drainage occurred. The column in the container containing oil dwindled at a higher rate because of its contact with the oil fluid level.

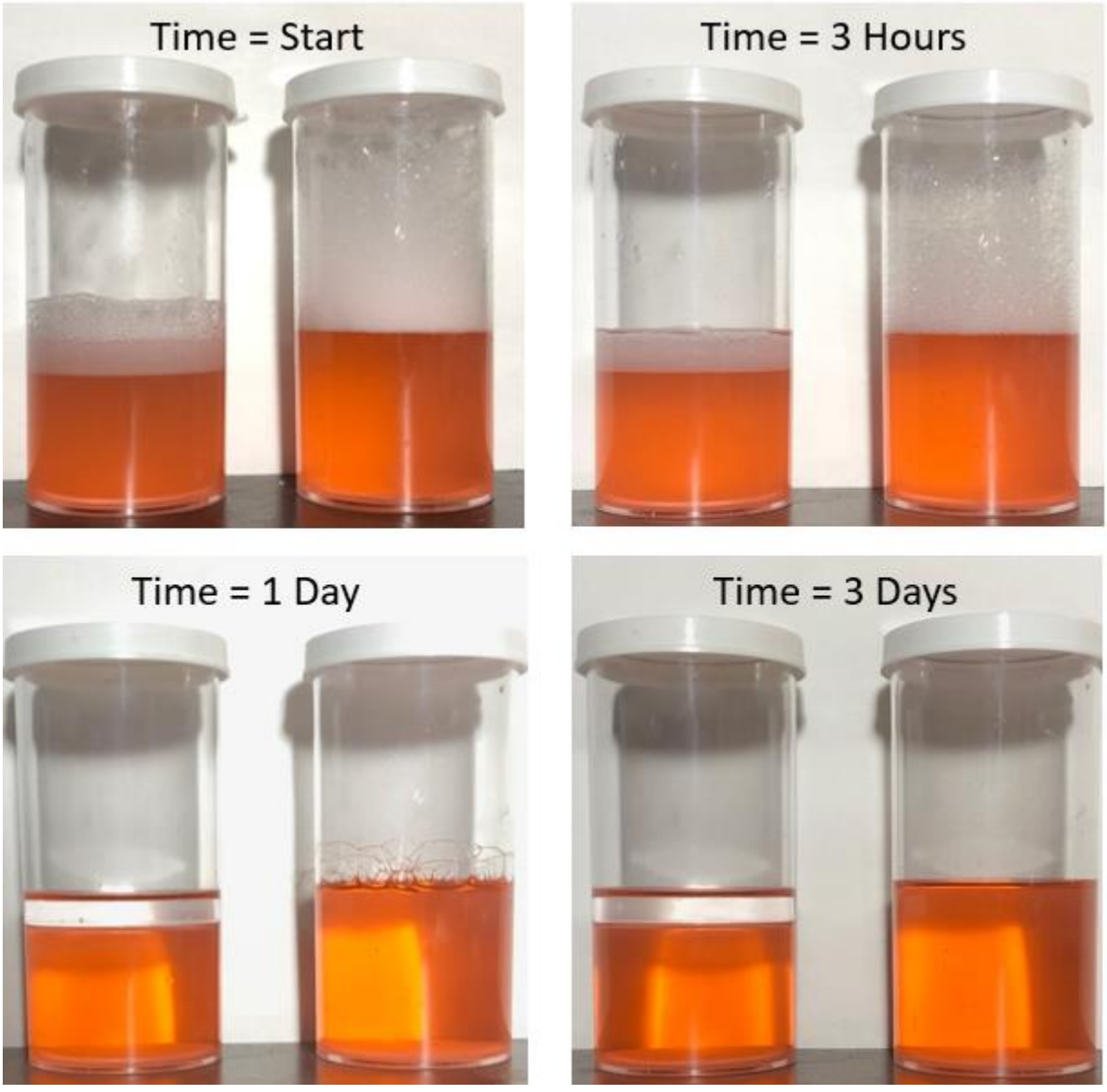

Figure 28 - A comparison of foam stability over time revealed that oil destabilizes micelles formed from SDS at standard conditions. The 20% mineral oil mixture is on the left, while the frac fluid with no oil is on the right.

The bubble column for the mixture without oil persisted for three days, but the bubble column in the mixture containing oil disappeared after three hours. The minutely sized bubbles suspended in the oil outlasted the oil-free column previously existing above it because of its wet nature (dry foam is much less stable than wet foam), however it did eventually degrade after a day passed.

5.2 Unloading Oil from Fracture Results

Oil obviously has a negative impact on both foam generation and stability with this particular surfactant at atmospheric conditions, however it is desired to observe the importance of this effect in the fracture cell under the same experimental conditions as previously tested. For these experiments, oil was added to the fracture already prepared with 0.1% SDS solution in broken hydraulic fracturing fluid to obtain an oil saturation of approximately 30%. Four test runs were then performed at different air injection rates and the results are shown in Figure 29.

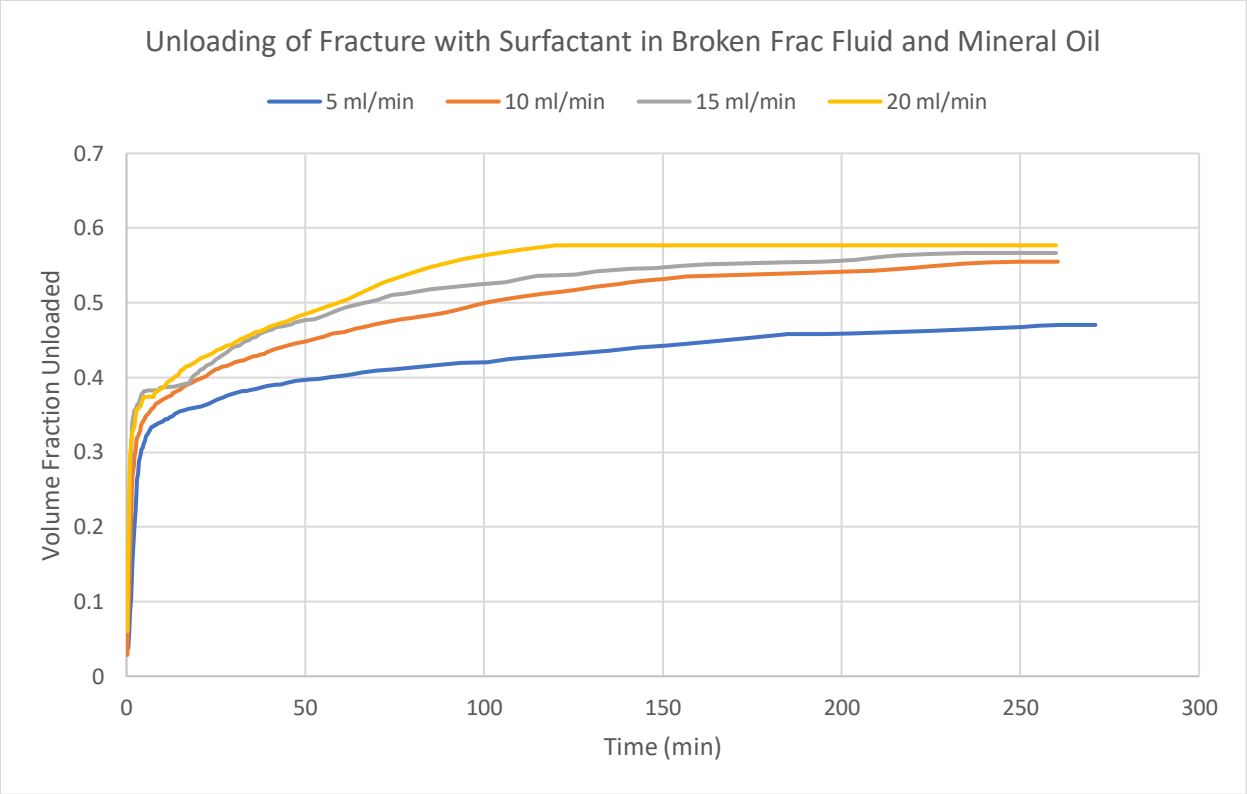

Figure 29 – Unloading results involving a mixture of mineral oil and broken hydraulic fracture fluid of surfactant concentration of 0.1%.

At first look, the curves do not have the same shapes as the experiments without oil. The unloading results during the mid-time appear less smooth. There even appears to be some overlap between the 15 and 20 ml/min curves. The aberration in shape is likely because these experiments exhibited all three types of transport (displacement, splashing, and bridging) and display as well the transitional periods between them. These will be discussed later.

The times to reach unloading limits increased dramatically with the addition of oil. At the fastest air injection rates, the time was increased by a factor of approximately four. The unloading limits decreased as well. With the exception of the slowest air injection rate, the limits reduced a proportional amount as seen in Table 5. The 5 ml/min air injection resulted in a greater decrease

in the unloading limit. Visually, the liquid removed from each flow rate was determined to have an oil cut of approximately 25%.

Table 5 - Unloading Limits of 0.1 SDS in Broken Frac Fluid

Air Injection Rate	$S_o = 0$	$S_o = 0.3$	**Percent Decrease**
5 ml/min	90.92	47.03	**48.27**
10 ml/min	92.74	55.50	**40.15**
15 ml/min	95.38	56.67	**40.58**
20 ml/min	97.26	57.69	**40.68**

Clearly, oil had a large detrimental effect on the surfactant's ability to improve unloading capabilities at these conditions. New observations can be made by presenting the data on different timescales, showing the results at early time and early-mid time in Figure 30. It should be noted that these results are still significantly greater than those seen without surfactant in Figure 21.

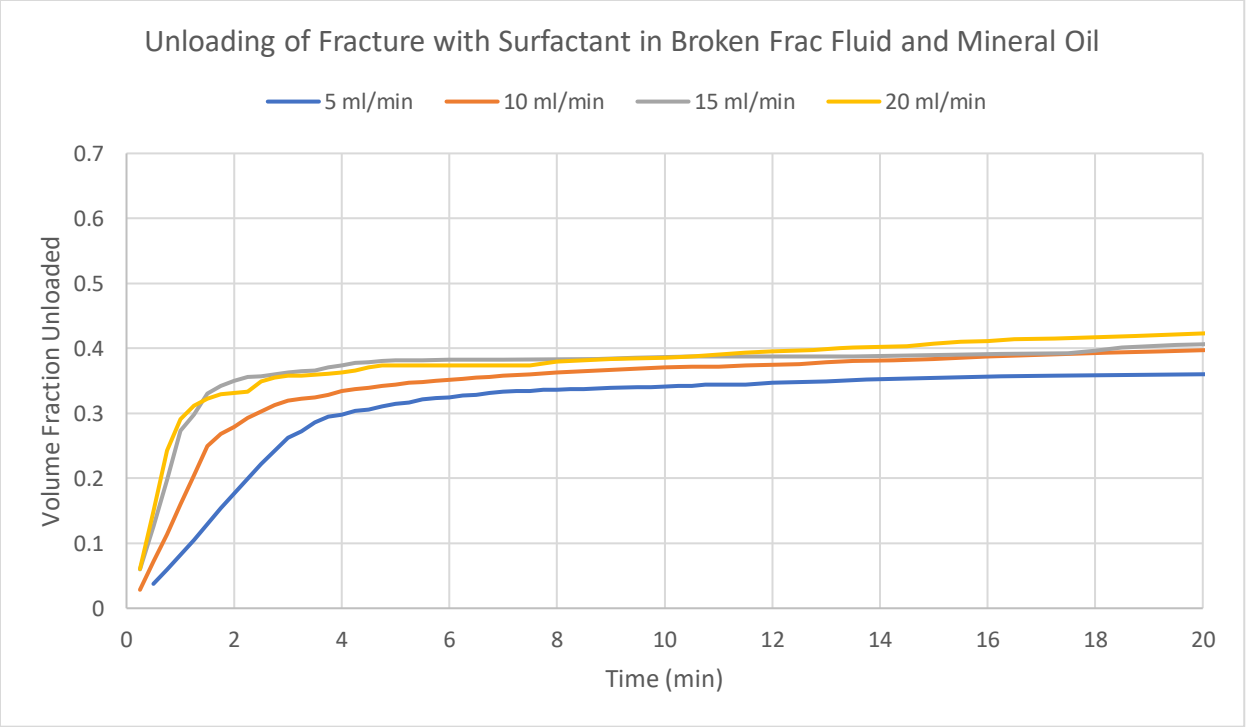

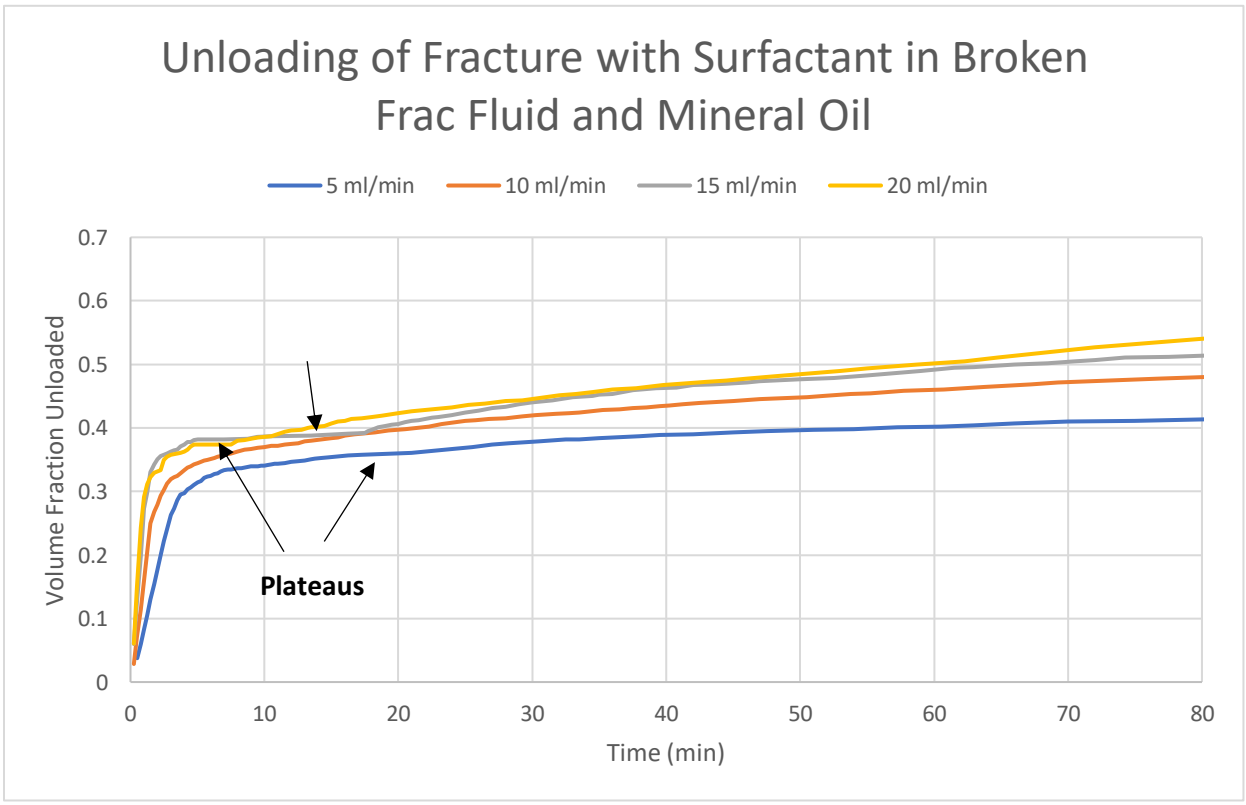

Figure 30 – Unloading results with mineral oil, surfactant, and broken frac fluid displayed at different timescales (early and early-mid time). The early-mid time figure reveals plateaus in unloading.

The early time curves reveal that displacement transport is still linear, indicating the lack of smoothness in Figure 29 does not start until the critical volume fraction has been reached. Interesting to note, the addition of oil did not cause the critical volume fraction to become air injection rate dependent; the critical volume fractions are still consistent across all flow rates at a value of about 0.27. However, this value is starkly different from the 0.74 obtained from the experiments without oil in Case 6. This critical volume fraction is much closer to those observed in Case 1 and Case 4 that contain no surfactant, the reason being an absence of piston-like displacement. Even though there is surfactant in the fracture, the oil prevents the mixture's mobility ratio from dropping below unity. As mentioned previously, areal sweep achieved by viscous fingering is not great, resulting in the low critical volume fraction.

Pictured in Figure 30, there are some minor overlaps of curves that contribute to the appearance of the data being less smooth compared to previous results that lack oil. The main reason for the overlap is because plateaus occurred during a transitional period. As the unloading behavior had mimicked liquids without surfactant so far, the mode of transport aptly became splashing after the critical volume fraction has been obtained. Splashing transport was able to occur until the gap between fluid level and fracture outlet became too great. It is at this point that the plateau occurred, and if no surfactant existed in the mixture, unloading would be complete.

Unloading did indeed resume eventually, as bubbles finally stabilized and started to bridge the gap. For some reason the inception of foam stability began when oil could be visually seen at the top of the fluid level. As time and bridging progressed, the volume of oil at the top increased due to its lighter density. Two distinct foam types could then be characterized: bubbles that bridge across through the oil and bubbles that bridge from the oil level to the outlet of the fracture. These

types are similar to those observed in Figure 28. Unloading continued to occur until the latter foam type destabilized and the bridge collapsed.

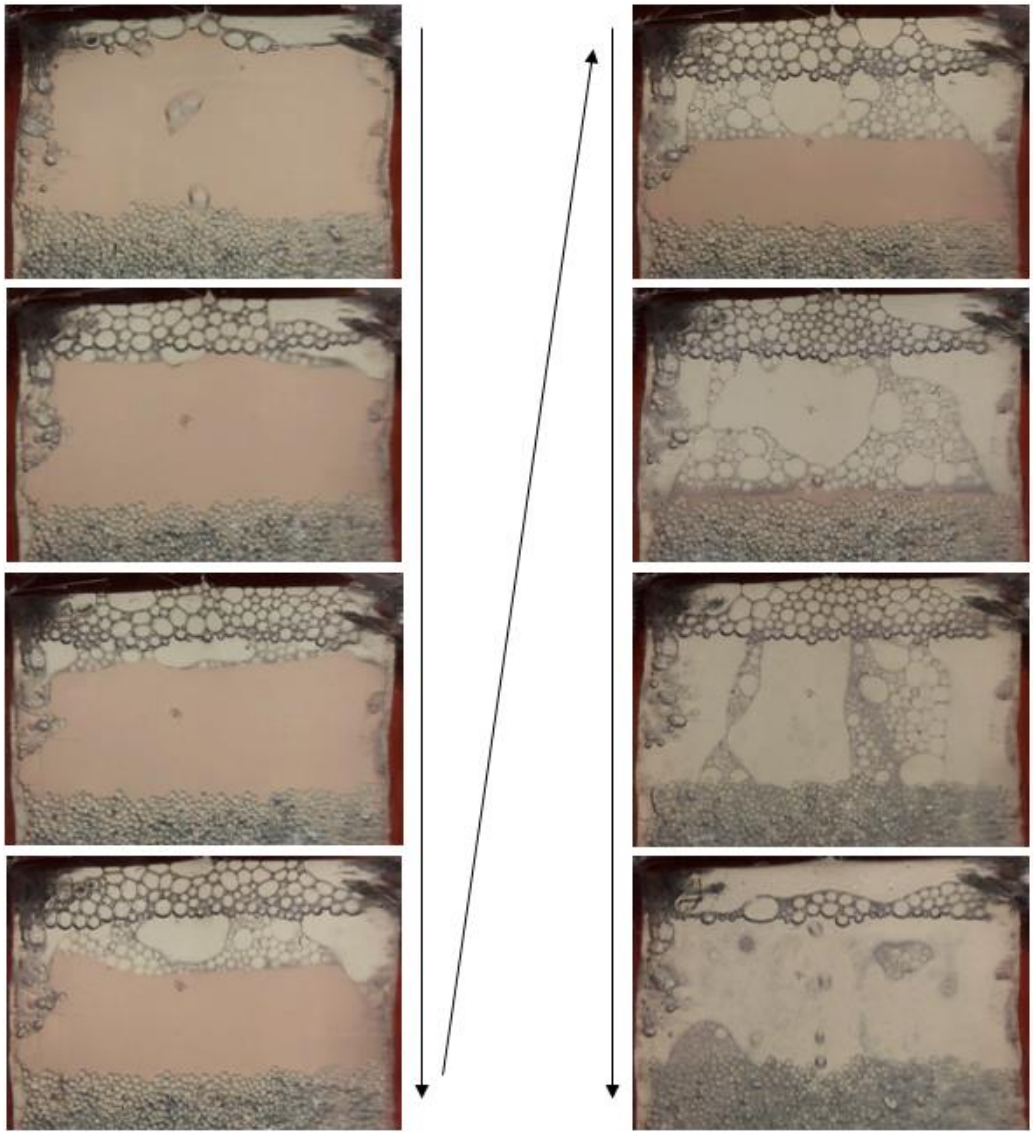

Figure 31 - Oil in the fracture cell with frac fluid and surfactant results in both splashing transport and foam bridging. There are two distinct bridges.

Figure 31 shows how the transport transitions from splashing to bridging and how the separate bridges evolve. The bubbles in the oil remained at much smaller sizes because foam is much less stable when in contact with oil and must reduce bubble radius as compensation. These bubbles are considered to be wet as they are surrounded by liquid and still retain their spherical

shape. The bubbles bridging the gap between the oil level and the fracture outlet ranged in size as time progressed, however they were larger than the other foam type and had more polygonal shape.

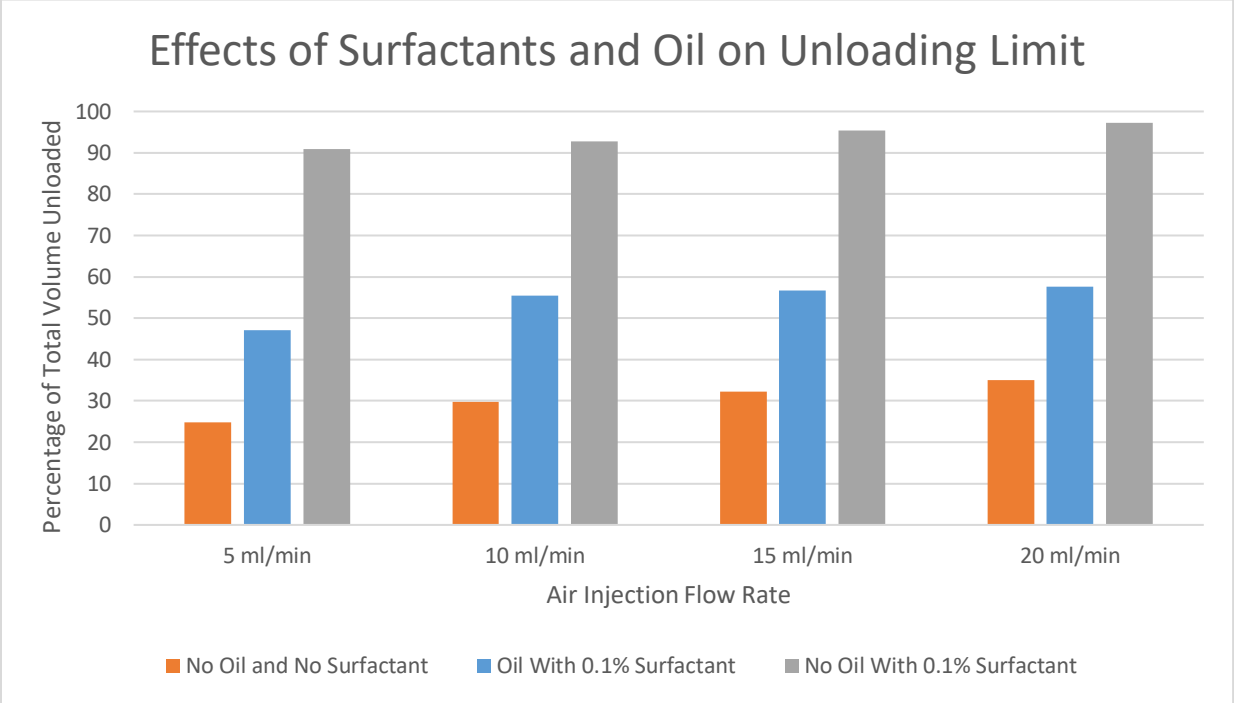

Figure 32 - Unloading limit comparison of hydraulic fracturing fluid with and without surfactant and with oil.

The experiments conducted with oil, surfactant, and frac fluid exhibited characteristics of cases run both with and without surfactant. Early time displacement involved viscous fingering rather than piston-like displacement. Also, initial foam instability forced the mechanism of transport to be splashing for continued unloading. When stable bubbles were able to form bridges, they allowed unloading to progress for long periods of time. Although stable enough to form bridges, these bridges were not as stable as those lacking oil. As the gap between fluid level and fracture outlet increased, the volume of foam required to form the bridge was too great and the weight of the bridge eventually caused the bubbles to collapse. This instability was further compounded as the load bearing bubbles were in contact with the oil. Final unloading limits

exceeded those of the cases unable to form bridges, however they were significantly lower than the results lacking oil in Case 6. This comparison can be seen in Figure 32.

Chapter 6: Using NMR to Investigate the Interaction between Shales and Water-Based Fluids

The desire to investigate unloading of water-based fracture fluids was driven by the fact that frac fluid leaks-off into the surrounding rock by imbibition. It is important to know what controls this imbibition process and if the use of surfactants can increase or decrease the extent of imbibition. Imbibition can result in clay softening, ionic transfer, fines generation, chemical reactions, etc. and change the fracture conductivity. The observations to be made in this chapter do not address these issues. Rather, they are limited to observations and quantification of the extent of imbibition of different aqueous solutions into shales. These observations come from analyzing NMR T_2 scans that are shown to provide a very good and convenient method for quantifying the extent of imbibition.

6.1 Nuclear Magnetic Resonance Background

T_2 distributions are often used to identify different types and amounts of molecules containing hydrogen in a variety of industries. For the oil and gas industry, T_2 distributions from NMR scanning give information about the fluids inside a rock. Specifically, for shales, scans can identify water saturation, as well as the type of porosity the water is located in (clay-bound water vs. bulk-water pore space). This allows an observer to acquire information about the imbibition of fluids into the rock.

When an external magnetic field is applied by a nuclear magnetic resonance machine, atomic nuclei precess around the direction of the field. The machine is able to measure signals

from the interaction between the spinning magnetic nuclei and the external magnetic field, one of these signals being the T_2 distribution. Because hydrogen has a relatively large magnetic moment as it only contains one proton and no neutrons, it produces a strong signal, so most results from NMR are based off the response of the hydrogen atom (Coates, Xiao, & Prammer, 1999). Because both water and hydrocarbons contain hydrogen, fluids in rocks can be measured through the use of nuclear magnetic resonance.

6.2 Experimental Preparation and Process

To study the interactions of shale with different fluids, small test samples of crushed rock were prepared in containers of fluid and allowed to soak over time. Crushed shale is used instead of cores because it allows a better surface area to volume ratio which promotes a better signal reading from the NMR as well as promotes more imbibition into the rock. It is noted that crushing the rock alters the porosity. However, as the purpose of this experiment is a relative comparison across fluid types, the true magnitudes of porosity and fluid saturation are unnecessary as long as the mesh size of the rock is consistent. For this testing, the shale is crushed to a particle size of US Mesh 5-10. After soaking, the samples are placed in an NMR machine and scanned. The NMR parameters can be seen in Table 6 . Three scans are taken for quality assurance. The T_2 distributions can be plotted and compared with other samples in MATLAB

Table 6 - NMR Parameters Used During Testing

Recycle Delay (ms)	750	Gain (dB)	54
SNR	100	Hydrogen Index	1
TAU	0.1	Relative Calibration	1
T_2 Max (ms)	100	Number of Points per Echo	4
Number of Echoes	2500		

6.2.1 Interpreting T_2 Distributions with Shale and Preliminary NMR Scans

Most of the scans are expected to appear similar in that they will contain two distinct peaks. The left peak is referred to as the first peak, and usually has a T_2 relaxation time between 0.1 and 1. The right peak is referred to as the second peak, and the T_2 relaxation time usually falls between 10 and 30. The first peak is known to be an indicator of clay-bound water, while the second peak indicates water in the effective pore space. Larger pores will result in greater relaxation times, while smaller pores as seen in shale will result in lower relaxation times. The magnitude of the peak indicates the volume of fluid in that particular region. The following subsections involve examples of interpretation as some initial testing was performed to practice and perfect test sample preparation and procedure.

6.2.1.1 Salinity Effects on Imbibition

Samples of unpreserved Eagleford shale source were soaked in different concentrations of brines for three days and then scanned by NMR. To obtain a baseline, a shale sample of equal volume from the same source was also scanned without being subjected to any fluid. These samples are from the Hawkville field, and their minerology can be found in Appendix A.

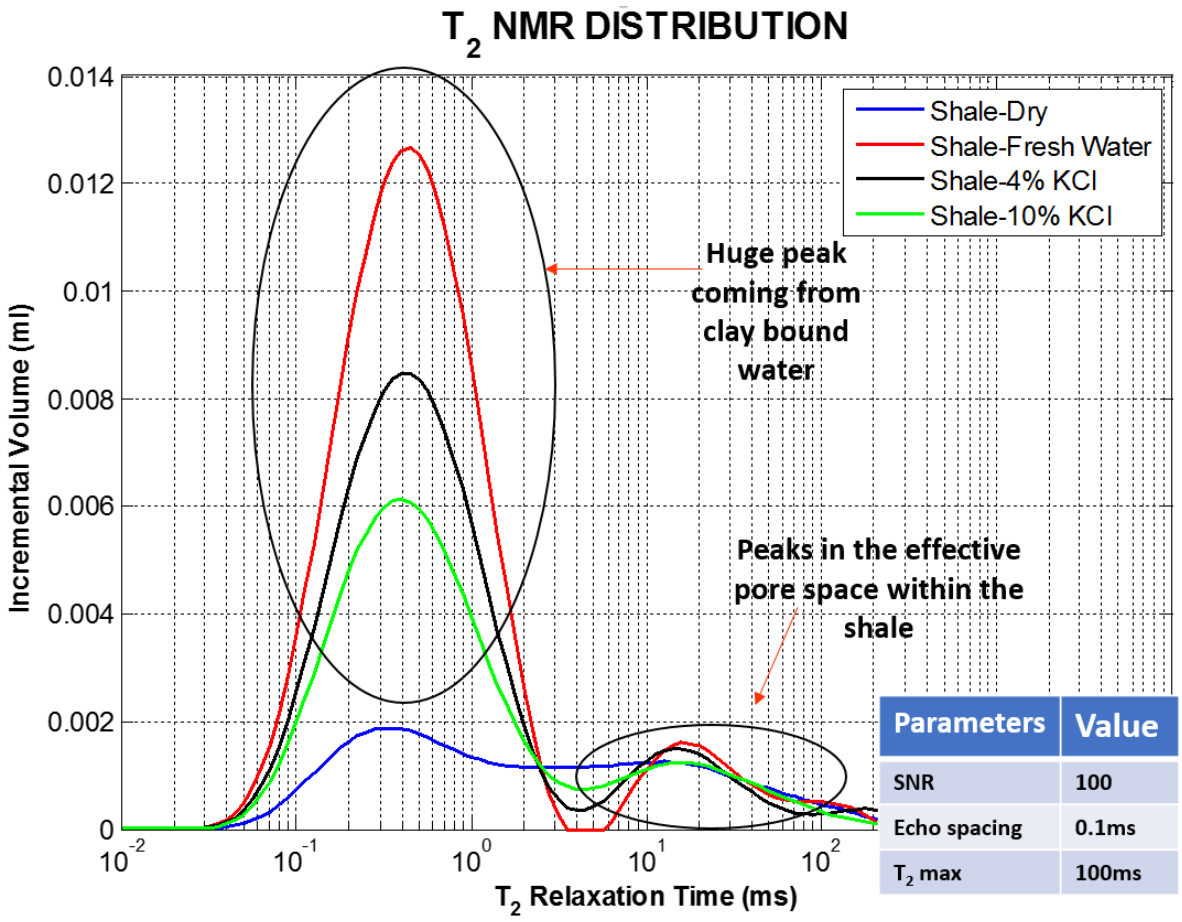

Figure 33 - Different NMR scans display the effect salinity has on the imbibition of fluid into shale.

From Figure 33, both the peak indicating water bound to clay minerals and the peak indicating water found in the effective pore space are very obvious. The distributions show what is already widely known—decreasing salinity promotes clay swelling. As one can see in both peaks, the shale soaked in DI water imbibed the most fluid, while the 10% KCl brine imbibed the least. The dry shale curve is plotted as a baseline for the observer. The differences in peaks are also much starker for the clay-bound water region. This is because this is the region where the clay swelling process takes place, as less saline water has a tendency to imbibe into the interlayer spaces in the clay minerals and become part of its crystal structure. The intrusion into clay minerals is much more sensitive to salinity than the intrusion into effective pore spaces.

6.2.1.2 Testing With Cores

Other initial testing was performed to compare NMR signals from crushed rock with signals from cores. Cores of equal volume as the crushed shale were prepared in a similar manner as before in both DI water and in a 4% KCl solution and then scanned with the NMR. Figure 34 shows the resulting T_2 distributions. The black curves indicate shale soaked in DI water, while the red curves indicate shale soaked in the brine. The solid lines represent crushed shale, while dotted lines represent cores.

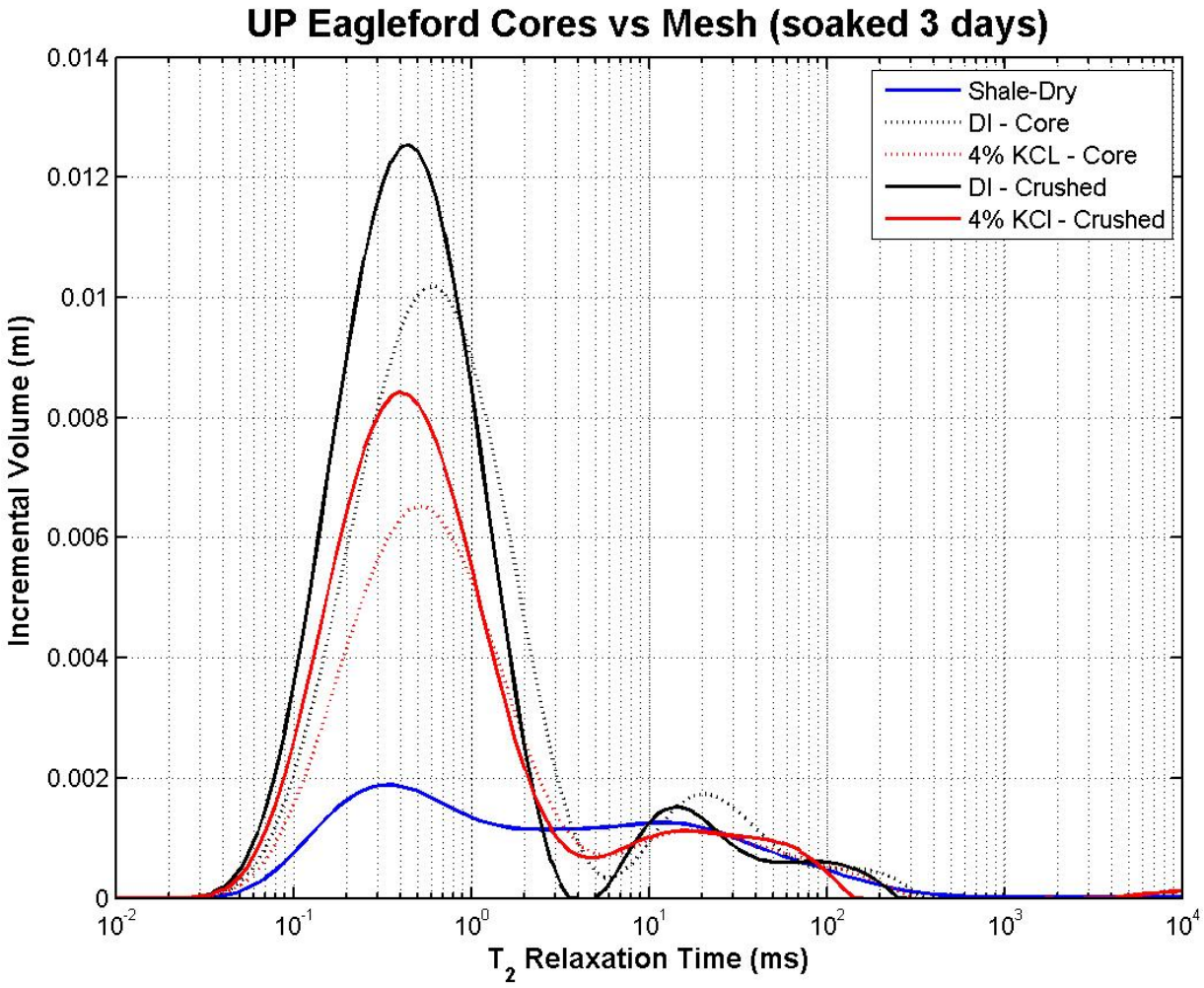

Figure 34 - For samples soaked for three days, a greater NMR signal was obtained with crushed shale rather than with cores.

The same trend is observed as before, as lower salinity promotes increased imbibition of liquid. The distributions also indicate fluid imbibition is greater in the crushed rocks compared to their core counterparts. The higher signal is thought to be due to the increased surface area to volume ratio, either encouraging more imbibition or allowing a for a greater magnetic resonance signal to occur with the crushed rock, or perhaps a combination of the two. As stated before, it is recognized that crushing the rock alters the true porosity of the sample. For a quantitative characterization of the sample, this practice would not be an accurate representation of the shale sample. However, the purpose of these tests are purely for a relative comparison, so the affected porosity is not an issue.

6.2.1.3 Time Dependency

A last round of initial testing was performed to observe the effect of the length of time the shale sample is allowed to soak in fluid. Equal volumes of crushed shale were soaked in DI water for different periods of time, and then they were scanned with the NMR. The results depicted in Figure 35 show an interesting trend occurring in the second peak. In the first hour of soaking, it appears a large amount of fluid initially resides in the effective pore space. However, as time passes, this volume of fluid seems to decrease. After three days, the fluid saturation of the effective pore space returned to a similar level as the first hour. Contrary to the second peak, the first peak steadily increases with time. Imbibition results after a full week are similar to the imbibition after three days. This indicates three days is enough time for testing. Allowing the samples extra time would simply be costing time.

A hypothesis for what is responsible for this phenomenon is that water initially imbibes into both the pore space and matrix. The matrix fills up quicker because the pores are larger. As time passes water imbibes from the pores to the interstitial layers in the clays. This competition between the water imbibing into the larger pores and into the clay bound layers results in complicated changes in the second peak. Because of this observation, future testing involves soaking samples for three days. Other research has also determined three days to be ample time for imbibition in crushed shale (Zeng, Miller, & Mohanty, 2018).

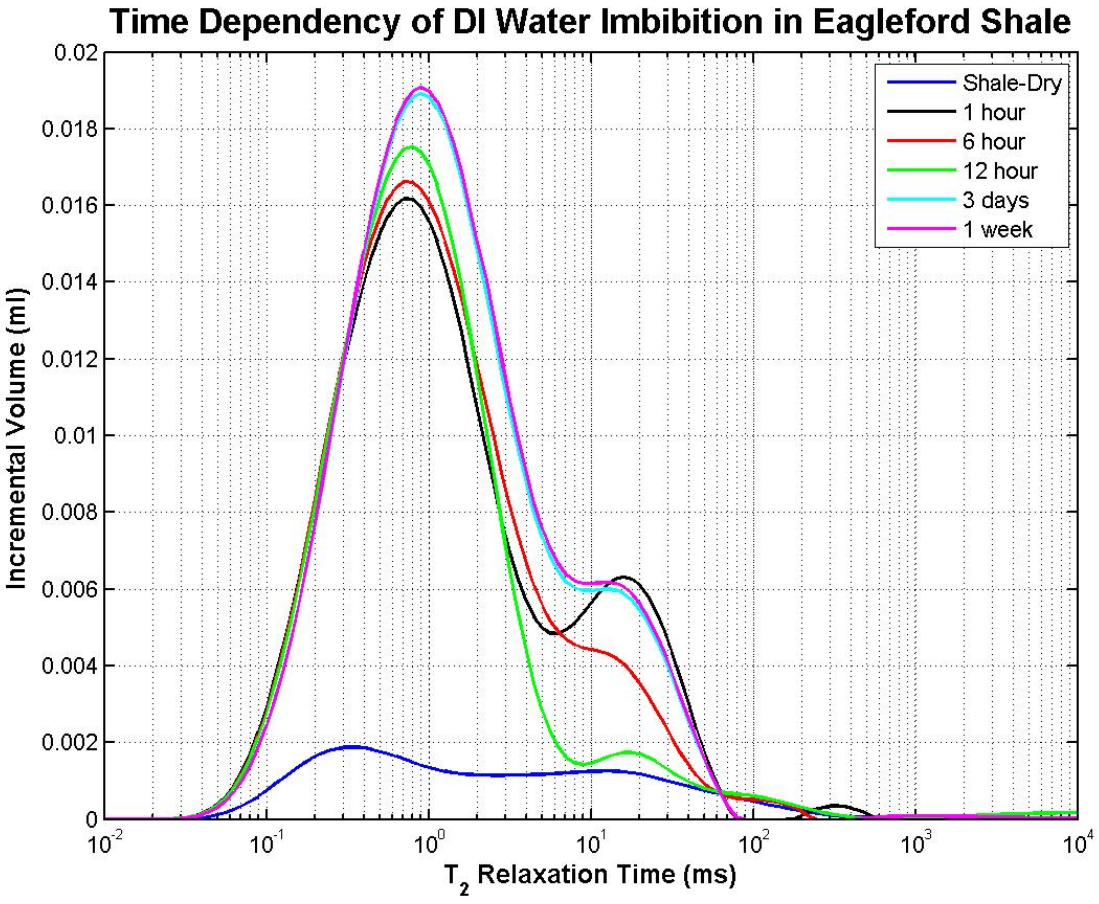

Figure 35 – The investigation of time dependency of imbibition in DI water determines three days of soaking to be sufficient.

6.2.2 Test Fluids

A variety of fluids and additives typically included in hydraulic fracturing fluid were tested on two different sources of shale—one with high clay content and the other with low clay content. These fluids include deionized water, brine, broken hydraulic fracturing fluid, clay inhibitors, and surfactants. Unpreserved Eagleford from the Hawkville field was used as the source for high clay content, while preserved Utica was used as the source for the low. Their minerology can be found in Appendix A. A matrix was created for testing combinations of these fluid types with different surfactants as seen in Figure 36.

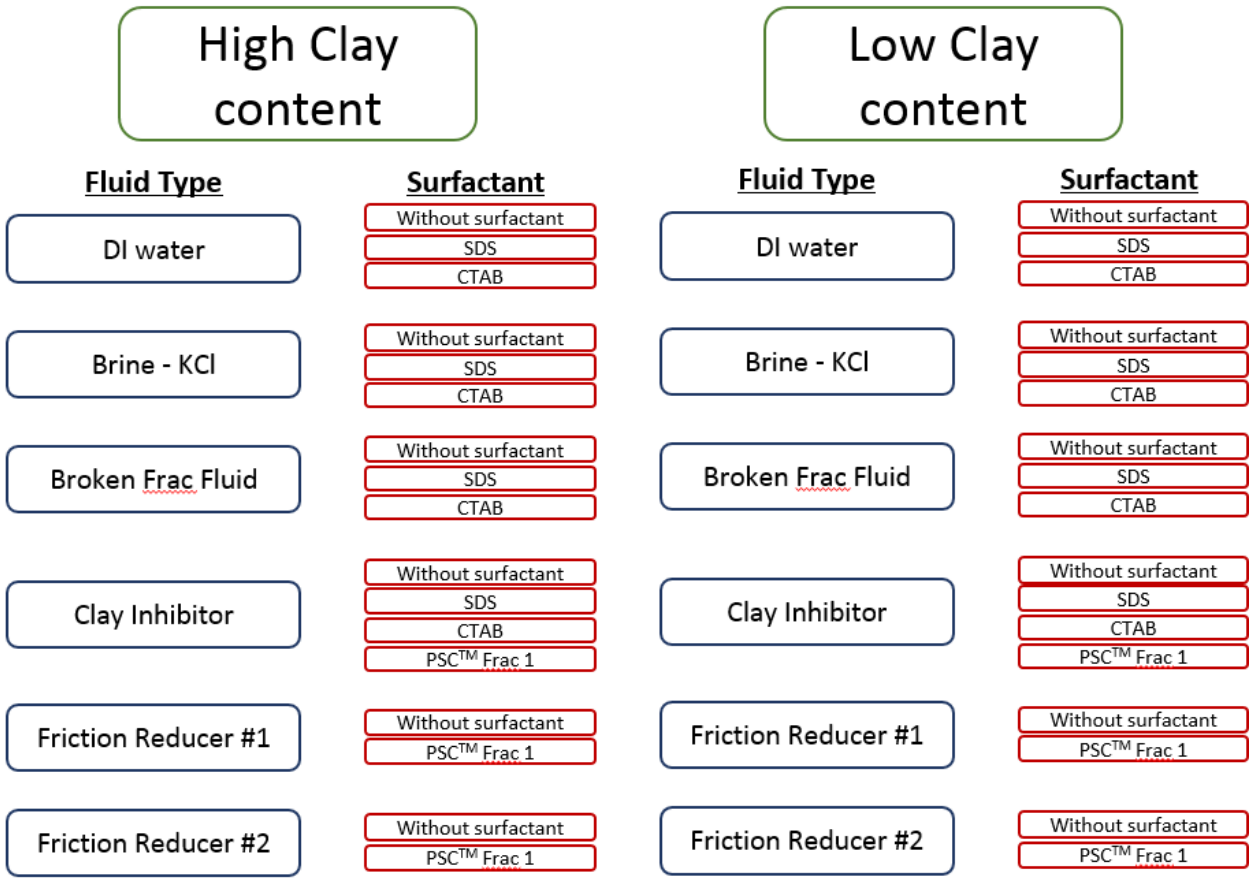

Figure 36 - Test matrix of combinations of shale and fluids to be tested with NMR.

The brine solution has a concentration of 5% by weight of KCl. The broken frac fluid is the same fluid utilized in the unloading experiments. Its preparation is briefly explained in Section 3.2. The clay inhibitor was prepared in deionized water with a proprietary chemical to a concentration of 0.1% by volume. The two friction reducers are also proprietary chemicals prepared in water, where the first is added as a liquid to form a concentration of 0.1% by volume and where the second is added as a solid to form a concentration of 0.26% by weight.

When surfactant was included, there was a concentration by weight of 0.1%. For most of the fluids to be tested, sodium dodecyl sulfate (SDS) and cetyl trimethyl ammonium bromide (CTAB) were used to observe the effects of different ionically charged surfactants. The former is anionic, while the latter is cationic. Advanced BioCatalytics provided a third surfactant, PSC Frac 1, to be included with the clay inhibitor and friction reducers. This surfactant is also anionic.

6.2.3 Sample Preparation and Experimental Procedure

This experiment was briefly explained in previous sections, however the following is a more detailed outline of the steps taken to prepare shale samples to be tested, as well as the experimental procedure.

Fluid Imbibition in Shale Testing Preparation and Procedure

- A shale sample is identified and then crushed with a pestle, mortar, and sieves to obtain particles sizes of 5-10 mesh (2-4 mm in diameter). For these tests, an entire mason jar was filled. The jar is then placed in an oven at 105°C for 24 hours to reduce preexisting water saturation. The oven is also placed under a vacuum to eliminate trapped air within the inter-granular pore space.

- Fluids to be tested are prepared in separate beakers. Fluid concentrations are described in Section 6.2.2 and 3.2.

- 15 mg of dry crushed shale is weighed in a metal tea strainer. Making sure the top is securely in place, the strainer is lowered into 100 mL of fluid to be tested. The entire strainer must be completely submerged to ensure all shale can be in contact with the fluid. The fluid container is covered to prevent interaction with air. The equipment is left alone for three days to allow shale particles to imbibe the fluids at atmospheric temperature and pressure.

- After the three days, the strainer can be removed from the test fluid and placed on Kimwipe delicate task wipers. The sample must next be subjected to a short drying process to ensure there are no water droplets on the faces of the rock or in spaces between particles. The particles are poured out of the strainer and onto clean Kimwipes that line a small plastic

weigh dish, taking care to ensure all the shale is removed. With more Kimwipes, the rock is patted down until the wipe is no longer wetted. All Kimwipes are disposed of while the rock remains inside the weigh dish. The weigh dish is then placed inside a fume hood to sit for 25 minutes. After the first 10 and 20 minutes, the dish is gently shaken to flip and move around the particles to ensure more consistent drying.

- After the 25 minutes have expired, the sample is funneled into a small glass sealed container and weighed (knowing the weight of the glass container one can determine the weight of the wet shale). These weight measurements are not actually used for the NMR experiment; they are simply obtained to maintain a record.

- The glass container is placed into the NMR machine. Some adjustments may be required with the NMR machine to ensure the applied magnetic field envelopes the entirety of the rock sample. Three back-to-back T_2 scans are run for redundancy. Depending on the test sample, the scan may take between 30 minutes to 3 hours.

- After scan completion, the data is exported to excel sheets, where they are organized and plotted on MATLAB

6.3 NMR Results

The test matrix depicted in Section 6.2.2 resulted in a total of 34 different combinations of shale-fluid interactions. The NMR results for these tests are depicted in the following subsections. Each figure depicts results of one fluid type and contains multiple distributions for the surfactant added to the mixture. The distributions displayed in red and green represent the respective results from anionic SDS and cationic CTAB surfactants. PCS Frac 1 is shown in

pink. Scans of the sample soaked in the test fluid with no surfactant is seen in black. The T_2 distribution of the dry sample is shown in blue as a baseline of comparison.

6.3.1 High Clay Content

As the samples taken from the Eagleford source are rich in clay minerals, it is expected that differences in fluid chemistry will have strong effects on imbibition. The following figures support this, in that the different surfactants have considerably different magnitudes of peaks.

6.3.1.1 Deionized water

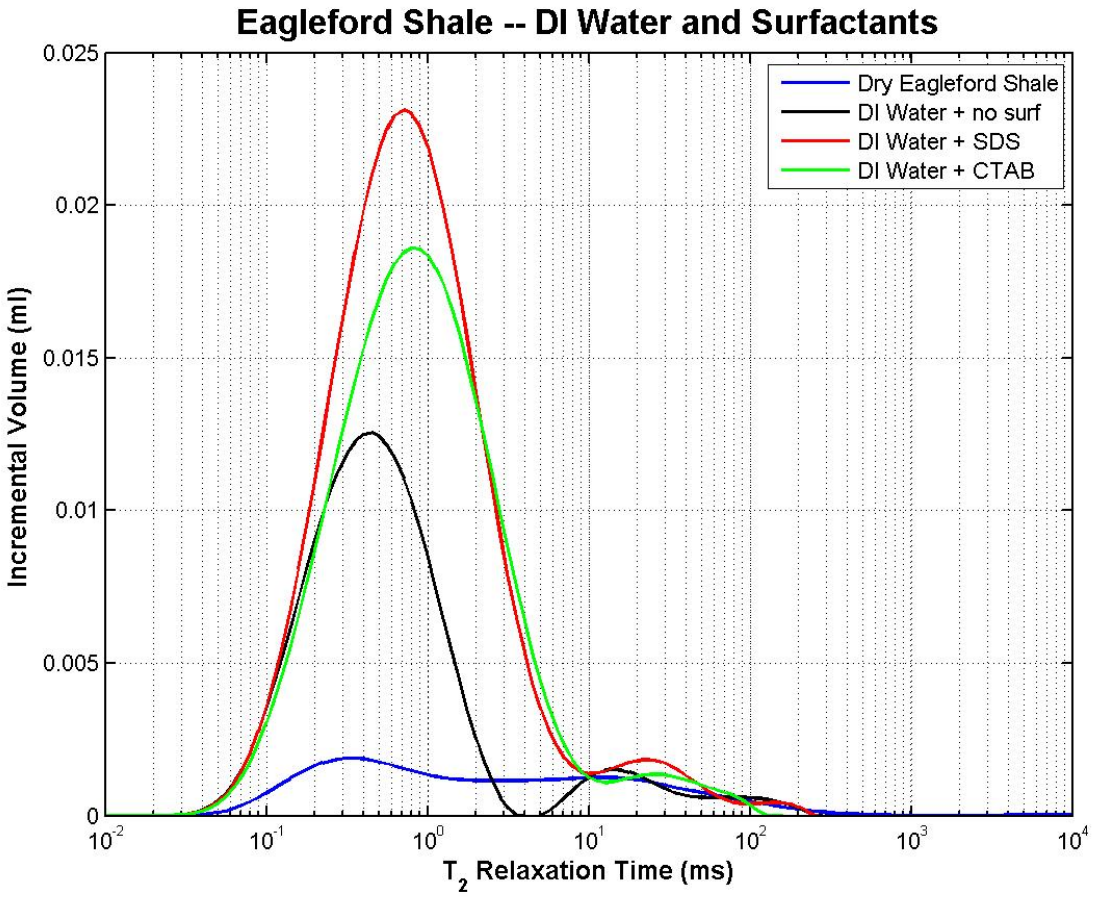

Figure 37 - Matrix testing of DI water and surfactants with high clay content shale.

Deionized water already has a high tendency to imbibe into shale. Surfactants appear to increase imbibition even more, as seen in Figure 37. From the first peak, it appears SDS almost doubled the volume of water imbibed into the clay minerals. Because clay minerals are mainly composed of alkali metals, alkaline earths, and other cations, it is reasonable that the anionic SDS would be attracted to the surfaces of these clays. The cationic surfactant CTAB also encouraged an increase of clay-bound water, however to a lesser extent compared to SDS. The differences are greater in the first peaks, rather than the second peaks. This suggests the magnitude of the clay mineral's tendency to absorb water is very large in relation to the volume of the pore space.

6.3.1.2 Brine

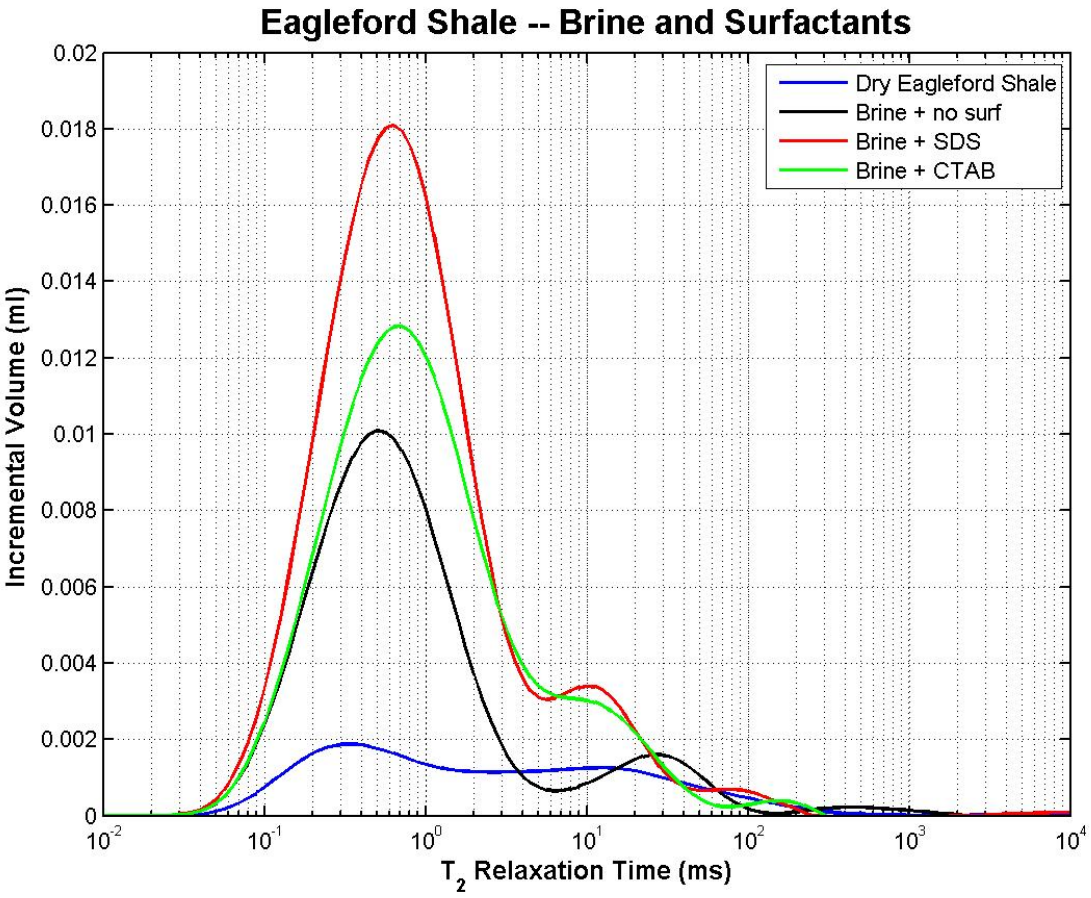

Figure 38 - Matrix testing of brine and surfactants with high clay content shale.

Scans of the samples soaked in brine and surfactants reveal similar behavior of imbibition into clay minerals, however the magnitudes of the peaks are lower due to the increased salinity as seen in Figure 38. Contrary to the DI water, the second peaks of the brine have greater separation, with both surfactants having larger volumes than the sample without. This indicates that surfactant can also affect imbibition into the effective pore space as well. There is a separation of curves in the second peaks of the brine but not the DI water because the degree of clay swelling is smaller. With less swelling, pore throats are larger and connectivity is better, allowing for greater saturation of the effective pore space.

6.3.1.3 Broken Hydraulic Fracturing Fluid

Looking at the values of the incremental volumes that were imbibed in Figure 39, the broken frac fluid encouraged much more imbibition than the brine and DI water. It appears the surfactants did not encourage an increase of intrusion into the clay minerals. However, it is possible that that no increase is observed because the clay minerals imbibed such a volume of fluid that it reached an "intrusion limit" and could not absorb any more.

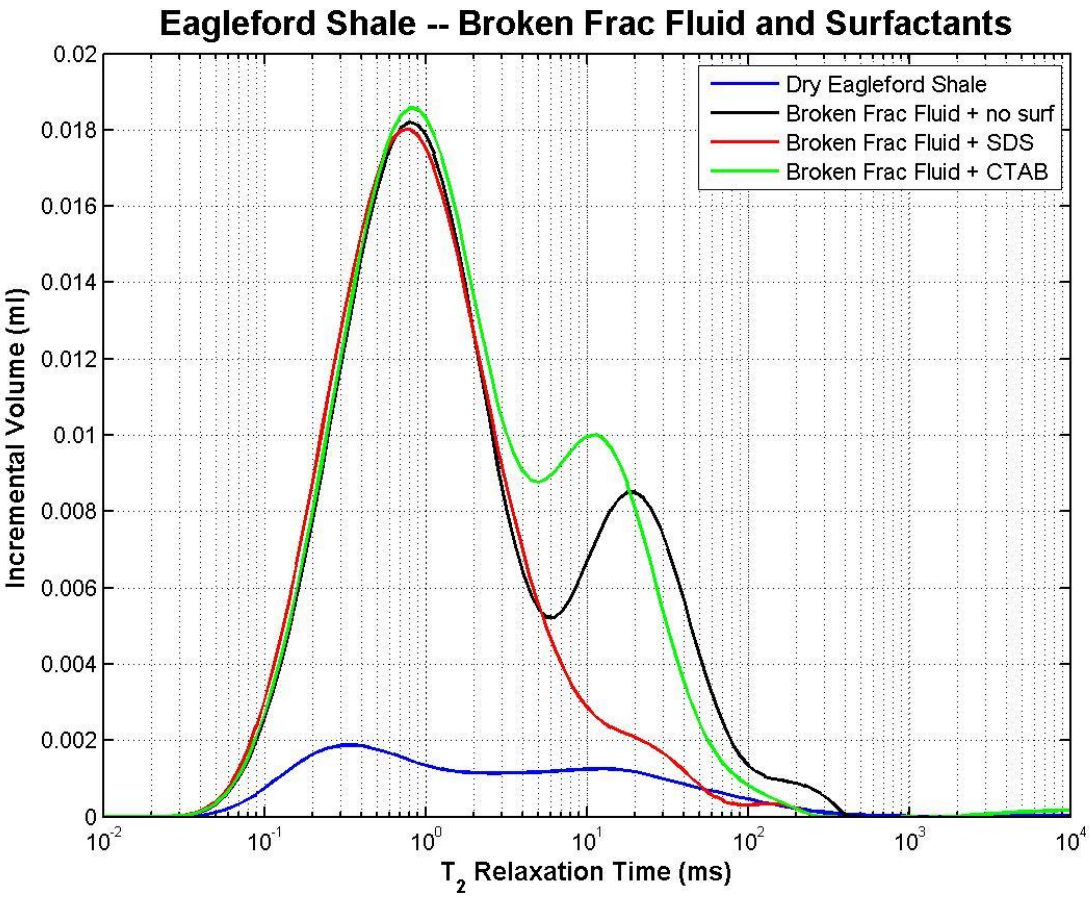

Figure 39 - Matrix testing of broken hydraulic fracturing fluid and surfactants with high clay content shale.

The surfactants did indeed have an effect on the second peak. This scan reveals CTAB being the surfactant to encourage increased imbibition, although this time in the effective pore

space. The SDS actually decreased intrusion into the pores. This phenomenon is likely due to the ionic interactions between the surfactant and the proprietary polyacrylamide.

6.3.1.4 Clay Inhibitor

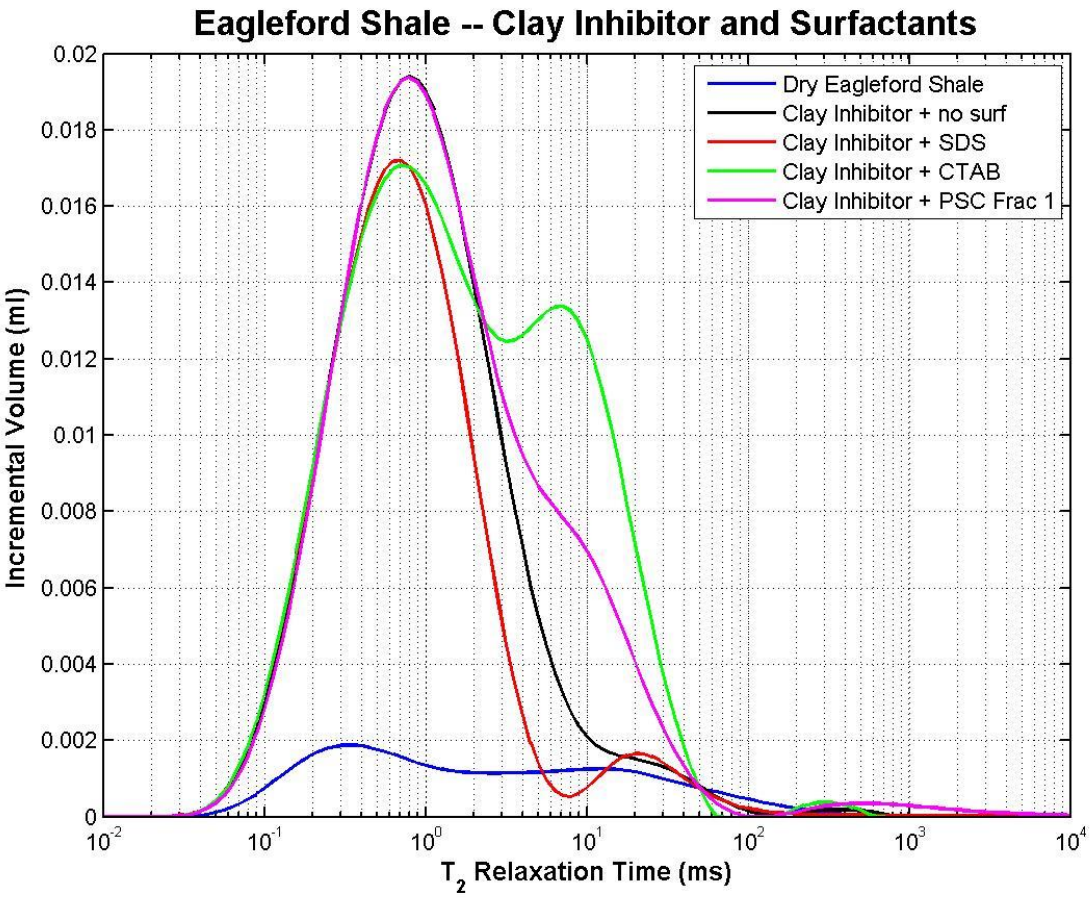

Figure 40 - Matrix testing of clay inhibitor and surfactants with high clay content shale.

Similar to the broken frac fluid results, CTAB mixed with the clay inhibitor strongly encouraged increased imbibition into the effective pore space, whereas SDS did not. Advanced BioCatalytic's surfactant also encouraged effective pore space imbibition although it is more ionically similar to SDS. It is clear that the shale-fluid interactions can be very diverse. Figure 40 reveals another interesting trend to note. The addition of SDS and CTAB inhibited imbibition into the clay-bound region. This is interesting because previous fluids have shown surfactant to

increase clay swelling. This observation likely occurs because the clay inhibitor is functioning as it was intended—to mitigate clay interactions. However, it is strange that the clay inhibitor samples imbibe a large amount of fluid when they are lacking surfactant.

6.3.1.5 Friction Reducer 1

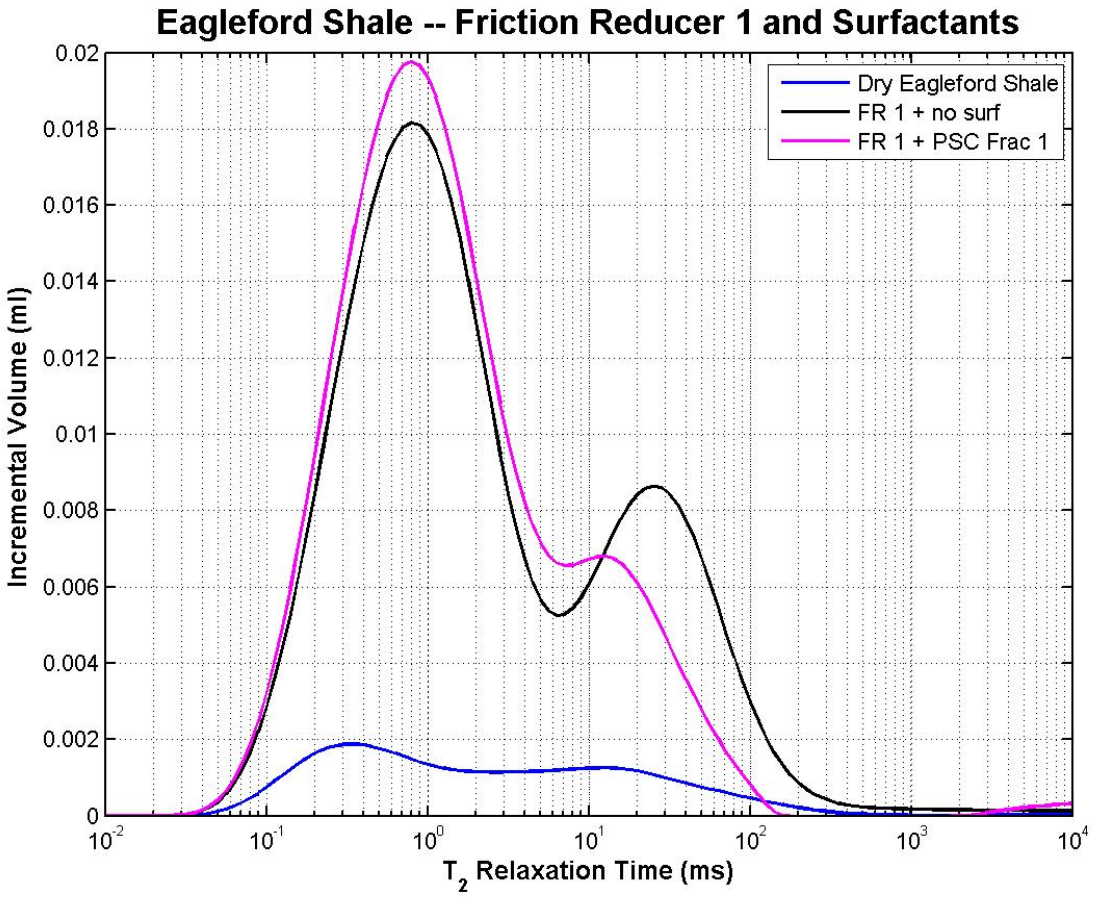

Figure 41 - Matrix testing of friction reducer 1 and surfactants with high clay content shale.

The only surfactant tested with the friction reducers was Advanced BioCatalytic's surfactant. Its addition, the first friction reducer increased clay swelling enough that pores were blocked and intrusion into the pore space was limited.

6.3.1.6 Friction Reducer 2

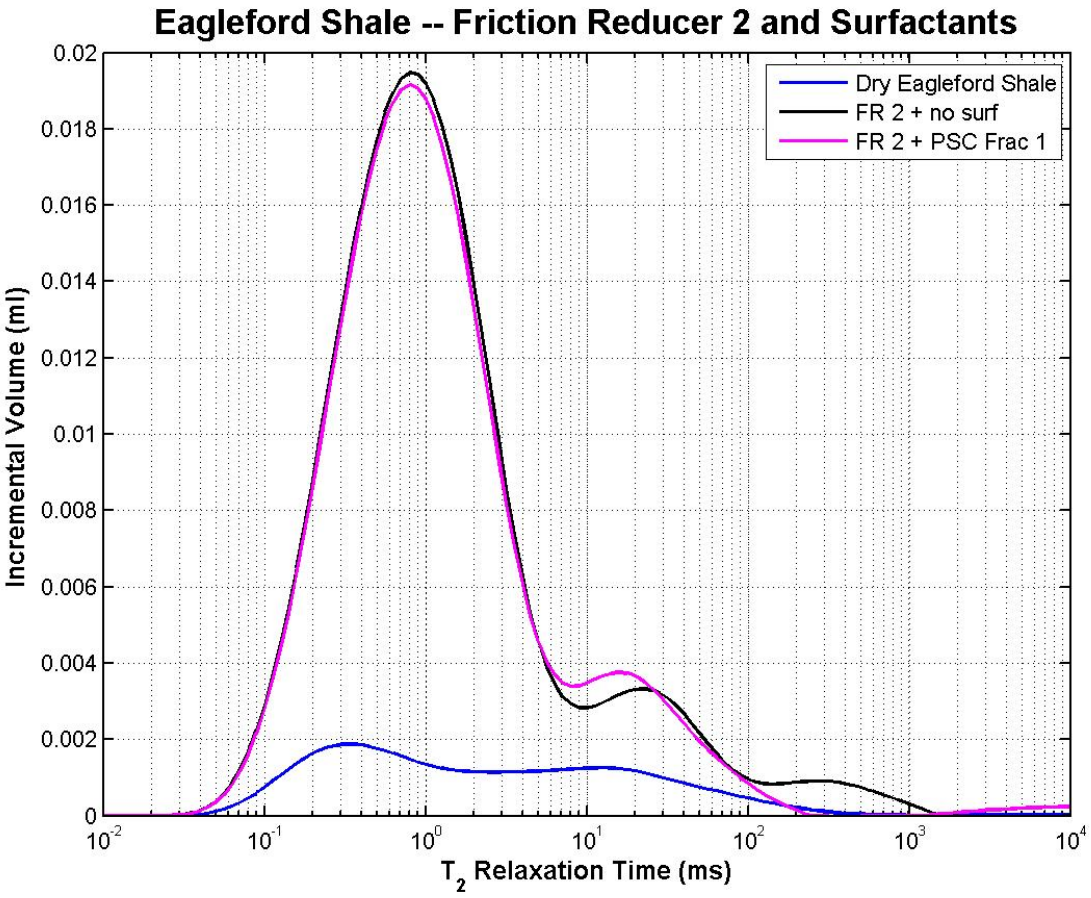

Figure 42 – Matrix testing of friction reducer 2 and surfactants with high clay content shale.

The opposite effect was seen with the second friction reducer. Addition of ABC's surfactant resulted in slightly less clay swelling, thereby allowing for marginally more imbibition into the pore space.

6.3.1.7 Fluid Types without Surfactant

Figure 43 displays the interaction of the different types of fluids with high clay content shale samples with no surfactants involved. It is obvious that the extent of fluid imbibition is highly dependent on the composition of that fluid. From the NMR scans, the different fluids appear to fall into different groups categorized by the magnitude of their peaks. The less "complex" fluids that are simply DI water and brine fall into one group, whereas the more "complex" fluids (friction reducers, clay inhibitor, and frac fluid) fall into another.

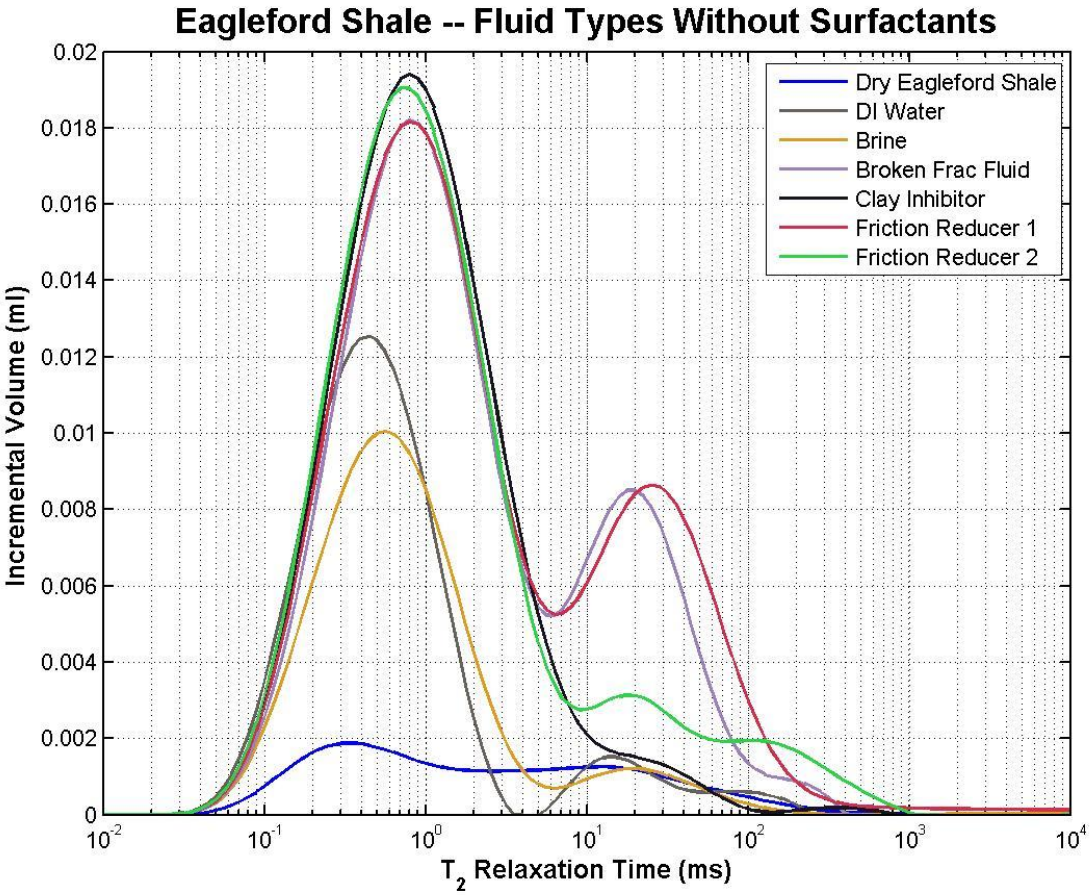

Figure 43 - Comparison of tested fluids with high clay content without surfactants.

The fluids in the first group solely involve water and salts and induce lower amounts of imbibition. The second group involves chemicals much more complicated than salt that interact

with the shale with more complex reactions, causing a higher degree of imbibition into both the clay minerals and effective pore space. The second group's distributions reveal how easily frac fluid can leak into the surrounding rock depending on what additives are included in its amalgam of chemicals. Figure 43 also reveals how fluids of the same category can interact with shale differently, as the degree of effective pore space imbibition is different for the two friction reducers.

6.3.2 Low Clay Content

The following subsections contain the results of the different fluid types interacting with the sample containing low clay content from the Utica play. Because there was less clay in these samples, the NMR scans have smaller peaks than those found in the previous section, indicating less imbibition occurred.

6.3.2.1 Deionized Water

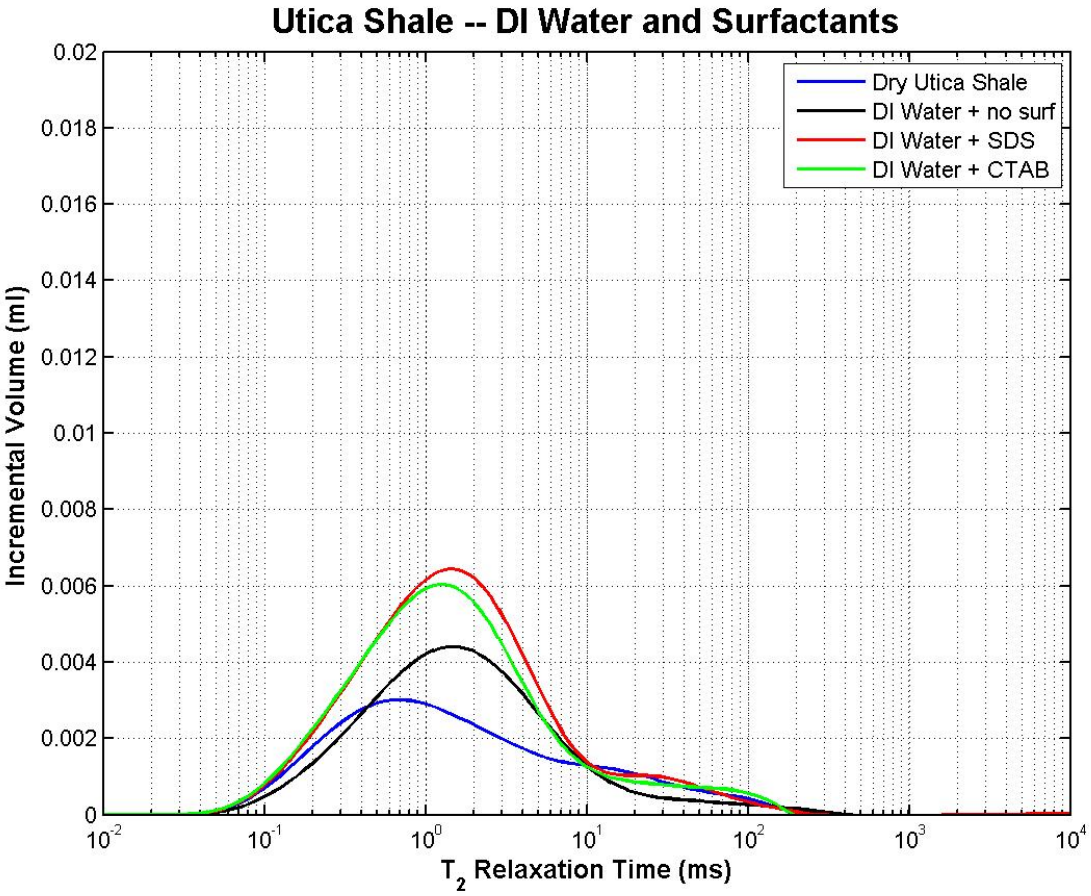

Figure 44 - Matrix testing of DI water and surfactants with low clay content shale.

Adding surfactants to DI water had the same effect to the low clay content sample as it did with the high. Both surfactants increased imbibition, having a greater increase with the SDS. As

mentioned previously, the magnitudes of the curves are significantly lower than those found in section 6.3.1 because there are less clay minerals to absorb water.

6.3.2.2 Brine

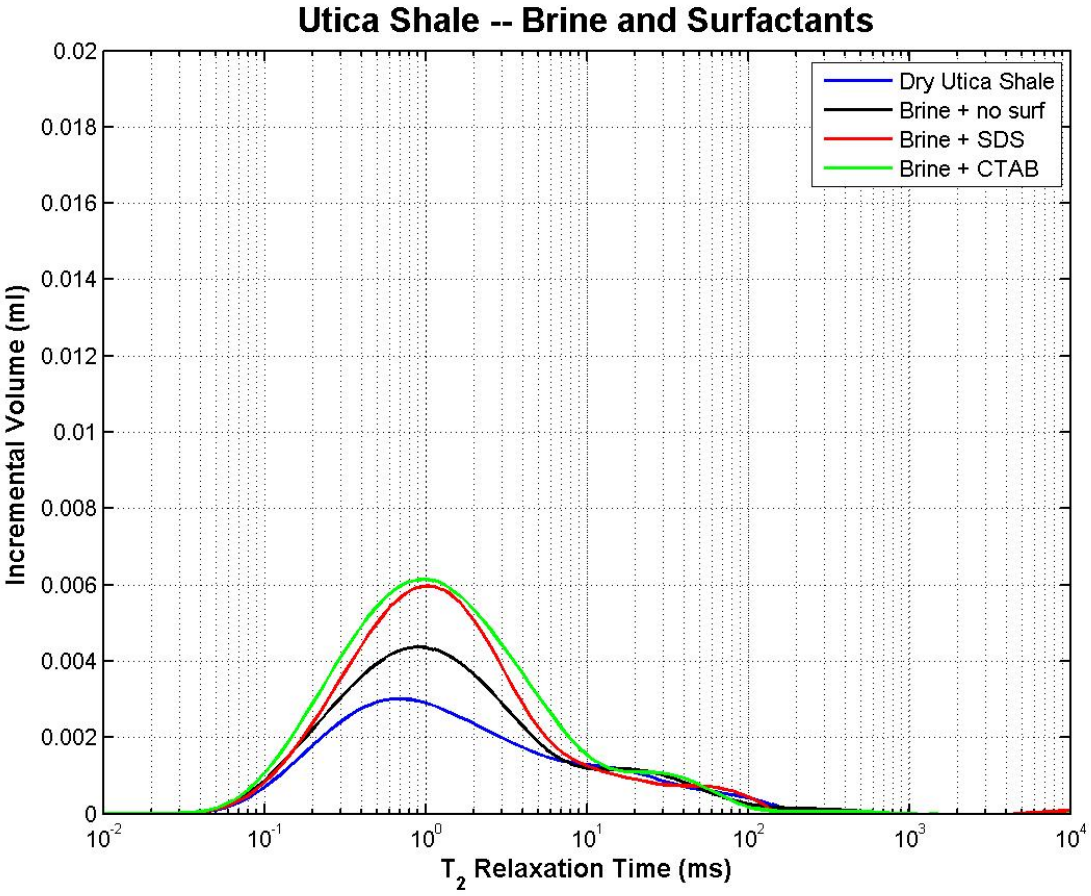

Figure 45 - Matrix testing of brine and surfactants with low clay content shale.

As presented in Figure 45, surfactants still increase imbibition when added to brine, however the peaks of the two surfactants are quite similar. The CTAB distribution actually shows slightly more clay swelling, contrary to observations seen in the Eagleford samples.

6.3.2.3 Broken Hydraulic Fracturing Fluid

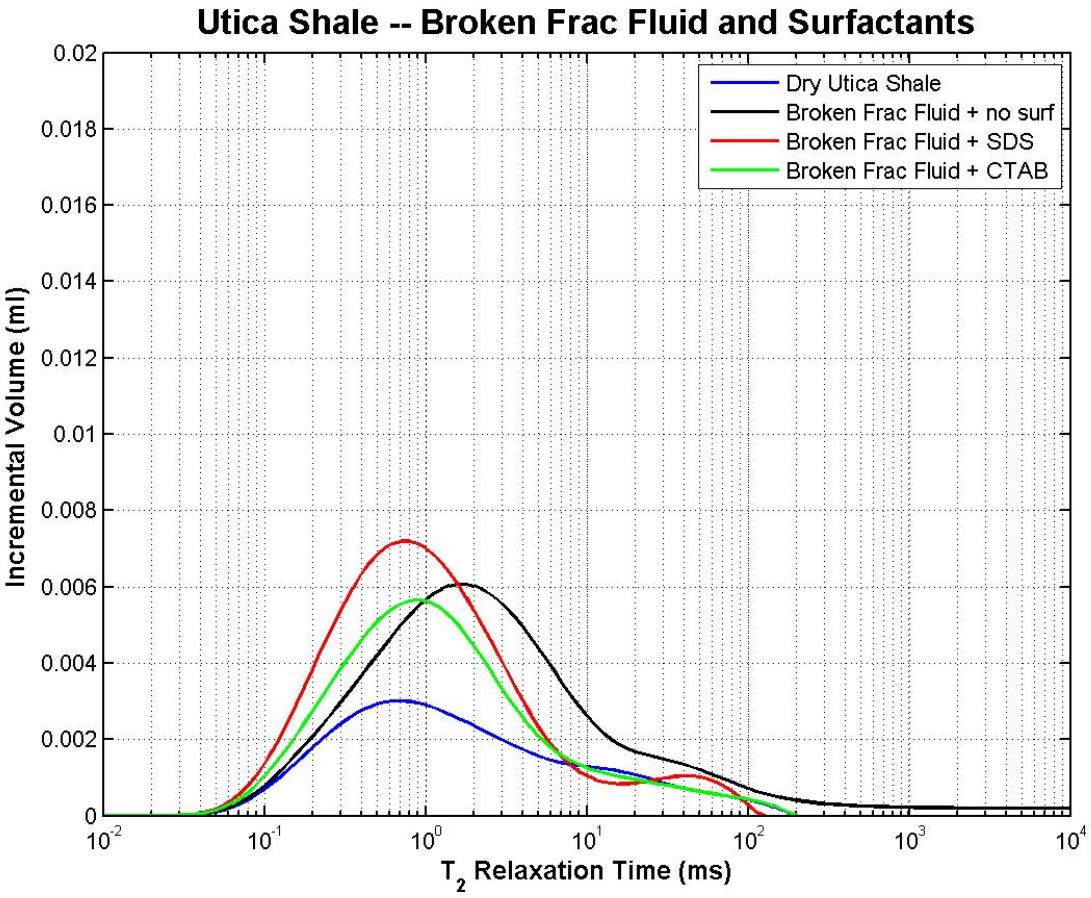

Figure 46 - Matrix testing of broken hydraulic fracturing fluid and surfactants with low clay content shale.

Similar to the scans of the high clay, the two surfactant's distributions are above and below the sample of broken frac fluid lacking surfactant as seen in Figure 46. However, the positions are switched, as SDS induced more imbibition into the low clay shale and CTAB induced less. The distribution of the interaction without surfactant appears shifted to the right. After believing the scan to be faulty, multiple trials of sample preparation and NMR scanning proved the distribution to be true.

6.3.2.4 Clay Inhibitor

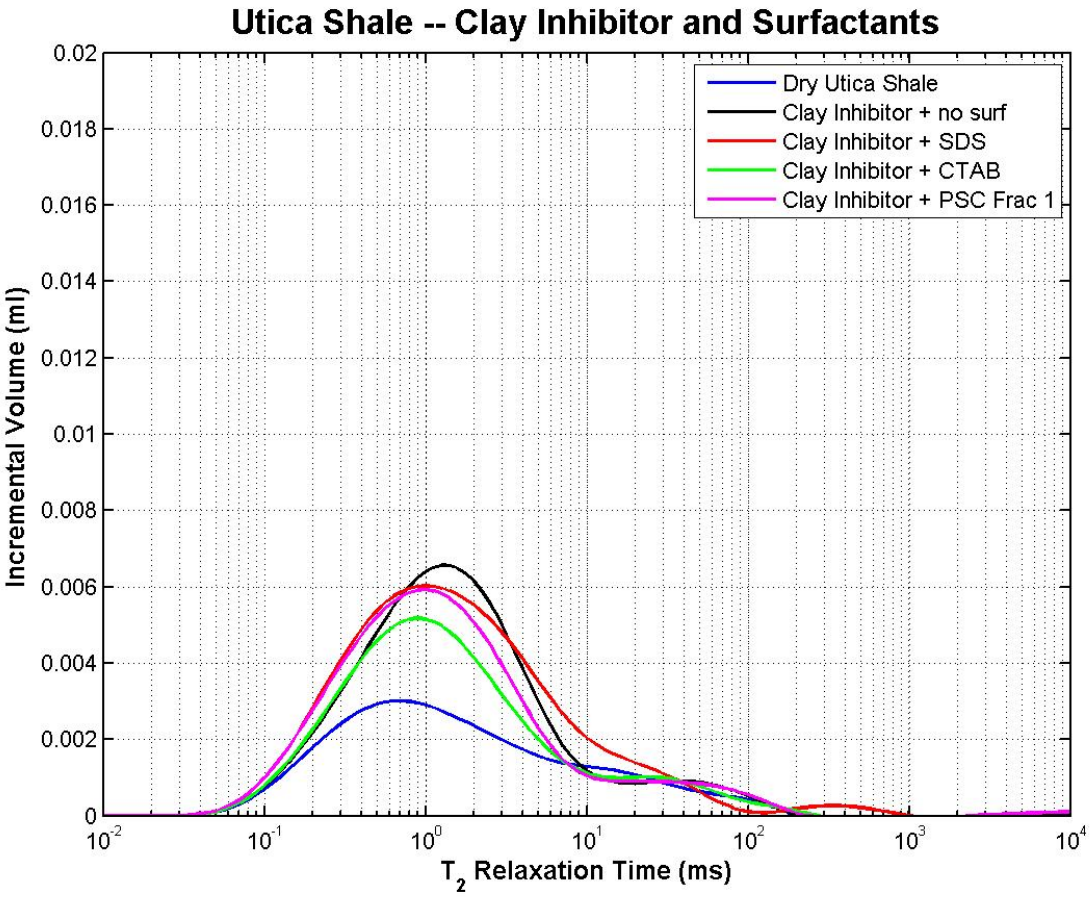

Figure 47 - Matrix testing of clay inhibitor and surfactants with low clay content shale.

Figure 47 reveals that surfactants and the clay inhibitor do not have the diverse behavior in the effective poor space seen with the high clay shale. With the Utica samples, none of the fluids with clay inhibitor saw much imbibition into the pore space regardless of the surfactant added. However, similar to the Eagleford, the addition of surfactant to the clay inhibitor reduced clay swelling.

6.3.2.5 Friction Reducer 1

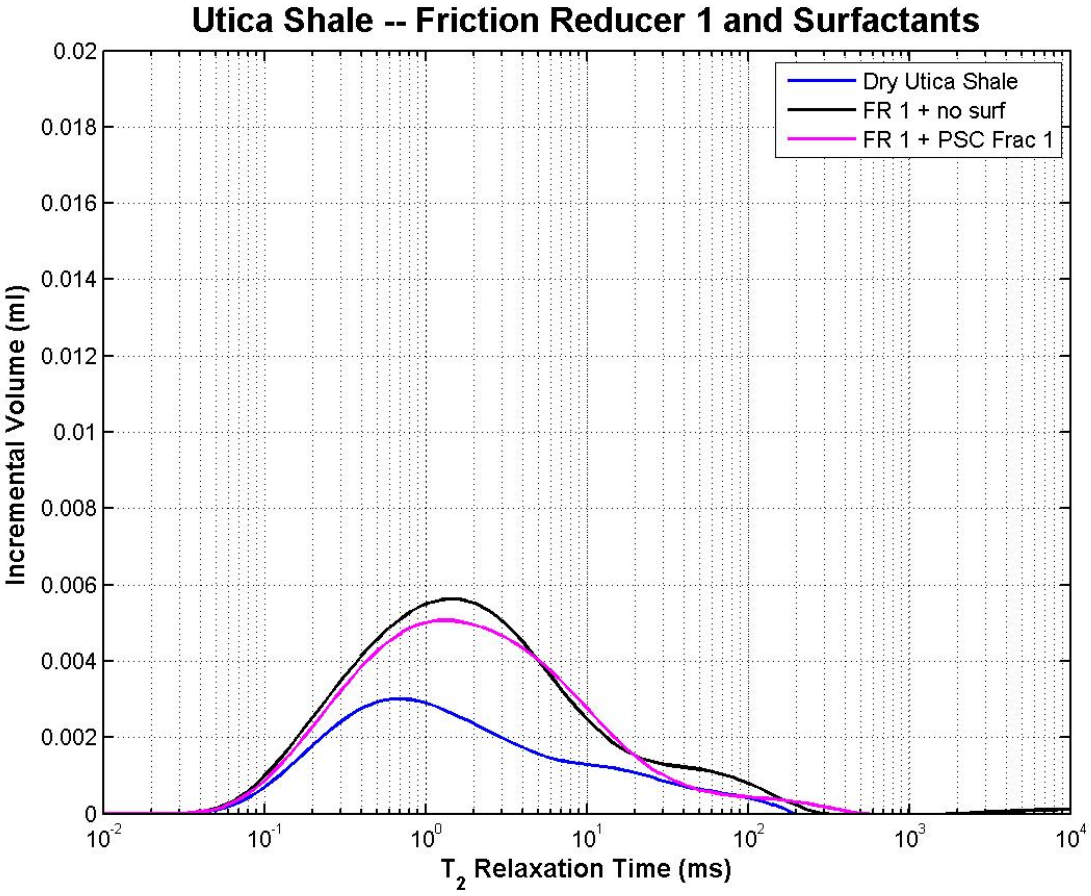

Figure 48 - Matrix testing of friction reducer 1 and surfactants with low clay content shale.

Also contrary to results with the high clay content, the amount of clay swelling is less when ABC's surfactant was added to the first friction reducer and allowed to interaction with the low clay content. This means not only the magnitudes of shale-fluid interactions are dependent on the concentration of clay content, but also the trends and behavior can vary as well.

6.3.2.6 Friction Reducer 2

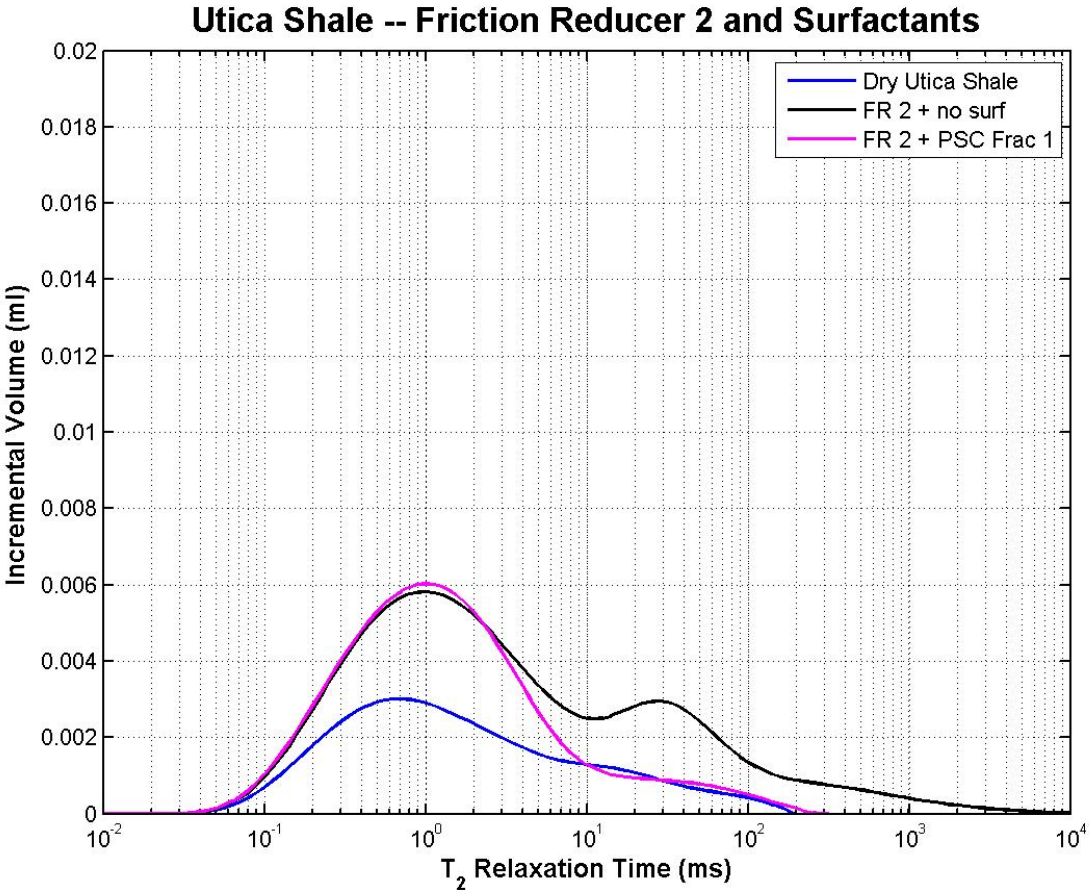

Figure 49 - Matrix testing of friction reducer 2 and surfactants with low clay content shale.

According to Figure 49, friction reducer 2 encourages imbibition into the effective pore space, whereas friction reducer 1 did not. The addition of ABC's surfactant stopped the pore space imbibition. This observation reveals that fluid-shale behavior cannot be specified for a given fluid type, as the two friction reducers exhibit different interactions.

6.3.2.7 Fluid Types without Surfactant

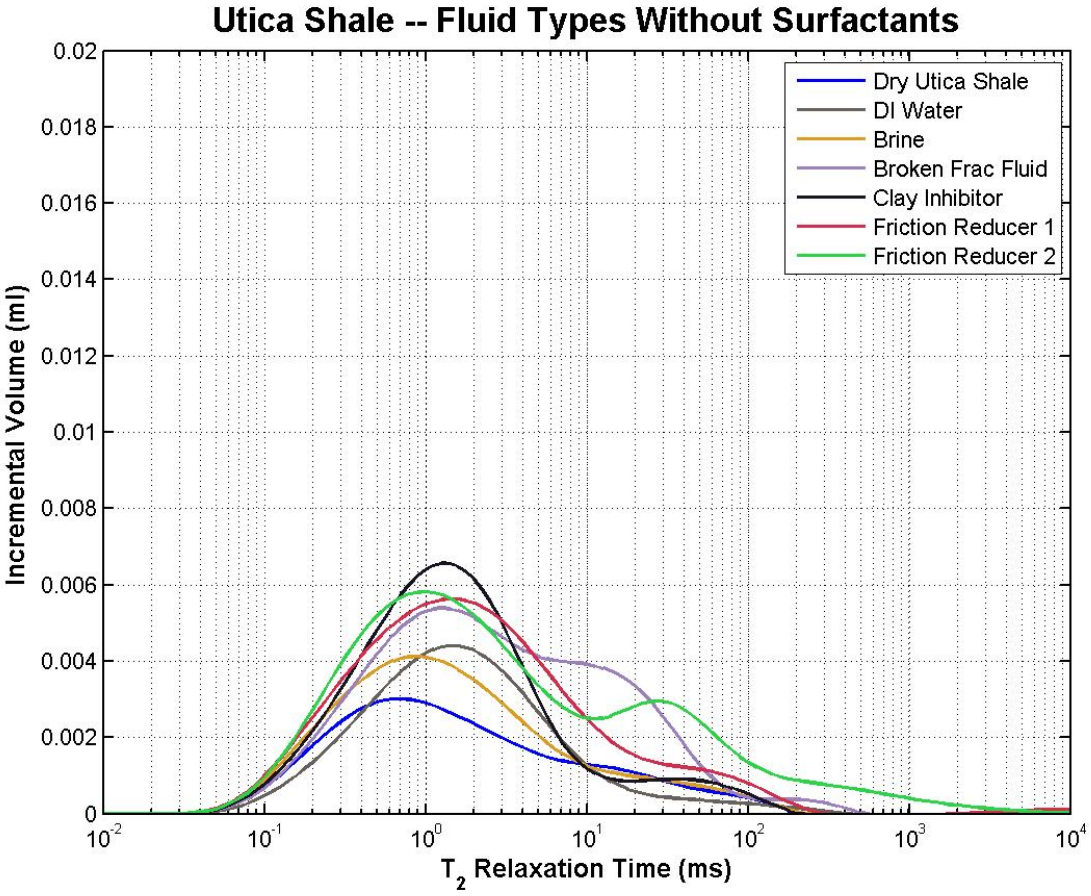

Figure 50 - Comparison of tested fluids with low clay content without surfactants.

Like the results of the high clay interactions, the distributions displayed in Figure 50 can be seen in two groups—the deionized water and brine in one group and the remaining fluids in the second. As stated before, the interactions of the second group appear to be much more complicated and varied, and their complexity only compounds further when mixed with surfactant. From the figure, it is very clear that fluid composition is a major contributor to the extent of imbibition into shale. Fluids of the same type, but different chemical makeup can also cause differing interactions, as one compares the green and red distributions of the two different friction reducers. Fluid behavior is also likely to differ with the addition of hydrocarbons.

6.3.3 Saturation Change

T_2 distributions can be related to the volumes of water imbibed in the rock, both in the clay minerals and in the effective pore space. Volumes are determined by converting the distribution's scale from T_2 to pore radius, then to volume. This scale conversion is performed with the following relationships:

$$\frac{1}{T_2} = \frac{1}{T_{2b}} + \rho \frac{S}{V}$$

Where: T_2 = The signal measured from the NMR
T_{2b} = Bulk relaxation of the fluid
ρ = Surface reflexivity of rock for a specific fluid
S = Surface Area
V = Volume

The T_{2b} value for water is approximately 3000 ms, however the parameter is not known for the rest of the fluids. Because the observed sample is shale, the reciprocal of the measured T_2 values are very large, and the T_{2b} term can be ignored through scale analysis. ρ is a parameter that is not known for each of the fluids either, however its value is typically between 1 and 20 μm/s. A value of 10 μm/s was assumed. The above conversion then simplifies to the following after assuming pores to be spherical:

$$R = 3\rho T_2$$

Where: R = pore radius (μm)

We could then create a distribution of pore volumes by using the radius distribution and assuming pores to be spherical. Fluid volumes can then be found by numerically integrating the volume distribution. Partial integration results in solving for volumes of fluid in different regions. This process was applied to all the samples tested to determine the

amount of fluid absorbed by the clay minerals and imbibed into the pore space. This information allowed us to determine the change in saturation in both regions. Saturation change was calculated by subtracting the area under the volume distribution of the dry samples from the area under the imbibition samples and dividing by the pore volume. Figure 51 and Figure 52 display the saturation changes for the rock samples in the different fluid types. Similar trends are found compared to the T_2 distribution results, however the bar graphs allow one to compare all the fluid types in one figure. One observation to notice is that even though the majority of clay bound peaks were much larger than the effective pore space peaks, integration reveals there to be greater fluid volumes in the pore spaces.

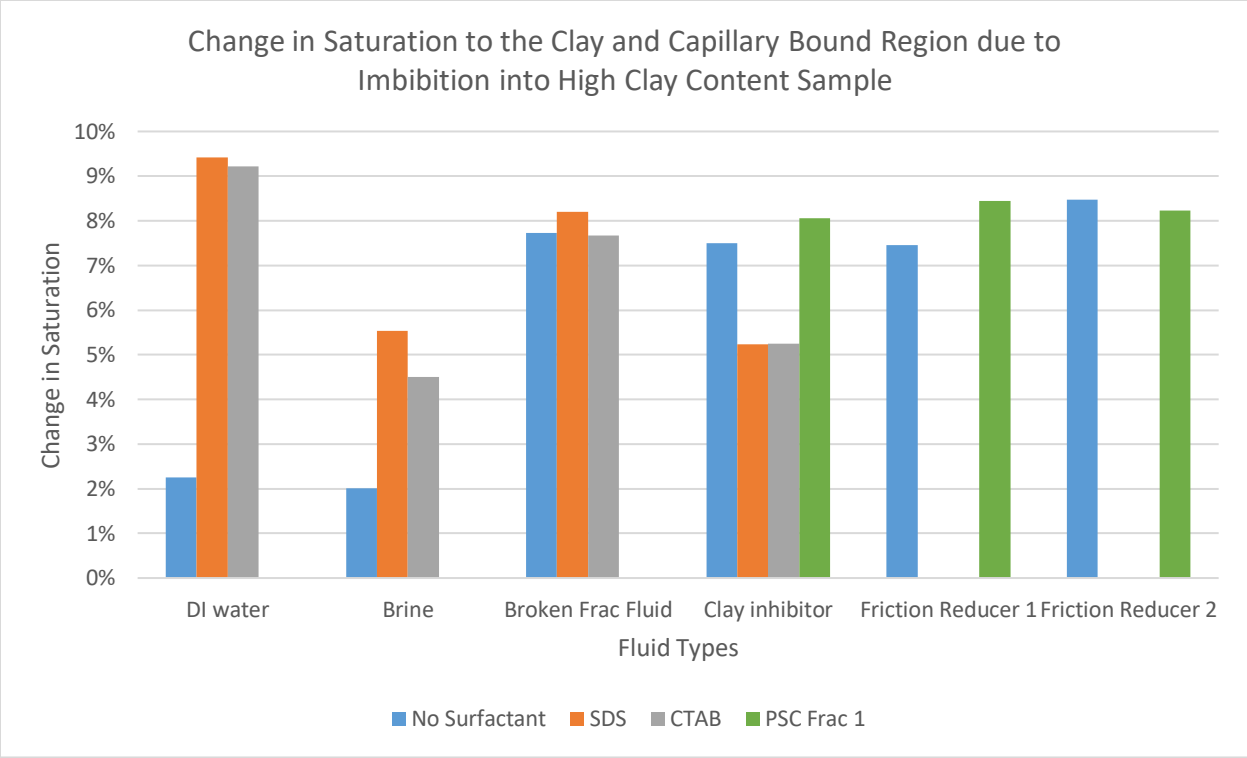

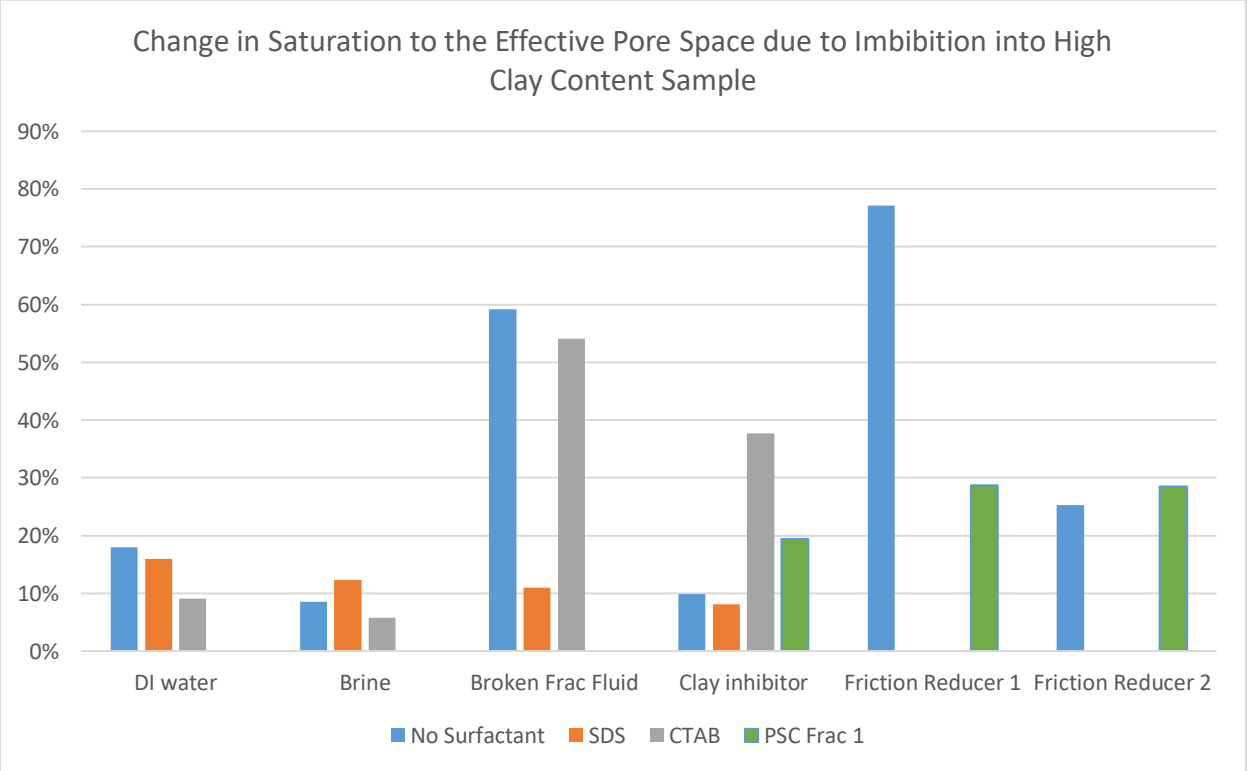

Figure 51 - Change in saturation due to imbibition from different fluids into the Eagleford sample.

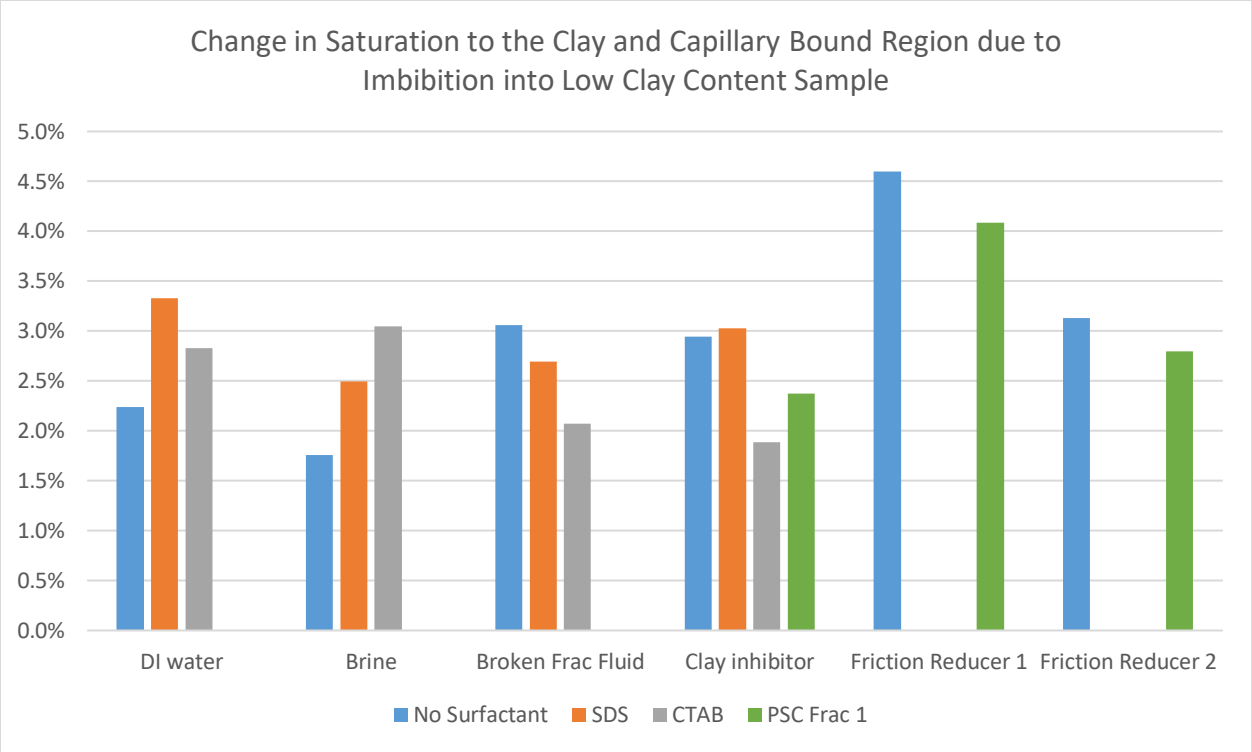

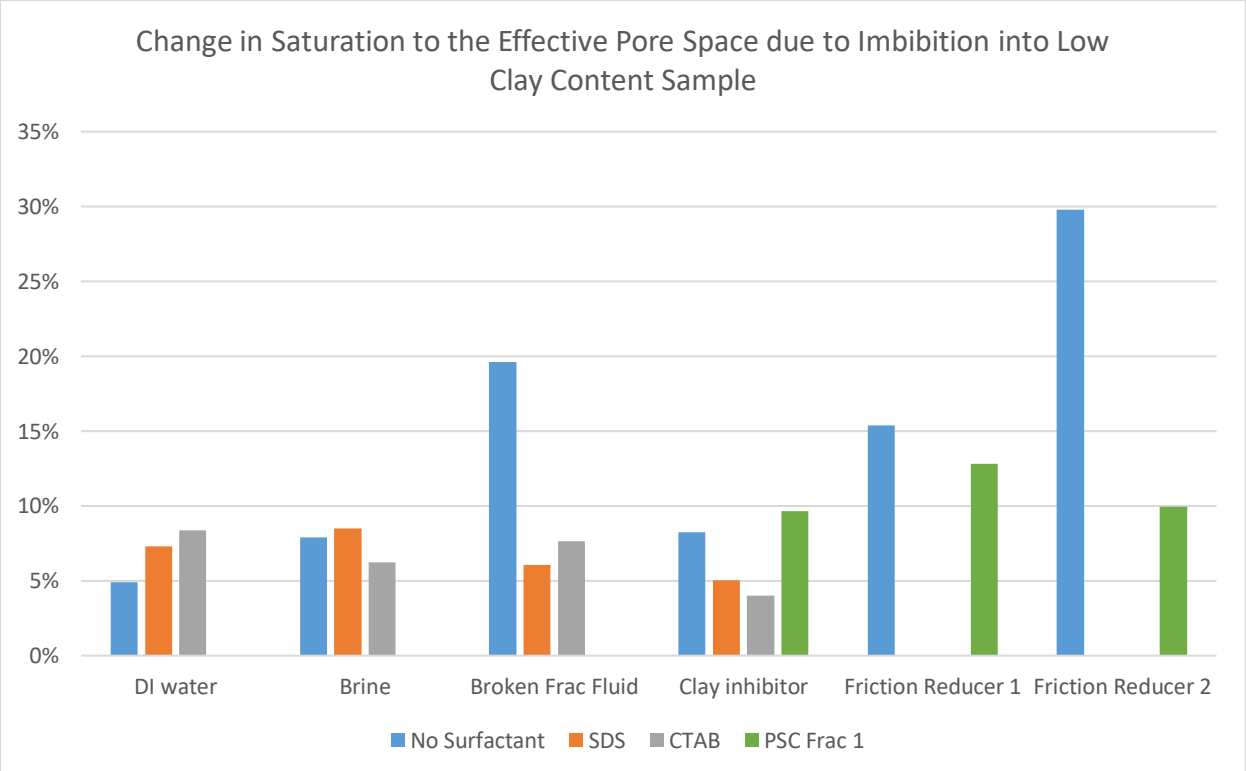

Figure 52 - Change in saturation due to imbibition from different fluids into the Utica sample.

Chapter 7: Conclusions and Recommendations for Future Work

7.1 Conclusions

The addition of surfactant is advantageous for the removal of liquids built up in a propped fracture. The cases involving surfactant performed significantly better than those without; the experiments with SDS at concentrations of 0.1% almost tripled the volume of liquid unloaded. The following observations were made regarding unloading performance:

- Foam generation within the proppant pack causes an increase in apparent viscosity and drives the mobility ratio down. When the mobility ratio is less than one, piston-like displacement occurs instead of viscous fingering. Because of this, the volume of liquid displaced up through the fracture increases appreciably (improved areal sweep efficiency). Areal sweep efficiency improves as surfactant concentration increases.
- Surfactant allows for the formation of foam bridges. As proppant distribution is not actually homogeneous in the fracture, this phenomenon allows liquids to travel across gaps in the proppant pack and allow fluid transport to continue. Transport through bridging is able to occur so long as the bridge remains stable. The main reasons for foam destabilization in a fracture include drainage effects from the natural decrease in liquid volume fraction as fluid unloads (wet bubbles are more stable than dry bubbles) as well interactions with defects such as film thinning caused by oil.
- At surfactant concentrations of 0.1%, the volumes of liquid able to be unloaded from piston-like displacement exceeded the volumes unloaded from bridging. This reveals

piston-like displacement to be the primary form of transport at high surfactant concentrations.

- Foam bridging was more important in cases with lower concentrations of surfactant compared to those cases with higher concentration, because the lower concentrations reached lower critical volume fractions (poorer areal sweep efficiency). Their mechanism of transport transitioned to bridging at much lower volume fractions and relied on bridging to obtain their unloading limits.
- Higher gas injection rates resulted in larger volumes of unloaded fluid. Although still a dependent relationship, the unloading limits appear to be less sensitive to surfactant concentration when gas flow rates increase. An increase in surfactant concentration does indeed unload more fluid, but the degree of improvement is greater at lower flow rates.
- The addition of oil into the system degraded unloading performance at most flow rates with a decrease in performance of about 40%. However, the performance was still significantly greater than experiments lacking surfactant.

If one's goal is to remove built-up liquid from a propped fracture, these observations indicate that surfactant can be utilized to improve unloading performance. For wells with fractures having low gas flow rates, unloading performance should be more dependent on surfactant concentration. Therefore if a fracture has a low gas flow rate, higher concentrations of surfactant should be added. If a fracture has a high gas flow rate, lower concentrations should be sufficient – increasing concentration would not be as beneficial as it would be at a lower flow rate.

One should also consider the interactions hydraulic fracturing fluid has with the rock formation. It is believed that when shale has a high tendency to imbibe fluid, the rock becomes more ductile. A product of clay swelling is that the shale becomes softer. This potentially leads to

proppant embedment and fines generation, which both are other potential contributors to productivity decline in fractured wells. From analyzing NMR scans of the imbibition of different fluid combinations into shale samples of differing clay content, it is obvious that the resulting interactions are extremely diverse. The following conclusions can be made:

- Samples with higher clay content can be more sensitive to fluid interactions because of the clay mineral's tendency to swell.
- Increasing salinity of a fluid generally will decrease imbibition, while other additives such as polymers can increase imbibition
- The addition of surfactants increases imbibition of water, both deionized and saline. The interaction resulting from their addition to other fluids is less obvious.
- Shale-fluid interactions are very complicated and diverse, and heavily depend on the chemistry of both the fluid and clay minerals.

7.2 Future Work

There is a lot of further research to be performed. These experiments were conducted at atmospheric conditions merely to determine the benefits and potential of surfactant utilization. During these experiments, oil definitely compromised the stability of foam generated by SDS. Generation and stability at reservoir conditions were not researched. Thus, the next step would be to identify a surfactant that can generate a stable foam at high temperatures, pressures, and when in contact with hydrocarbons. The surfactant also must not compromise the formation's integrity, and its interaction with clay minerals must be considered. Currently, there is ongoing research for such a surfactant by those intending to include it as an additive in gas injection for EOR purposes and some possible candidates or blends of candidates have been identified (Nguyen, Rommerskirchen, Fernandez, & Nguyen, 2018; Zeng, Miller, & Mohanty, 2018).

If a surfactant candidate can be selected, then liquid unloading experiments should be performed with fracture fluid and oil at high temperatures and pressures to validate trends observed in these experiments. Those results would determine future paths taken. If successful, a field trial could be conducted using the stable surfactant, giving one information about the surfactant's true performance in the field. A field trial would also reveal production benefits that can be achieved and the cost parameters needed to make this an economic success.

Appendices

Appendix A

Minerology of clay samples that were tested.

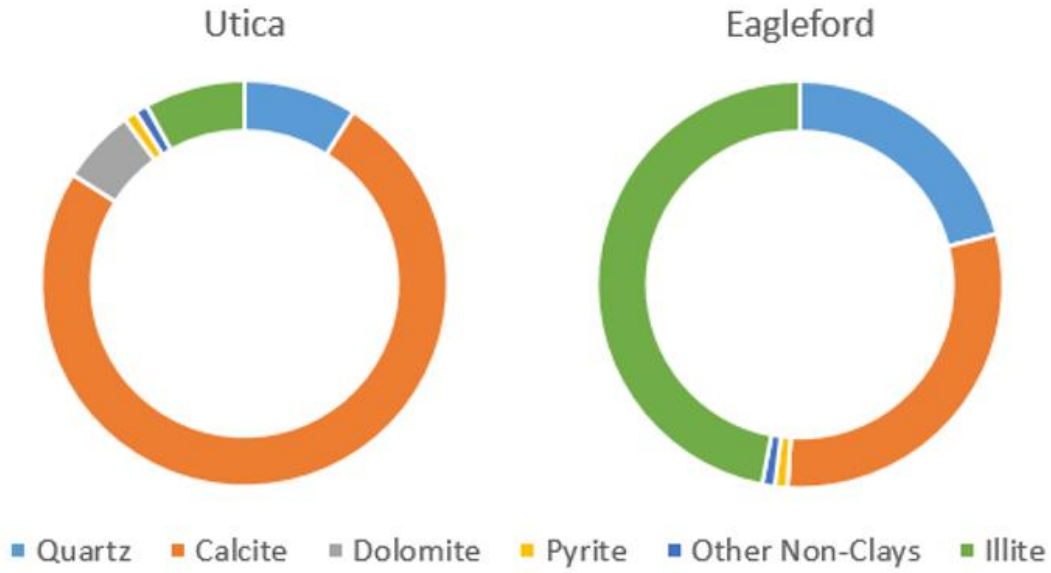

Utica Porosity = 11.2%

Eagleford Porosity = 11.9%

Appendix B

MATLAB code used to generate T2 distribution curves from Excel sheets containing NMR data.

```
clf; clear all
clc

%% Import data for T2 plot

T_2 = logspace(-2,4,121); % Generates 31 lograthimically spaced numbers from 0.01 to 10000

Shale_Dry = xlsread('UPE dryshale','dry','B2:B122')';    % Read Incremental Volume data from
excel file
a = xlsread('Uticaclayinhibitor.xlsx','nosurf','B2:B122')';
b = xlsread('Uticaclayinhibitor.xlsx','SDS','B2:B122')';
c = xlsread('Uticaclayinhibitor.xlsx','CTAB','B2:B122')';

% a = xlsread('UPE DI Water.xlsx','nosurf','B2:B122')';
% b = xlsread('UPE Brine.xlsx','nosurf','F2:F122')';
% c = xlsread('UPE PA.xlsx','nosurf','B2:B122')';

%% Plot T2 NMR data

figure(1)
semilogx(T_2, Shale_Dry,'b','LineWidth',1.5); hold on;
semilogx(T_2, a,'k','LineWidth',1.5); hold on;
semilogx(T_2, b,'r','LineWidth',1.5); hold on;
semilogx(T_2, c,'g','LineWidth',1.5); hold on;



% semilogx(T_2, a,'Color',[.411 .388 .368],'LineWidth',1.5); hold on;
% semilogx(T_2, b,'Color',[.859 .619 .137],'LineWidth',1.5); hold on;
% semilogx(T_2, c,'Color',[.61 .51 .74],'LineWidth',1.5); hold on;


ylim([0 .02])

grid on;

title('Utica Shale -- Clay Inhibitor and Surfactants','FontSize',16,'FontWeight','bold')
xlabel('T_2 Relaxation Time (ms)','FontSize',12,'FontWeight','bold')
ylabel('Incremental Volume (ml) ','FontSize',12,'FontWeight','bold')

% set(gca,'fontsize',12)  % set font size of axes
set(gca,'LineWidth',1.0,'TickLength',[0.01 0.01]);
legend ('Dry Eagleford Shale','Clay Inhibitor + no surf','Clay Inhibitor + SDS','Clay Inhibitor +
CTAB','location','Northeast')
% legend ('Dry Eagleford Shale','DI Water','Brine','Slickwater')

legend boxon
set(gca,'XGrid','on')
% ylim([0 0.1])
% saveas(gcf,'Utica -- Clay Inhibitor with Surfactants','jpg')
% saveas(gcf,'UPE -- Fluid Types without Surfactants','jpg')
```

References

Abbasi, M., Dehghanpour, H., & Hawkes, R. V. (2012, January 1). Flowback Analysis for Fracture Characterization. Society of Petroleum Engineers. doi:10.2118/162661-MS

Abbott, S. (2017). Surfactant science: Principles & practice. Lancaster, PA: DEStech Publications.

Acharya, A. R. (1986, March 1). Particle Transport in Viscous and Viscoelastic Fracturing Fluids. Society of Petroleum Engineers. doi:10.2118/13179-PA

Agrawal, S., & Sharma, M. M. (2015). Practical insights into liquid loading within hydraulic fractures and potential unconventional gas reservoir optimization strategies. Journal of Unconventional Oil and Gas Resources,11, 60-74. doi:10.1016/j.juogr.2015.04.001

Alramahi, B., & Sundberg, M. I. (2012, January 1). Proppant Embedment And Conductivity of Hydraulic Fractures In Shales. American Rock Mechanics Association.

American Chemistry Council. (2019, January 03). Surfactants | Use, Benefits, and Chemical Safety Facts. Retrieved January 28, 2019, from https://www.chemicalsafetyfacts.org/surfactants/

Aronson, A., Bergeron, V., Fagan, M., & Radke, C. (1994). The influence of disjoining pressure on foam stability and flow in porous media. Colloids and Surfaces A: Physicochemical and Engineering Aspects, 83(2), 109-120. doi:10.1016/0927-7757(94)80094-4

Aveyard, R., Cooper, P., Fletcher, P. D., & Rutherford, C. E. (1993). Foam breakdown by hydrophobic particles and nonpolar oil. Langmuir, 9(2), 604-613. doi:10.1021/la00026a041

Behera, M. R., Varade, S. R., Ghosh, P., Paul, P., & Negi, A. S. (2014). Foaming in Micellar Solutions: Effects of Surfactant, Salt, and Oil Concentrations. Industrial & Engineering Chemistry Research, 53(48), 18497-18507. doi:10.1021/ie503591v

Cho, Y., Ozkan, E., & Apaydin, O. G. (2013, May 1). Pressure-Dependent Natural-Fracture Permeability in Shale and Its Effect on Shale-Gas Well Production. Society of Petroleum Engineers. doi:10.2118/159801-PA

Coates, G. R., Xiao, L., & Prammer, M. G. (1999). NMR Logging Principles & Applications. Halliburton Energy Services Publication.

Falls, A. H., Musters, J. J., & Ratulowski, J. (1989, May 1). The Apparent Viscosity of Foams in Homogeneous Bead Packs. Society of Petroleum Engineers. doi:10.2118/16048-PA

Fan, L., Thompson, J. W., & Robinson, J. R. (2010, January 1). Understanding Gas Production Mechanism and Effectiveness of Well Stimulation in the Haynesville Shale Through Reservoir Simulation. Society of Petroleum Engineers. doi:10.2118/136696-MS

Fisher, M. K., & Warpinski, N. R. (2012, February 1). Hydraulic-Fracture-Height Growth: Real Data. Society of Petroleum Engineers. doi:10.2118/145949-PA

Fredd, C. N., McConnell, S. B., Boney, C. L., & England, K. W. (2001, September 1). Experimental Study of Fracture Conductivity for Water-Fracturing and Conventional Fracturing Applications. Society of Petroleum Engineers. doi:10.2118/74138-PA

Gdanski, R. D., & Walters, H. G. (2010, January 1). Impact of Fracture Conductivity and Matrix Relative Permeability on Load Recovery. Society of Petroleum Engineers. doi:10.2118/133057-MS

Ghanbari, E., & Dehghanpour, H. (2016). The fate of fracturing water: A field and simulation study. Fuel, 163, 282-294. doi:10.1016/j.fuel.2015.09.040

Green, D. W., & Willhite, G. P. (1998). SPE Textbook Series, Volume 6: Enhanced Oil Recovery. Society of Petroleum Engineers.

Koehler, S. A., Hilgenfeldt, S., & Stone, H. A. (2000). A Generalized View of Foam Drainage: Experiment and Theory. Langmuir, 16(15), 6327-6341. doi:10.1021/la9913147

Kumar, P., & Mittal, K. L. (1999). Handbook of Microemulsion Science and Technology. CRC Press

Lichtarowicz, M. (2013, March 18). Surfactants. Retrieved January 28, 2019, from http://www.essentialchemicalindustry.org/materials-and-applications/surfactants.html

McClure, M. W., Babazadeh, M., Shiozawa, S., & Huang, J. (2016, August 1). Fully Coupled Hydromechanical Simulation of Hydraulic Fracturing in 3D Discrete-Fracture Networks. Society of Petroleum Engineers. doi:10.2118/173354-PA

Mejia, L., Tagavifar, M., Xu, K., Mejia, M., Du, Y., & Balhoff, M. (2019). Surfactant flooding in oil-wet micromodels with high permeability fractures. Fuel, 241, 1117-1128.

Negin, C., Ali, S., & Xie, Q. (2017). Most common surfactants employed in chemical enhanced oil recovery. Petroleum, 3(2), 197–211.

Nguyen, T., Rommerskirchen, R., Fernandez, J., & Nguyen, Q. P. (2018, March 26). Surfactants As Steam Foam Additives for Thermal EOR Processes. Society of Petroleum Engineers. doi:10.2118/190473-MS

Princen, H., & Mason, S. (1965). The permeability of soap films to gases. Journal of Colloid Science,20(4), 353-375. doi:10.1016/0095-8522(65)90082-6

Saint-Jalmes, A. (2006). Physical chemistry in foam drainage and coarsening. Soft Matter, 2(10), 836-849. doi:10.1039/b606780h

Sarma, D. S., Pandit, J., & Khilar, K. C. (1988). Enhancement of stability of aqueous foams by addition of water-soluble polymers—measurements and analysis. Journal of Colloid and Interface Science, 124(1), 339-348. doi:10.1016/0021-9797(88)90356-6

Sarna, A., Xing, Q., Mork, J., & Ershaghi, I. (2014, April 17). Impact of Fracture Closure on Productivity Decline of Unconventional Wells. Society of Petroleum Engineers. doi:10.2118/169590-MS

Schramm, Laurier L., Stasiuk, E. N., & Marangoni, D. G. (2003). 2 Surfactants and their applications. Annu. Rep. Prog. Chem., Sect. C: Phys. Chem., 99, 3–48.

Sedev, R., & Exerowa, D. (1999). DLVO and non-DLVO surface forces in foam films from amphiphilic block copolymers. Advances in Colloid and Interface Science, 83(1-3), 111-136. doi:10.1016/s0001-8686(99)00007-x

Sharma, M., & Agrawal, S. (2013, February 4). Impact of Liquid Loading in Hydraulic Fractures on Well Productivity. Society of Petroleum Engineers. doi:10.2118/163837-MS

Stevenson, P. (2010). Inter-bubble gas diffusion in liquid foam. Current Opinion in Colloid & Interface Science, 15(5), 374-381. doi:10.1016/j.cocis.2010.05.010

Tcholakova, S., Mitrinova, Z., Golemanov, K., Denkov, N. D., Vethamuthu, M., & Ananthapadmanabhan, K. P. (2011). Control of Ostwald Ripening by Using Surfactants with High Surface Modulus. Langmuir, 27(24), 14807-14819. doi:10.1021/la203952p

U.S. Department of Energy. (2009). Modern Shale Gas Development in the United States: A Primer. Work Performed Under DE-FG26-04NT15455. Prepared by The Ground Water Protection Council and ALL Consulting.

Wang, L., & Yoon, R. (2008). Effects of surface forces and film elasticity on foam stability. International Journal of Mineral Processing, 85(4), 101-110. doi:10.1016/j.minpro.2007.08.009

Worland, J. (2018, March 06). U.S. Fracking Is About to Transform the Global Energy Market. Retrieved January 7, 2019, from http://time.com/5187074/fracking-energy-oil-natural-gas/

Zeng, T., S. Miller, C., & Mohanty, K. (2018, April 14). Application of Surfactants in Shale Chemical EOR at High Temperatures. Society of Petroleum Engineers. doi:10.2118/190318-MS